UPPSALA
UNIVERSITET

Digital Comprehensive Summaries of Uppsala Dissertations from the Faculty of Science and Technology 1631

Theoretical studies of lattice- and spin-polarons

NINA BONDARENKO

ACTA
UNIVERSITATIS
UPSALIENSIS
UPPSALA
2018

ISSN 1651-6214
ISBN 978-91-513-0235-5
urn:nbn:se:uu:diva-340947

Dissertation presented at Uppsala University to be publicly examined in Häggsalen, Ångströmlaboratoriet, Uppsala, Tuesday, 27 March 2018 at 09:30 for the degree of Doctor of Philosophy. The examination will be conducted in English. Faculty examiner: Professor Maria Roser Valenti Vall (Institute for Theoretical Physics. Goethe University Frankfurt).

Abstract

Bondarenko, N. 2018. Theoretical studies of lattice- and spin-polarons. *Digital Comprehensive Summaries of Uppsala Dissertations from the Faculty of Science and Technology* 1631. 103 pp. Uppsala: Acta Universitatis Upsaliensis. ISBN 978-91-513-0235-5.

Theoretical studies of lattice- and spin-polarons are presented in this thesis, where the primary tool is ab-initio electronic structure calculations. The studies are performed with employment of a variety of analytical and computational methods. For lattice-polarons, we present an analytical study where multipolaron solutions were found in the framework of the Holstein 1D molecular crystal model. Interestingly, we found a new periodic, dnoidal, solution for the multipolaron system. In addition to it, we examined the stability of multipolaron solutions, and it was found that cnoidal and dnoidal solutions stabilize in different ranges of the parameter space. Moreover, we add to the model nonlocal effects and described dynamics in terms of internal solitonic modes.

Hole-polaron localization accompanying the formation of a cation vacancy in bulk MgO and CaO and at the (100) MgO/CaO interfaces is presented. We show that the ground state is found to be the O1-O1 bipolaronic configuration both in bulk oxides and at their interfaces. Moreover, the one-centered O2-O0 bipolaron was found to be metastable with its stability being enhanced at the interfaces compared to that in bulk oxides. Also, for several bipolaronic configurations, we analyzed possible transitions from O1-O1 to O2-O0. On the same line of reasoning, electron localization and polaron mobility in oxygen-deficient and Li-doped monoclinic tungsten trioxide has been studied. It is shown for WO3, that small polarons formed in the presence of oxygen vacancy prefer bipolaronic W5+-W5+ configuration rather than W6+-W4+ configuration, which is found to be metastable state. Also, it is demonstrated that the bipolarons are tightly bound to vacancies, and consequently exhibit low mobility in the crystal. On the other hand, we show that polarons formed as a result of Li intercalation are mobile and that they are being responsible for electrochromic properties discovered in the compound.

Spin-polaron formation in La-doped CaMnO3, with G-type antiferromagnetic structure, was also studied. We found that for this material, spin-polarons are stabilized due to the interplay of magnetic and lattice-effects at lower La concentrations and mostly due to the lattice contribution at larger concentrations. We show that the formation of SP is unfavourable in the C- and A-type antiferromagnetic phase, in agreement with previously reported experimental studies. We have also studied dynamical and temperature dependent properties of spin-polarons in this compound. We estimated material specific exchange parameters from density functional theory and found that 3D magnetic polarons in the Heisenberg lattice stabilize at slightly higher temperatures than in the case of 2D magnetic polarons. Next, we have proposed a method to calculate magnetic polaron hopping barriers and studied spin-polaron mobility CaMnO3 using additional methods such as atomistic spin dynamics and kinetic Monte Carlo. We make a suggestion of using this system in nano-technological applications.

Keywords: Polaron, Nonlinear Schrödinger Equation, Nonlocality, Solitons, Integrable systems, Quantum field theory (low energy), Electron-phonon interaction, Density functional theory, Electronic structure of atoms and molecules, Spin-polaron, Langevin equation, Transport properties, Hubbard model, Heisenberg lattice

Nina Bondarenko, Department of Physics and Astronomy, Materials Theory, Box 516, Uppsala University, SE-751 20 Uppsala, Sweden.

ISSN 1651-6214
ISBN 978-91-513-0235-5
urn:nbn:se:uu:diva-340947 (http://urn.kb.se/resolve?urn=urn:nbn:se:uu:diva-340947)

To all those who are on their challenging way of the scientific discovery

List of papers

This thesis is based on the following papers, which are referred to in the text by their Roman numerals.

I Multi-polaron solutions, nonlocal effects and internal modes in a nonlinear chain.
N. Bondarenko, O. Eriksson, N. V. Skorodumova, and M. Pereiro.
Submitted to Physical Review A

II Hole bipolaron formation at (100) MgO/CaO epitaxial interface.
N. Bondarenko, O. Eriksson, and N. V. Skorodumova.
Physical Review B **89**, 125118 (2014).

III Polaron mobility in oxygen-deficient and lithium-doped tungsten trioxide.
N. Bondarenko, O. Eriksson, and N. V. Skorodumova.
Physical Review B **92**, 165119 (2015).

IV Spin-polaron formation and magnetic state diagram in La-doped $CaMnO_3$.
N. Bondarenko, Y. Kvashnin, J. Chico, A. Bergman, O. Eriksson, and N. V. Skorodumova.
Physical Review B (R) **95**, 220401 (2017).

V Static and dynamical properties of spin-polaron in La-doped $CaMnO_3$.
N. Bondarenko, J. Chico, A. Bergman, Y. Kvashnin, N. V. Skorodumova, O. Eriksson.
Submitted to Physical Review X

Reprints were made with permission from the publishers.

During the work in this thesis, I also co-authored the following papers which are not included in this thesis:

- Elastic phase transitions in metals at high pressures.
  O. M. Krasilnikov, Yu. Kh. Vekilov, I. Yu. Mosyagin, E. I. Isaev, **N. G. Bondarenko**.
  Journal of Physics: Condensed Matter **24**, 195402 (2012).

- Structural transformations at high pressure in the refractory metals (Ta, Mo, V).
  O. M. Krasilnikov, Yu. Kh. Vekilov, A. V. Lugovskoy, I. Yu. Mosyagin, M. P. Belov, **N. G. Bondarenko**.
  Journal of Alloys and Compounds **586**, S242 (2014).

Contents

1. Introduction

> Cheshire Cat: You may have noticed that I'm not all there myself.
>
> *Alice's Adventures in Wonderland. Lewis Carroll*

Condensed matter physics explores physical properties of condensed phases of matter. The studies are mainly focused on many-body systems where many particles bond to each other. Under certain assumptions, such systems admit a description in the *language* of interacting subsystems, nuclear (ionic) and electronic. The perturbation of the electronic state in the crystal leads to the local changes of the interatomic interaction and hence to the excitation of atomic vibrations, i.e., excitation of phonon modes. Vice versa the lattice perturbations affect the electronic density that reflect the manifestation of so-called *electron-phonon interaction* responsible for numerous cooperative effects in solids. Thus, current carrier scattering, anharmonic renormalisation of the phonon frequencies, carrier quantum confinement, or conventional superconductivity are possible examples.

One of the most extraordinary collective phenomena which arises as a consequence of the *electron-phonon interaction* is a charge localisation in a lattice in the self-induced potential well. In this regards, a localised carrier is dressed in the lattice polarisation and it forms a quasiparticle, called a polaron. This entity has its own characteristics reflecting its inner structure: radius, formation energy, charge, magnetic momentum and other quantum numbers. Polaron admits a description in the frame of the effective mass approximation and since it is a dressed quasiparticle, the polaronic effective mass is usually greater than the effective mass of a Bloch particle, i.e, an undressed electron in a crystal lattice.

Despite the simplicity of the main concept, exact solution of the polaron problem has been obtained only in a few limiting cases and the problem continues to attract the extensive attention of the scientific community. In statistical mechanics and quantum field theory, the problem is the simplest case of a system where nonrelativistic quantum particle interacts with a bosonic quantum field. Numerous sophisticated theoretical methods had been developed and employed to solve the problem.

Initially, the concept was introduced by L.D. Landau [1]. S.I. Pekar [2], suggested a common term − polaron and investigated the self-energy and the effective mass of this new quasi-particle in continuum polar media. Later, Fröhlich [3] in studies on polaron model in the continual limit has adapted Pekar's approach to the adiabatic or strong-coupling regime. The functional integral method, developed by R. Feynman especially to study polaron problem, became one of the most used methods in statistical mechanics and quantum field theory [4]. An essential contribution to the polaron theory has been constructed by Bogolyubov which developed a consistent adiabatic perturbation theory of polaron formation [5]. Later he returned to the problem and also applied the well-known method of chronological orderings or T-products [6]. The technique appeared effective for the theory of polarons with a large radius (radius much larger than the characteristic lattice period) for all electron-phonon interactions (weak, intermediate and strong). Moreover, the T-product method based on the path integral formalism has a variety of applications in many areas of quantum physics.

A proper theoretical analysis of a polaron also includes studies with employment of the Lattice Hamiltonian in the context of a microscopic picture. The studies dealing with a spatially well-localised wave function (small polaron limit) form another branch of research which question Fröhlich picture. Seminal papers corresponding to the subject are dated back to the 50's of the previous century [7]. Nowadays, studies on the polaron in the discrete picture form a broad field including numerous studies with employment of advanced theoretical and computation technics such as Diagrammatic Monte Carlo [8], the Density Matrix Renormalization Group technics (DMRG) [9] or Exact Diagonalisation [10] among others. Recently, it has been shown that a proper theoretical analysis of a lattice polaron in microscopic pictures requires ab-initio techniques [11]. They precisely account for material dependent wave function and reflecting the motion of every single atom in the area of the lattice distortion surrounding the localised electron.

Interest in the polaron problem increases if, in addition to the previously described spatially homogeneous systems, a charged particle with elementary excitations in spatially inhomogeneous media is considered. In this regards, polaron localisation in quantum dots, interfaces and surfaces, in systems with low-dimensionality also constitute as an emerging subject. Moreover, the polaron concept extended to systems, with a different type of interaction enriched the family of quasiparticles. Thus, the family of polaron-like quasiparticles has been extended and are listed in the following as: spin-polaron − a localized, due to the magnetic interaction, charge in a magnetic lattice [12], excitonic-polaron − an exciton coupled to the optical phonon branches [13], ripplonic polaron [14] − a

charge carrier localised due to the topological defects, plasmapolaron [15] – an electron coupled to a plasmon excitation and many more.

Polarons is a broad field of experimental research in solid-state physics since they are not only theoretical, abstract constructions, but also experimentally observable objects. Nowadays, the experimental evidence allows studying a variety of polaronic fingerprints in systems with variable structures and compositions. For example, optical absorption spectra and electron spin resonance (ESR) indicate the formation of a polaronic state [16]. Moreover, studies of the optical absorption for small polarons as compared to large polarons exhibit different characters of the spectra [17]. Usually, experimental X-ray absorption measurements are employed to detect polaronic band formation [18]. Very recently, two-dimensional electronic spectroscopy (2DES) has been employed to study bipolaron pair absorption in polymer thin films [19]. Measurements of electrical conductivity and Seebeck coefficient are methods of choice in order to study polaron mobility [20]. The sample magnetisation curves carry information regarding spin-polaron state formation [21]. Overall, these experimental data plays an important role in the understanding of a variety of phenomena such as charge transport and optical properties of semiconductors [17, 22], high-temperature superconductivity [23] and giant magnetoresistance [24].

Of course, it is impossible to highlight all aspects of the polarons in this short introduction. With this, we just aimed to familiarize the reader with the methods and achievements of modern physics developed in the context of the polaron theory. Undoubtedly, the following chapters of this work are devoted to several problems in the framework of polaron theory. However, for a complete description, we refer the reader to specialised literature [25, 26, 27, 28].

Here, we present a theoretical study of lattice- and spin-polarons with employment of several theoretical methods. Our research is done in systems with various dimensionalities, such as, one-dimensional chain of harmonic oscillators, two-dimensional surfaces, interfaces and three-dimensional oxide bulk. Moreover, we analysed polaron formation and dynamics accounting for the influence of anisotropy, non-locality, temperature and electric field. Studies are done with employment of both analytical as well as modern computational methods of solid state physics. The thesis is organised as follows: in Chapter I, we give an overview of main theoretical models and approaches of polaron theory, in Chapter II, we discuss polarons and multi-polarons in Holstein molecular-crystal model with introduced non-local term and some of our results achieved in the frame of this model. In Chapter III, we give an overview of main aspects of spin-polaron theory related to our studies in this field. In Chapter IV, we discuss methods and approaches of the density functional theory (DFT). In Chapter V, we discuss methods and approaches of the

density functional theory (DFT) we used in order to model polarons in oxides. Chapter VI of this thesis is devoted to our results of the polaron numerical modelling in the frame of DFT. In Chapter VII, we report analytical calculation of the polaronic nonadiabatic transition rate. Finally, in Appendices we discuss analitical derivation of polaron nonadiabatic transition rate.

2. Polaron models

Formation of a polaronic state is a consequence of the lattice polarization induced by a charge carrier. The crystal polarization lowers the crystal energy towards the delocalized state and a local potential well forms. In polar crystals, the carrier's wave function is well localized in the potential well and rapidly decays in the surrounding media. Therefore, the polaronic state develops in a self-consistent manner: a localized charge state induces lattice polarization and in its turn, the locally polarized lattice traps the carrier.

In the continual limit when the localized wave function is spread over a region significantly larger than the characteristic interatomic spacing, the so-called large polaron is discussed. In this approach, the crystal can be considered as a continuous dielectric media with the corresponding material constants.

Another attempt to describe polarons is given within mesoscopic models which account for the internal structure of the media. Polarons in this model are usually strongly onsite localised. Below we describe both continual and discrete polaron model. Also, we discuss bipolaron state which may form.

2.1 Pekar's model

We start assuming a self-trapped, large polaronic state in the tight-binding picture [29]. In the framework of the model, we distinguish inertial polarization responsible for the state localization and the periodic potential formed due to the ionic shell polarization which follows the carrier motion without any interruption. Thus, the localized state can be determined as a solution of the Schrödinger equation:

$$-\frac{\hbar^2}{2m}\nabla^2\psi(\boldsymbol{r})+\left[V(\boldsymbol{r})+W(\boldsymbol{r})\right]\psi(\boldsymbol{r})=\mathcal{E}\psi(\boldsymbol{r}), \tag{2.1}$$

where $\psi(\boldsymbol{r})$ is the electronic wave function, $V(\boldsymbol{r})$ is lattice periodic potential, and $W(\boldsymbol{r})$, the interaction energy of the electron with the trapping self-induced polarization field. For a large polaron, it is possible to drop the periodic lattice polarization term replacing the electronic mass m by effective mass m*:

$$-\frac{\hbar^2}{2m^*}\nabla^2\psi(\boldsymbol{r})+W(\boldsymbol{r})=\mathcal{E}\psi(\boldsymbol{r}). \tag{2.2}$$

The Eq. (2.2) can be obtained as a variation of the following functional and accounting for the normalization condition $\int d\tau\,|\psi|^2=1$:

$$\mathcal{E}\,[\psi]=\int d\tau\frac{\hbar^2}{2m^*}(\nabla\psi)^2+\int d\tau W\psi^2, \tag{2.3}$$

hereby we notice that the second term in this equation is the average of the electron-media interaction energy $\bar{W}$.

For the polarized anisotropic media $\bar{W}$ can be expressed in terms of the dipole interaction energy as:

$$\begin{aligned}\bar{W}=-\int\int d\tau d\tau'\boldsymbol{P}(\boldsymbol{r})q(\boldsymbol{r}')\frac{\boldsymbol{r}-\boldsymbol{r}'}{|\boldsymbol{r}-\boldsymbol{r}'|^3}=\\ -e\int\int d\tau d\tau'\boldsymbol{P}(\boldsymbol{r})\,|\psi(\boldsymbol{r}')|^2\,\frac{\boldsymbol{r}-\boldsymbol{r}'}{|\boldsymbol{r}-\boldsymbol{r}'|^3},\end{aligned} \tag{2.4}$$

where $\boldsymbol{P}(\boldsymbol{r})$ is the crystal polarization vector and $q(\boldsymbol{r}')$ is the electron charge distribution function.

At the same time the electrical induction vector is :

$$\boldsymbol{D}(\boldsymbol{r})=e\int d\tau'\,|\psi(\boldsymbol{r}')|^2\,\frac{\boldsymbol{r}-\boldsymbol{r}'}{|\boldsymbol{r}-\boldsymbol{r}'|^3}. \tag{2.5}$$

Accounting for Eq. (2.5), the functional (2.3) finally obtains the following form:

$$\mathcal{E}\,[\psi]=\int d\tau\frac{\hbar^2}{2m^*}(\nabla\psi)^2-\int d\tau\boldsymbol{P}\boldsymbol{D}\,[\psi]\,. \tag{2.6}$$

Next, relation between $\boldsymbol{P}(\boldsymbol{r})$ and $\boldsymbol{D}(\boldsymbol{r})$ can be found using material dependent constants :

$$\boldsymbol{P}(\boldsymbol{r})=\frac{1}{4\pi\varepsilon^*}\boldsymbol{D}(\boldsymbol{r}), \tag{2.7}$$

where ε^* is the effective permittivity (called also Pekar's factor) determined by the ionic polarization displacements and can be defined as $\varepsilon^{*-1}=\varepsilon_\infty^{-1}-\varepsilon_0^{-1}$, where ε_∞ and ε_0 are static and high-frequency permittivity, respectively.

The ground state energy corresponding to the polaronic state can be found by applying a minimization procedure to the functional (2.6) at the constant $\boldsymbol{P}$. After the minimization, the vector $\boldsymbol{P}$ can be defined using first the relation (2.7) and then Eq. (2.5). A similar result can be obtained first redefining $\boldsymbol{P}(\boldsymbol{r})$ through $\boldsymbol{D}(\boldsymbol{r})$, and then minimizing the obtained functional but only multiplying the potential term by factor 1/2. Thus, the ground state wave function can be found solving the following integro-differential equation:

$$\mathcal{J}[\psi] = \int d\tau \frac{\hbar^2}{2m^*}(\nabla\psi)^2 - \frac{1}{8\pi\varepsilon^*}\int d\tau \boldsymbol{D}[\psi]^2 . \tag{2.8}$$

Adopting Pekar's choice for the trial function $\psi = A(1+r/r_p+\beta r^2)e^{-r/r_p}$, where r_p is the characteristic radius of the polaronic cloud, β is the variational parameter and A is a normalizing coefficient. After minimizing the functional indicated in Eq. (2.8) with respect to the variables, we obtain:

$$\begin{aligned} A &= 0.12/r_p^{3/2}, \\ \beta &= 0.45/r_p^2, \\ r_p &= 1.51\frac{\hbar^2\varepsilon^*}{e^2 m^*}. \end{aligned} \tag{2.9}$$

Taking into account Eq. (2.6), the obtained parameters for the electronic wave function lead to:

$$\mathcal{E}_0 = \mathcal{E}[\psi_0] = -0.164\frac{m^* e^4}{\varepsilon^{*2}\hbar^2}. \tag{2.10}$$

This energy can be considered as the lowest photon energy E_b to excite the polaronic electron into the bare electron band, so that $E_b = \mathcal{E}_0$. The thermal polaron dissociation energy can be estimated as $E_d = -\mathcal{E}_0 - W_p$, where $W_p = \frac{1}{4\pi\varepsilon^*}\int \boldsymbol{D}^2$ is the inertial part of the polarization energy. By using Eq. (2.10) and the definition of the inertial part of the polarization energy, it is straightforward to show that $W_p = -2/3\mathcal{E}_0$ and consequently $E_d = -1/3\mathcal{E}_0$. Finally, the averaged potential energy according to Eq. (2.4) and Eq. (2.10) is $\bar{W} = 4/3\mathcal{E}_0$. Thus, we arrive to the fundamental ratio $|E_d| : |W_p| : |E_b| : |\bar{W}|$ =1:2:3:4 for characteristic energies of the Pekar's continual polaron.

2.2 Fröhlich versus Holstein model

The Fröhlich Hamiltonian [3, 30] describes an electron coupled to non-dispersive (optical) phonons of a dielectric medium via its polarisation.

The model is mostly popular in the polaron problem and has attracted broad interest of researchers working in the field, well describing many aspects of polaron behaviour in a wide range of systems. The Fröhlich model postulates the following main principles (Fig. 2.1 a)): 1) in the system one considers optical modes with the same frequencies; 2) the dielectric crystal is treated as a continuum medium; 3) in the undistorted lattice the carrier moves freely with a quadratic dispersion relation. In the standard description, the Fröhlich Hamiltonian reads as [3]:

$$H = -\frac{\hbar^2}{2m^*}\nabla^2 + \sum_{\boldsymbol{k}} \hbar\omega_{LO} a^\dagger_{\boldsymbol{k}} a_{\boldsymbol{k}} + \sum_{\boldsymbol{k}} (V_k a_{\boldsymbol{k}} e^{i\boldsymbol{kr}} + H.c.), \tag{2.11}$$

where $\boldsymbol{r}$ is electron position coordinate operator, m^* is the electron effective mass, $a^\dagger_{\boldsymbol{k}}$ and $a_{\boldsymbol{k}}$ are the creation and annihilation operators of the longitudinal optical phonons with the wave vector $\boldsymbol{k}$ and energy $\hbar\omega_{LO}$. The Fourier components of the electron-phonon interaction are:

$$V_k = -i\frac{\hbar\omega_{LO}}{k}\left(\frac{4\pi\alpha}{V}\right)^{\frac{1}{2}}\left(\frac{\hbar}{2m^*\omega_{LO}}\right)^{\frac{1}{4}}, \tag{2.12}$$

where V is the crystal volume and constant α is the strength of the electron-phonon interaction:

$$\alpha = \frac{e^2}{\hbar}\sqrt{\frac{m^*}{2\hbar\omega_{LO}}}\frac{1}{\varepsilon^*}. \tag{2.13}$$

In the weak coupling regime (valid in the limit $\alpha < 1$) the Lee, Low and Pines [31] approach is the method of choice. The method is based on the unitary transformation which eliminates the electronic variables in the Hamiltonian. Using the variational wave function, the method finds a shifted polaronic ground state energy under the assumption that new, successive virtual phonons are emitted independently.

When the coupling is very strong ($\alpha \gg 1$) all features of polaron behavior are well described by Pekar's model [29]. The theory includes variational calculations based on the idea that in the strong coupling regime the quantum effects are negligible and a carrier is adiabatically followed by the surrounding polarization field.

An excellent formalism, that is accurate at all couplings, was already introduced by Feynman [32]. He developed a variational all-coupling path-integral polaron theory. The starting point of the formalism is the imaginary-time path-integral for the Fröhlich Hamiltonian, with a single impurity. With employment of the Feynman-Jensen [33] inequality, for

which the full path integral calculation is a difficult task, is replaced with a simpler variational model action. After the procedure, the problem is formulated in terms of a model Hamiltonian which approximately describes the interaction of the electron with the lattice. In the new Hamiltonian, an electron is coupled to a fictitious mobile mass, which models the cloud of phonons. In this description, the model consists of two variational parameters: the mass of the fictitious particle and the spring constant. The diagrammatic quantum Monte Carlo [34] and renormalization group studies [35] have demonstrated the remarkable accuracy of the Feynman method for the Fröhlich electron self-energy.

In contrast to the Fröhlich model, mainly dealing with long-range interactions, the Holstein model was adopted to describe microscopic properties of the localized state and focuses on the polaron formation at the presence of short-range interactions (Fig. 2.1 b)). The Holstein Hamiltonian in one dimensional, spin-less picture reads as:

$$H = -j\sum_i (a_i^\dagger a_{i+1} + H.c.) - g\sum_i a_i^\dagger a_i (b_i^\dagger + b_i) + \omega_0 \sum_i b_i^\dagger b_i, \qquad (2.14)$$

where $a_i^\dagger$ (a_i) and $b_i^\dagger$ (b_i) are creation (annihilation) operators for electrons and dispersionless optical phonons on i-th site, j is the nearest-neighbor hopping integral, g is the electron-phonon coupling parameter and ω_0 is the phonon frequency.

The model has successfully been applied to a vast range of physical problems [25, 36]. For instance, studying band structure of the strongly correlated systems [37, 38] and thermoelectric properties of molecular junctions [39]. Polaron paring (bipolaron) mechanism in the frame of the model has been suggested to understand high-(Tc) superconductivity phenomena in cuprates [40] and hydrides under high pressure [41]. In the last decades, the model also has gained much attention due to polaronic effects which play an important role in charge transport in organic semiconductors [42].

According to the value of the system parameters, several different limits of the model can be distinguished. The first important dimensionless ratio (the adiabaticity ratio) t/ω_0 determines characteristic time scale of the electronic or atomic subsystems. In the case of adiabatic regime, $t/\omega_0 \gg 1$, the dynamics of the charge carrier is affected by quasi-static crystal deformations and as a consequence of this, the quantum lattice fluctuations can be neglected. Lattice oscillators, in this case, may involve dispersive character having many levels and can be considered as classical variables in the Hamiltonian.

However, in the so called anti-antiadiabatic regime ($t/\omega_0 \ll 1$), the electronic subsystem is slower than the ionic subsystem, so that, the latter immediately adapts to the perturbations of the electronic state renormal-

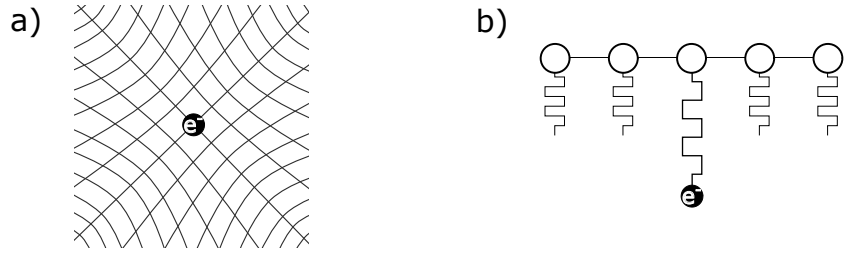

Figure 2.1. Illustration for two different polaronic models. a) Fröhlich continual model. b) Discrete Holstein polaron.

izing the mass of the carrier. If the Einstein oscillator energy is not too small compared to the energy of the coupling strength, the phonons in the Hamiltonian can be fully described as quantum particles.

Now, we move the discussion to the second ratio g/ω_0 which characterizes electron-phonon coupling strength (the ratio is also called dimensionless coupling constant). The strong (weak)-coupling regime simply holds when $g/\omega_0 > 1 (g/\omega_0 < 1)$. The electron-phonon coupling strength can be also characterized via $\alpha = g^2/2\omega_0 Dt$, where 2Dt is the half bandwidth of the free electron (here D refers to the dimensionality of the system).

Since the seminal Holstein [7] paper, the model has extensively been studied using a variety of theoretical techniques. Introduced at the early stages of theory development, Lang-Firsov (LF) and modified Lang-Firsov (MLF) transformation [43] turned out to be a powerful tool for numerous studies. The transformations renormalize the system energy and incorporate the electron-phonon interaction into the electronic hopping integral. Perturbative approaches [44], which can also be combined with the transformations [36], are methods well established in the weak and strong coupling limits.

Recently, the field theory development together with numerical and computational technics extended coverage of the coupling constant also to intermediate regimes. Relevant for this discussion are Exact Diagonalization [45], variational [46] and Quantum Monte Carlo [47] algorithms. Unfortunately, the current computational capabilities highly limit these calculations in terms of the lattice size. To overcome this problem, the DMRG method [9], optimal for one dimensional systems, has successfully been implemented. Dynamical mean-field theory also has been applied to the Holstein polaron problem [41, 48]. The approach, exact in infinite dimensions, has been interpolated for 3D systems with use of the semiempirical electronic density of states.

Even though numerical calculations have significantly increased our understanding of polaron physics in the Holstein's picture, the rigorous analytical solution still has a tremendous value. Moreover, they are im-

portant not only from the mathematical point of view, but also increasing our insight into the details of the physical nature of the problem.

2.3 Bipolaron concept

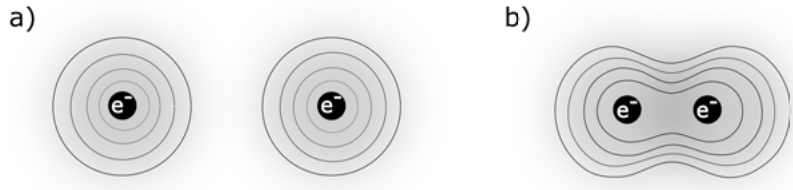

Figure 2.2. Cartoon illustrating bipolaron formation. a) Two separated polarons each in its own polarisation well. b) Bipolaron where two electrons are localized in the same potential well. Formation of the joint bipolaron potential overcomes Coulomb repulsion of the electrons. The potential wells are schematically shown via concentric isolines.

For certain system parameters, two polarons with the same charge can become mutually coupled, forming a new type of a quasiparticle named bipolaron [40]. Therefore, the energy gain for creating a bipolaron from two separated polarons (Fig. 2.2 a)) is the net result of the Coulomb repulsion which tends to separate polarons, and the lattice deformation energy gained by having two particles in the same potential well (Fig. 2.2 b)). Electron or hole bipolaron has an electric charge equal either to $2e^-$ or $2e^+$, respectively. The two electrons may localize at the same atomic site in the lattice. In this case, the so-called one-centre bipolaron forms [49]. In the simplest models, such bipolaron configuration is usually described by a helium atom-like Hamiltonian. Two polarons localised at different sites form a two-centred bipolaron. The two-centred polaron, unlike two unbound polarons, is characterised by a nonzero formation energy of the bound state. Bipolaron can stabilise in two equilibrium magnetic configurations. If two polarons form an s-orbital configuration, where the net angular momentum of two united polarons is zero, it will occur in the spin-singlet state. This scenario is common for the one-centred bipolaron. Otherwise, two polarons with the same spin component along a common quantization axis will form a bipolaron in the spin-triplet state. For example, two-centred hole-bipolarons in the magnesium oxide stabilise in the spin-triplet state.

The bipolaron has an integer spin so that the bipolarons obey the Bose-Einstein statistics. Moreover, it is thought that at low tempera-

tures they form a Bose condensate similarly to Cooper pairs in superconductors [50]. Due to their unique properties bipolarons formation takes a special place in the polaron physics. Bipolaron models have successfully been applied to the study of the transport properties of conducting polymers [51], organic magnetoresistance [52] and hight T_c superconductivity [53]. Moreover, recently it has been shown that bipolaron model leads to a straightforward interpretation of the isotope effect observed in the latter [54].

3. Polaron in Holstein Molecular Crystal model in the continuous limit

Since the seminal work of S. Pekar that initiated studies of polarons more than 70 years ago, nowadays the polaron theory has developed into a wide field of research. However, some of the aspects of the theory as, for example, non-local electron effects had not been fully discussed in the literature up today. The main reason for the circumstance is caused by the complexity of the non-local problem applied to the interacting electron-lattice systems. In this chapter, we make an attempt to introduce the non-local extensions to the Molecular-Crystal Model, which describes interacting electrons in the tight-binding picture. Holstein has shown that in one-dimension, continual case the model can be mapped onto a so-called Non-Linear Shrödinger Equation (NLSE). Interestingly, in this limit, the robust stable solitonic solution of the NLSE corresponds to a polaron. Below, we describe our studies of the non-local extensions of the polaronic NLSE. Moreover, we discuss the new, periodic solutions of the model and their stability with respect to a weak, periodic perturbation.

3.1 Nonlocal extensions of the Holstein Molecular Crystal model in the continuous limit

Following Holstein's seminal paper [7], we reformulate the model starting from the Hamiltonian:

$$H = H_{el} + H_{lat} + H_{el-lat} + H_{n-loc}, \tag{3.1}$$

where

$$\begin{aligned} H_{el} &= -j\sum_n a_n^\dagger (a_{n+1} + a_{n-1}), \\ H_{lat} &= \sum_n \left(\frac{p_n^2}{2M} + \frac{1}{2} M\omega_0^2 x_n^2 \right), \\ H_{el-lat} &= -g\sum_n x_n a_n^\dagger a_n, \\ H_{n-loc} &= \sum_n W_n a_n^\dagger a_n. \end{aligned}$$

The first term H_{el} describes tight-binding electrons with nearest-neighbor overlap integral j. The second term of the Hamiltonian, H_{lat}, describes 1D lattice of N identical diatomic molecules with mass M and momentum operator $p_n \equiv (\hbar/i)\partial/\partial x_n$. Nucleus harmonically oscillate around the stationary mass center with frequency ω_0 and deviation x_n, which counts with respect to the equilibrium interatomic separation. In the zero-order adiabatic approach, assumed in the present work, the vibrational term only remains to be considered. The next term, H_{el-lat}, stands for the electron-lattice interaction with the characteristic coupling constant g. Finally, the nonlocal term $W_n(x_1, ..., x_n)$, in a simple picture, is assumed to be taken in the form of the Pöschl-Teller potential [55]. This term represents the perturbation on site n due to the presence of the other atomic sites. It can be calculated, in the continuum limit, as the following Coulomb integral [7]:

$$W_n(x_1, ..., x_n) = \int \mid \phi(x - na, x_n) \mid^2 \sum_{m \neq n} U(x - ma, x_m) dx, \tag{3.2}$$

where $\phi_n \equiv \phi(x - na, x_n)$ are the "single-site" atomic electron wave functions, U is the single-site atomic potential and a is the lattice parameter. As commented above, the atomic potential can be modelled by using the Pöschl-Teller potential given by:

$$U(x - ma, x_m) = \frac{-V_m}{\cosh^2\left(\frac{x - x_m}{\beta a}\right)}, \tag{3.3}$$

where V_m is the height of the potential and β is the parameter accounting for the potential overlapping with nearest neighbours.

For the single-site electronic wave function, we used a localised function as:

$$\phi(x - na, x_n) = \gamma_n \operatorname{sech}^2(\frac{x - x_n}{\beta a}). \tag{3.4}$$

Here, γ_n represents the maximum of the wave function. For simplicity, we used the same β parameter for both U and ϕ since they are related to the overlapping of the electron wave function and this is precisely what the W_n term is meant to describe. Consequently, it is expected that W_n will be proportional to β. By inserting Eqs. (3.3)-(3.4) in Eq. (3.2), the nonlocal term W_n can be recast in the form:

$$W_n = -\sum_{m \neq n} \gamma_n^2 V_m \int_{-\eta}^{\eta} \operatorname{sech}^4\left(\frac{x - x_n}{\beta a}\right) \operatorname{sech}^2\left(\frac{x - x_m}{\beta a}\right) dx, \tag{3.5}$$

where η represents half of the size of the 1D system, i.e. half of the number of diatomic molecules.

The overlap integral between neighbouring diatomic molecules is defined, in the continuum limit, as:

$$j(x_n, x_m) \equiv \int \phi^*(x - na, x_n) U(x - na, x_n) \phi(x - ma, x_m) dx. \tag{3.6}$$

Using the same picture as described above and assuming for simplicity that $\gamma_n = \gamma_m$, then the hopping integral can be recast in the following form:

$$j(x_n, x_m) = -\gamma_n^2 V_n \int_{-\eta}^{\eta} \frac{\operatorname{sech}^2\left(\frac{x - x_m}{\beta a}\right)}{\cosh^4\left(\frac{x - x_n}{\beta a}\right)} dx. \tag{3.7}$$

In order to ensure that the boundary conditions of the chain of diatomic molecules are periodic, we take a finite chain in the range [-η,η] and assume the periodic boundary conditions.

The general Hamiltonian, as defined in Eq. (3.1), projected onto a single-electron state solves the following eigenvalue problem:

$$\mathcal{E} a_n = \frac{1}{2} \sum_m M \omega_0^2 x_m^2 a_n - g x_n a_n + W_n a_n - j(a_{n-1} + a_{n+1}). \tag{3.8}$$

We multiply Eq. (3.8) by a complex-conjugated amplitude a_n^* and sum over all sites (here we employ normalisation condition $\sum_n |a_n|^2 = 1$). The procedure leads to an expression for the total energy:

$$\mathcal{E} = \frac{1}{2} \sum_m M \omega_0^2 x_m^2 - \sum_n g x_n |a_n|^2 + \sum_n W_n |a_n|^2 - \sum_n j(a_{n+1} + a_{n-1}) a_n^*. \tag{3.9}$$

In order to find equilibrium positions, we differentiate energy with respect to position, x_p, and if the dependence on electronic hopping is neglected one obtains:

$$\frac{\partial \mathcal{E}}{\partial x_p} = M \omega_0^2 x_p - (g - \frac{\partial W_p}{\partial x_p}) |a_p|^2, \tag{3.10}$$

and near the equilibrium point ($\frac{\partial \mathcal{E}}{\partial x_p} \equiv 0$) this leads to an important analytical relation expressing dependency of the electronic and new, lattice degrees of freedom $\mathcal{X}_p$:

$$\mathcal{X}_p = \frac{(g - \frac{\partial W_p}{\partial x_p})}{M \omega_0^2} |\mathfrak{a}_p|^2, \tag{3.11}$$

where $\mathfrak{a}_p$ is the solution of Eq. (3.8) for the minimum energy $\mathcal{E}$ (notice that we introduce gothic font for the variable at the equilibrium point).

Substituting Eq. (3.11) into Eq. (3.8) and introducing an convenient notation $\Upsilon_p = \frac{g - \frac{\partial W_p}{\partial x_p}}{M\omega_0^2}$, we obtain an electronic discrete Schrödinger-type equation:

$$\mathcal{E}\mathfrak{a}_n = \frac{1}{2}\sum_n M\omega_0^2 \mathcal{X}_n^2 \mathfrak{a}_n - g\Upsilon_n |\mathfrak{a}_n|^2 \mathfrak{a}_n + W_n \mathfrak{a}_n - j(\mathfrak{a}_{n-1} + \mathfrak{a}_{n+1}). \quad (3.12)$$

After introducing the convenient substitution: $\varepsilon = -\mathcal{E} + \frac{1}{2}\sum M\omega_0^2 \mathcal{X}_n^2 - 2j$, Eq. (3.12) takes the following form:

$$j(\mathfrak{a}_{n-1} - 2\mathfrak{a}_n + \mathfrak{a}_{n+1}) + g\Upsilon_n |\mathfrak{a}_n|^2 \mathfrak{a}_n - (\varepsilon + W_n)\mathfrak{a}_n = 0. \quad (3.13)$$

In the continuum limit, $\mathfrak{a}_n$ is assumed to be a differentiable function of the continuous position variable n:

$$\mathfrak{a}_{n\pm1} = \mathfrak{a}_n \pm \frac{\partial \mathfrak{a}_n}{\partial n} + \frac{1}{2}\frac{\partial^2 \mathfrak{a}_n}{\partial n^2}. \quad (3.14)$$

In the case of the strongly localised wave function ($W_n = 0$ as $\beta \to 0$), the approach turns Eq. (3.13) into the so-called classical continuous nonlinear Schrödinger equation (CNLSE) [7, 56, 57]:

$$j\frac{\partial^2 \mathfrak{a}_n}{\partial n^2} + \frac{g^2}{M\omega_0^2}|\mathfrak{a}_n|^2 \mathfrak{a}_n - \varepsilon \mathfrak{a}_n = 0. \quad (3.15)$$

Interestingly, the first term in Eq. (3.15) can be generalised for the case of the higher order overlap integrals. We found that, in the continuum limit, for the case of hopping to the arbitrary δ-th nearest neighbour:

$$j_\delta \mathfrak{a}_{n+\delta} + j_\delta \mathfrak{a}_{n-\delta} = j_\delta(2\mathfrak{a}_n + \delta^2 \frac{\partial^2 \mathfrak{a}_n}{\partial n^2}). \quad (3.16)$$

It is easy to prove that in the case of the first-nearest neighbour ($\delta = 1$), this relation converges to Eq. (3.14):

$$j\mathfrak{a}_{n+1} + j\mathfrak{a}_{n-1} = j(2\mathfrak{a}_n + \frac{\partial^2 \mathfrak{a}_n}{\partial n^2}). \quad (3.17)$$

Thus, accounting for δ-nearest neighbours, we finally reformulate the problem in terms of the extended CNLSE with variable coefficients:

$$\sum_\delta j_\delta \delta^2 \frac{\partial^2 \mathfrak{a}_n}{\partial n^2} + g\Upsilon_n |\mathfrak{a}_n|^2 \mathfrak{a}_n - (\varepsilon + W_n)\mathfrak{a}_n = 0, \quad (3.18)$$

where we have disregarded the functional dependence of the functions for the sake of simplicity. Finally, the extended time-dependent CNLSE with

variable coefficients is obtained after adding the time-dependent derivative:

$$i\hbar\frac{\partial \mathfrak{a}_n}{\partial t}+\sum_{\delta} j_\delta \delta^2 \frac{\partial^2 \mathfrak{a}_n}{\partial n^2}+g\Upsilon_n\left|\mathfrak{a}_n\right|^2\mathfrak{a}_n-(\varepsilon+W_n)\mathfrak{a}_n=0. \tag{3.19}$$

3.2 On the periodic solutions of the one dimensional polaronic model

In this section, we describe derivations on the periodic solutions in more detail. The initial electron-lattice Hamiltonian in the absence of the non-local term can be mapped into the continuous NLSE:

$$j\frac{\partial^2 \mathfrak{a}_n}{\partial n^2}+\frac{g^2}{M\omega_0^2}\left|\mathfrak{a}_n\right|^2\mathfrak{a}_n-\varepsilon\mathfrak{a}_n=0. \tag{3.20}$$

It is convenient to introduce the following notation: $\mathfrak{f}^2=\frac{g^2}{\varepsilon M\omega_0^2}\left|\mathfrak{a}_n\right|^2$ and $n=(\frac{j}{\varepsilon})^{\frac{1}{2}}n'$, which leads to:

$$\mathfrak{f}''_{n'n'}+\mathfrak{f}^3-\mathfrak{f}=0. \tag{3.21}$$

Periodic solutions of Eq. (3.21) are sought in the form of Jacobi elliptic functions $\zeta_0\,\mathrm{cn}[\zeta n,\mathfrak{m}]$ and $\zeta_0\,\mathrm{dn}[\zeta n,\mathfrak{m}]$, where ζ_0 and ζ are coefficients that can be expressed as a function of $\mathfrak{m}$, the square of the elliptic function modulus. After some algebra we obtain:

$$\begin{aligned}\mathfrak{f}^{(cn)}&=\left(\frac{2\mathfrak{m}}{|2\mathfrak{m}-1|}\right)^{\frac{1}{2}}\mathrm{cn}\left[\frac{1}{|2\mathfrak{m}-1|^{\frac{1}{2}}}n',\mathfrak{m}\right],\\ \mathfrak{f}^{(dn)}&=\left(\frac{2}{2-\mathfrak{m}}\right)^{\frac{1}{2}}\mathrm{dn}\left[\frac{1}{(2-\mathfrak{m})^{\frac{1}{2}}}n',\mathfrak{m}\right].\end{aligned} \tag{3.22}$$

By using the notation $\sigma=\frac{g^2}{4M\omega_0^2 j}$, we can rewrite the periodic cnoidal and a previously not discussed, dnoidal solutions of Eq. (3.20) as:

$$\begin{aligned}&\frac{\mathfrak{m}^{\frac{1}{2}}\zeta^{(cn)}}{(2\sigma)^{\frac{1}{2}}}\,\mathrm{cn}\left[\zeta^{(cn)}n,\mathfrak{m}\right];\quad \zeta^{(cn)}=(\frac{\varepsilon^{(cn)}}{j})^{\frac{1}{2}}\frac{1}{|2\mathfrak{m}-1|^{\frac{1}{2}}},\\ &\frac{\zeta^{(dn)}}{(2\sigma)^{\frac{1}{2}}}\,\mathrm{dn}\left[\zeta^{(dn)}n,\mathfrak{m}\right];\quad \zeta^{(dn)}=(\frac{\varepsilon^{(dn)}}{j})^{\frac{1}{2}}\frac{1}{(2-\mathfrak{m})^{\frac{1}{2}}}.\end{aligned} \tag{3.23}$$

The normalisation condition of $\mathfrak{a}_n$ in case of $\mathfrak{N}$-well solutions will lead to (the solutions are presented in Fig. 3.1 a),b)):

$$\begin{aligned}\frac{\mathfrak{N}}{\sigma}\mathfrak{m}\zeta^{(cn)}\int_0^K \mathrm{cn}^2\left[\zeta^{(cn)}n,\mathfrak{m}\right]dn=\frac{\mathfrak{N}}{\sigma}\zeta^{(cn)}(E-\mathfrak{m}'K)=1,\\ \frac{\mathfrak{N}}{\sigma}\zeta^{(dn)}\int_0^K \mathrm{dn}^2\left[\zeta^{(dn)}n,\mathfrak{m}\right]dn=\frac{\mathfrak{N}}{\sigma}\zeta^{(dn)}E=1,\end{aligned} \tag{3.24}$$

where K is the complete elliptic integral of the first kind, E is the complete elliptic integral of the second kind and $\mathfrak{m}'$ is the complementary to $\mathfrak{m}$ parameter [58].

After some algebra, the relations shown in Eq. (3.24) lead to the following expressions for the energy of the localised electron represented by the parameter ε:

$$\begin{aligned}\varepsilon^{(cn)}&=j\left(\frac{\sigma}{\mathfrak{N}}\right)^2\frac{2\mathfrak{m}-1}{(E-\mathfrak{m}'K)^2},\\ \varepsilon^{(dn)}&=j\left(\frac{\sigma}{\mathfrak{N}}\right)^2\frac{2-\mathfrak{m}}{E^2}.\end{aligned} \tag{3.25}$$

The length of the chain 2η and number of the wells along the chain $\mathfrak{N}$ are related as $2\eta\zeta=\mathfrak{N}K$. Considering this relation we find it convenient to present the energy of the localised electron in the following form:

$$\begin{aligned}\varepsilon^{(cn)}&=\left(\frac{g^2}{4M\omega_0^2}\right)\left(\frac{K}{2\eta}\right)\frac{2\mathfrak{m}-1}{E-\mathfrak{m}'K},\\ \varepsilon^{(dn)}&=\left(\frac{g^2}{4M\omega_0^2}\right)\left(\frac{K}{2\eta}\right)\frac{2-\mathfrak{m}}{E}.\end{aligned} \tag{3.26}$$

3.3 The modulation instability of the periodic solutions

Investigating the stability problem is the key method to clarify the system behaviour in case of non-degenerate tree of solutions. We focus on the cnoidal and the dnoidal solutions as the most probable candidates describing the behaviour of the multi-polaron chain and examine their modulation instability [59] against small perturbations. We start considering the time dependent CNLSE (Eq. (3.19)) in the form:

$$i\hbar\frac{\partial\mathfrak{a}_n}{\partial t}+j\frac{\partial^2\mathfrak{a}_n}{\partial n^2}+\frac{g^2}{M\omega_0^2}\left|\mathfrak{a}_n\right|^2\mathfrak{a}_n-\mathcal{W}\mathfrak{a}_n=0. \tag{3.27}$$

where $\mathcal{W}$ plays the role of an external potential which we assume to be constant in order to study the perturbation near the manifold of the analytically obtained periodic solutions (it is easy to prove that the conditional relation for the slowly changing non-local term W_n in Eq. (3.2) sets a criterion that $V_p << \gamma_n$ and $2\eta > \beta a$). Hereby we also find it convenient to introduce the following substitutions: $\phi^2 = \frac{g^2}{jM\omega_0^2} |\mathfrak{a}_n|^2$ and $t = \frac{\hbar}{j}\tau$. That leads to the following equation:

$$i\phi_\tau^{'} + \phi_{nn}^{''} + |\phi|^2 \phi - \frac{\mathcal{W}}{j}\phi = 0. \tag{3.28}$$

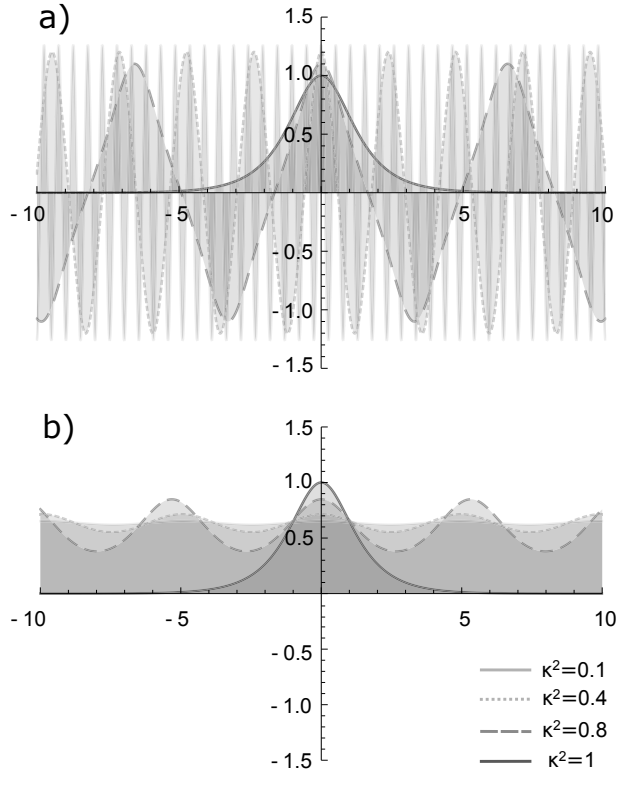

Figure 3.1. Normalized periodic cnoidal a) and the dnoidal b) solutions of Eq. (3.20) for κ^2 varied in the range of 0.1-1. Notice that both solutions converge to a soliton as soon as $\kappa^2 \to 1$.

In order to find the solutions in this study, we use the following ansatz in the form of the travelling wave function:

$$\phi(\xi,\tau) = A(\mathfrak{f}(\xi) + \phi_1(\xi,\tau) + i\phi_2(\xi,\tau))e^{i(A^2-k^2)\tau + ikx}, \tag{3.29}$$

where we redefine $\xi = A(n - 2k\tau)$. In this notation $\mathfrak{f}(\xi)$ represents the stationary part of the solution; $\phi_1(\xi,\tau)$ and $i\phi_2(\xi,\tau)$ are assumed to be the lower-order terms with respect to the unperturbed solution. They play the role of small perturbations in the system.

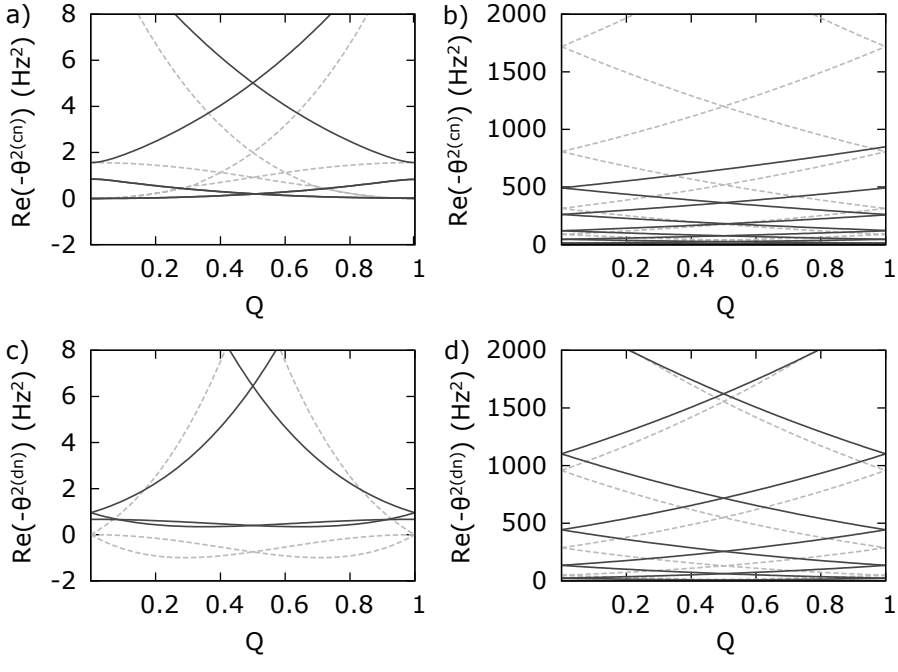

Figure 3.2. Real part of the Θ_{mn} matrix eigenvalues. Low-lying (left panel) and upper-lying (right panel) branches are obtained over 15x15 matrix diagolization for cnoidal (**a)**, **b)**) and dnoidal (**c)**, **d)**) solutions. Branches are plotted in the range of Q=0-1, for $\mathfrak{m} = 0.1$ (dashed line), $\mathfrak{m} = 0.9$ (solid line) and parameter $\varpi = 1$.

Substituting Eq. (3.29) into Eq. (3.28), leads us to the following system of equations:

$$\begin{cases} \mathfrak{f}''_{\xi\xi}(\xi) + \mathfrak{f}^3(\xi) - \varpi\mathfrak{f}(\xi) = 0, \\ \frac{\partial\phi_1(\xi,\tau)}{\partial\tau} = A^2(\varpi - \mathfrak{f}^2(\xi) - \frac{\partial^2}{\partial\xi^2})\phi_2(\xi,\tau) = A^2\hat{\mathcal{O}}_1\phi_2(\xi,\tau), \\ i\frac{\partial\phi_2(\xi,\tau)}{\partial\tau} = -iA^2(\varpi - 3\mathfrak{f}^2(\xi) - \frac{\partial^2}{\partial\xi^2})\phi_1(\xi,\tau) = -iA^2\hat{\mathcal{O}}_2\phi_1(\xi,\tau). \end{cases} \tag{3.30}$$

Here we find it convenient to introduce the dimensionless parameter $\varpi = 1 + \frac{\mathcal{W}}{jA^2}$. Moreover, we have introduced $\hat{\mathcal{O}}_1$ and $\hat{\mathcal{O}}_2$ are the operators acting in the real and complex space, respectively.

After some simple algebra, we obtain the following relation:

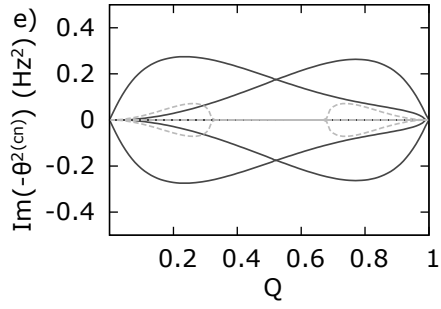

Figure 3.3. Imaginary part of the 15x15 Θ_{mn} matrix eigenvalues obtained after diagolization procedure in case of the cnoidal solution, in the range of Q=0-1, for $\mathfrak{m} = 0.1$ (dashed line) and $\mathfrak{m} = 0.9$ (solid line).

$$\frac{\partial^2 \phi_1(\xi,\tau)}{\partial \tau^2} = -A^4 \hat{\mathcal{O}}_1 \hat{\mathcal{O}}_2 \phi_1(\xi,\tau). \tag{3.31}$$

Further, we introduce time factorisation of the $\phi_1(\xi,t)$ in the form:

$$\phi_1(\xi,\tau) = \phi_1(\xi) e^{A^2\theta\tau}, \tag{3.32}$$

where the θ parameter is so called the instability increment. Substituting the factorised function into Eq. (3.31) leads us to following relation:

$$\hat{\mathcal{O}}_1 \hat{\mathcal{O}}_2 \phi_1(\xi,\tau) = -\theta^2 \phi_1(\xi). \tag{3.33}$$

We substitute small, periodic perturbation in the form of the Bloch-Floquet set: $\phi_1(\xi) = \sum_q \mathfrak{f}(\xi) e^{iq\xi}$. Fourier series expansion of $\mathfrak{f}(\xi)$ at the given q, leads us to $\phi_1^{(q)} = \sum_n C_n e^{inq_0\xi} e^{iq\xi} = \sum_n C_n e^{iq_n\xi}$ which we substitute into Eq. (3.33). Here C_n are constant coefficients. We find it convenient to introduce $q_n = nq_0 + q = q_0(n+Q)$, where Q and n are numerical parameters (n is an integer) and normalise integrals with respect to l. Furthermore multiplying the obtained relation by $e^{-iq_m\xi}$ and integrating over l which stands for the period of the $\mathfrak{f}(\xi)$ function, we end up with:

$$\frac{1}{l}\sum_n C_n \int_0^l e^{-iq_m\xi} \hat{\mathcal{O}}_1 \hat{\mathcal{O}}_2 e^{iq_n\xi} d\xi = \sum_n \Theta_{mn} C_n \equiv -\theta^2 C_m. \tag{3.34}$$

Thus, the analysis of the system stability is being reformulated in terms of the Θ_{mn} matrix eigenvalue problem. Taking into account exponential

behaviour presented in Eq. (3.32), it is easy to see that $-\theta^2 \in \mathbb{R}^+$ is the condition for the system to be stabilized with respect to the small perturbation, but if otherwise, $-\theta^2 \in \mathbb{R}^-$ or $-\theta^2 \in \mathbb{C}$, the system instability exponentially diverges with time.

Replacing the operators in Eq. (3.34) by using Eq. (3.30), we finally find the matrix Θ_{mn}. The relation is very similar to the one obtained previously in studies of the nonlinear waves in plasma physics [60]:

$$\begin{aligned}\Theta_{mn} = (\varpi + q_n^2)^2\delta_{mn} + 3\frac{1}{l}\int_0^l \mathfrak{f}(\xi)^4 cos(q_n - q_m)d\xi - \\ \frac{1}{l}\int_0^l (4\varpi + 3q_m^2 + q_n^2)\mathfrak{f}(\xi)^2 cos(q_n - q_m)d\xi.\end{aligned} \tag{3.35}$$

In order to solve eigenvalue problem for Θ_{mn}, we substitute the periodic solutions given in Eq. (3.23) into Eq. (3.35). Then for the cnoidal solution we find the following relation:

$$\begin{aligned}\Theta_{mn}^{(cn)} = \varpi^2\{(1+(\frac{\pi(Q+n)}{2K(2\mathfrak{m}-1)^{\frac{1}{2}}})^2)^2\delta_{mn} + 3(\frac{2\mathfrak{m}}{2\mathfrak{m}-1})^2\int_0^1 \mathrm{cn}\,[4K\xi,\mathfrak{m}]^4\cos[2\pi(n-m)\xi]\,d\xi - \\ (\frac{2\mathfrak{m}}{2\mathfrak{m}-1})\int_0^1 (4+3(\frac{\pi(Q+m)}{2K(2\mathfrak{m}-1)^{\frac{1}{2}}})^2 + (\frac{\pi(Q+n)}{2K(2\mathfrak{m}-1)^{\frac{1}{2}}})^2)\,\mathrm{cn}\,[4K\xi,\mathfrak{m}]^2\cos[2\pi(n-m)\xi]\,d\xi\},\end{aligned} \tag{3.36}$$

and for the dnoidal:

$$\begin{aligned}\Theta_{mn}^{(dn)} = \varpi^2\{(1+(\frac{\pi(Q+n)}{K(2-\mathfrak{m})^{\frac{1}{2}}})^2)^2\delta_{mn} + 3(\frac{2}{2-\mathfrak{m}})^2\int_0^1 \mathrm{dn}\,[2K\xi,\mathfrak{m}]^4\cos[2\pi(n-m)\xi]\,d\xi - \\ (\frac{2}{2-\mathfrak{m}})\int_0^1 (4+3(\frac{\pi(Q+m)}{K(2-\mathfrak{m})^{\frac{1}{2}}})^2 + (\frac{\pi(Q+n)}{K(2-\mathfrak{m})^{\frac{1}{2}}})^2)\,\mathrm{dn}\,[2K\xi,\mathfrak{m}]^2\cos[2\pi(n-m)\xi]\,d\xi\}.\end{aligned} \tag{3.37}$$

It can be seen that the eigenvalues $-\theta^2$ of the infinite dimensional matrix Θ_{mn} form a band structure with respect to $\mathfrak{m}$ and Q parameters. In practice, to perform a numerical diagonalisation of Eqs. (3.36-3.37), a square matrix with a finite size has been considered. In order to examine matrix size effects, we have diagonalised 7x7, 15x15 and 33x33 matrices and noticed qualitatively similar results. In this section, we present results obtained over 15x15 matrix diagonalisation. Based on the obtained $-\theta^{2(cn)}$ and $-\theta^{2(dn)}$, the dispersion law of both solutions is described as follows.

In the case of cnoidal solution Fig. 3.2 a),b), the real part of the $-\theta^2$ matrix eigenvalues, for $\mathfrak{m}$=0.1 and $\mathfrak{m}$=0.9 all branches of $-\theta^{2(cn)}$ remain real and positive for Q parameter in the range of 0-1. However, the non-zero imaginary part of $-\theta^{2(cn)}$ eigenvalues indicates an instability of

cnoidal solution for $\mathfrak{m} = 0.1$ (see Fig. 3.3). At the same time for $\mathfrak{m} = 0.9$ the cnoidal solution remains stable in the range of Q=0.32-0.68 where the imaginary part of $-\theta^{2(cn)}$ eigenvalues remain vanished. As for the dnoidal solution, for $\mathfrak{m} = 0.1$ the solution is unstable due to the negative values of the low lying branches (Fig. 3.2 c)). For $\mathfrak{m} = 0.9$ dnoidal solution is stable over the whole range of Q values since all branches of $-\theta^2$ matrix eigenvalues remain positive (Fig. 3.2 d)). The results described in Chapter 3 form the basis of Paper I, that contains a full account of this analysis.

4. Spin-polaron: general concepts

The polaron concept extended to systems with magnetic interaction leads to a new phenomenon, the so-called spin-polaron. Similarly to the classical polaron, we have described in previous chapters, spin-polaron describes a localised charge carrier. However, in this case, the quasiparticle stabilises due to the strong magnetic interaction of the impurity spin and the spin states of the host material. Spin-polaron physics stems from Zener's study on the double-exchange interaction [61]. He has shown that the interaction is induced via electron doping and it forces two neighbouring Mn spins in manganese compounds with perovskite lattice become aligned parallel. Anderson and Hasegawa's [62] studies have also contributed to the theory development. Finally, in the seminal research on the spin-polaron formation, de-Gennes [63] discovered that in diluted antiferromagnetic semiconductors, a charge carrier localises in the ferromagnetic cloud of polarised spins. Studies on the half-filled, single-band Hubbard [64] model led Nagaoka [65] to the conclusion that in the limit of the infinite electron-electron repulsion the system will converge to a ferromagnetic ground state. This work is conceptually related to the spin-polaron theory since it predicts an infinite size, or limited by the size of the crystal, ferromagnetic cloud formation in the large-U limit. Thus, different models, have explained the mechanisms of a spin-polaron formation emerged by the strong magnetic interactions in the system. Nowadays, in the literature, there are several terms, which refer to the phenomenon − spin polaron [66], magnetic polaron [67], ferron [68], fluctuon [69] and perhaps many more.

In this chapter, we discuss theoretical models of spin-polaron formation and transport. Also, we describe Langevin dynamics in the context of the spin-polarons. This discussion is relevant for our studies presented in Chapter 7.

4.1 Exchange interactions

In magnetic materials, magnetic moments are rarely free of interaction with each other. Usually, they exhibit a collective behaviour manifested due to the magnetic exchange interactions dominating in magnetic systems. Below a critical temperature, magnetic moments stabilise in ferromagnetic or antiferromagnetic, or other more exotic structures such as

ferrimagnetic, helimagnetic, spin-glass, etc. The exchange interaction effects arise as a combination of the electrostatic Coulomb repulsion, Pauli exclusion principle which keeps electrons with parallel spins apart and reduces the Coulomb repulsion and kinetic energy.

Magnetic ordering manifested in magnetic systems is a result of direct or indirect interactions between the onsite localised moments or delocalised electronic moments in the crystal. For magnetic systems several mechanisms of the exchange interaction are most frequently considered:

1. Direct exchange which arises as a consequence of the Pauli exclusion principle and depends strongly on the overlap of the participating wave functions [70]. At shorter distances between the interacting particles, the interactions usually manifests an antiferromagnetic (AFM) character (Cr, Mn). However, as soon as the distance between the particles increases, the interaction changes its character to ferromagnetic (FM) (Fe, Co, Ni). Finally, when the overlap between the participating wave functions is neglectable small, the paramagnetic phase stabilises.
2. Superexchange interaction [71, 72, 73] takes place in most of the magnetic insulators, for example, MnO. The interaction is mediated by the magnetic coupling between the two next-neighbour cation atoms (Mn) situated at distances too far for their 3d wave functions to overlap. Thus, the exchange interactions is mediated by a non-magnetic anion (O) through the overlap of 3d and 2p wave orbital. The electrons involved in the superexchange interaction are strongly localised and its value and sign can vary depending on the cation-anion-cation bond angle and the occupancy of the d orbitals which is either the same for the cations or differs by two. According to Goodenough-Kanamori rules, [74, 75] superexchange interactions leads to an antiferromagnetic structure if a virtual electron transfer between overlapping orbitals that are each half-filled and leads to ferromagnetic structure formation if the transfer is performed between a half-filled (filled) to an empty (half-filled) orbital.
3. Double-exchange interaction [61] also takes place in the Mn-O-Mn bond alignment and differs from the superexchange interaction by the occupation of the d-orbitals and the delocalised character of the electrons involved in the interaction. The interaction is manifested in the material both by the magnetic exchange coupling as well as metallic conductivity.
4. Finally, we describe RKKY indirect exchange interaction named after Rudermann, Kittel, Kasuya and Yosida [76, 77, 78] which suggested the mechanism of the magnetic interaction. The interaction refers to the magnetic interaction of the two nuclear magnetic moments or localised inner d- or f- magnetic sites through the electronic gas of the conduction electrons (s, p). RKKY interaction takes place

over at distances beyond a few atomic spacings between the interacting spins and leads to the formation of a complex magnetic structure such as in helimagnets or spin-glass systems. Most of the rare-earth magnets have RKKY coupling.

4.2 Heisenberg Hamiltonian

The modern theory of magnetism begins with the Langevin's theory [79] explaining the Curie law [80] of magnetic susceptibility by means of local magnetic moments. Subsequently, Weiss introduced the molecular field as a notion of interaction between the atomic magnetic moments. In the frame of Langevin-Weiss [79, 81] approach was possible to describe the temperature effects observed in the ferromagnetic 3d transition metals. The theory correctly explained magnetisation behaviour observed both below and above the transition (Curie) temperature. However, despite its success, the theory failed to explain the magnitude of the molecular field within the classical description. Therefore, it became clear that the fundamental features of the magnetic exchange interactions invoke a quantum mechanical approach.

In 1928 Heisenberg [82, 83] proposed the quantum mechanical formulation of magnetic interaction. He has attributed the origin of the Weiss molecular field to the quantum mechanical exchange interaction. For the simplest case of two interacting electrons, the exchange Hamiltonian formulated by Heisenberg reads as follows:

$$\hat{H}_{ex} = -J_{12}\hat{s}_1\hat{s}_2, \tag{4.1}$$

where $\hat{s}_1$ and $\hat{s}_2$ are spin operators corresponding to electrons labelled as 1 and 2, and J_{12} is the exchange integral which characterises the relative proximity of the two interacting spins and can be estimated as:

$$J_{12} = \int\int d\tau_1 d\tau_2 \phi_1(r_1)\phi_2(r_2)\hat{H}_{ex}\phi_1(r_2)\phi_2(r_1). \tag{4.2}$$

where $\phi_1(r_1)$ and $\phi_1(r_2)$ are wave functions corresponding to electron 1 and 2, respectively. The parameter J_{12} has a short-range nature and decreases with the distance between two electrons. A positive value of J_{12} leads to the parallel spin orientation (ferromagnetic ordering) while a negative value produces an antiparallel orientation of spins (antiferromagnetic ordering).

At the earlier stages of the theory development, empirical values of the exchange interaction parameters have been calculated for a variety of ferromagnetic metals from specific heat measurements and from spin-wave

spectra. However, a fully theoretical estimation of the parameters has been one of the most challenging problems in magnetism. Early attempts to estimate exchange integrals based on model Hamiltonian approaches failed even to describe the magnetic structure in 3d systems [70]. Successful material specified parameters become possible to be estimated only during the last decades due to the recent developments of novel methods based on ab-initio calculations of the electronic structure of materials [84, 85]. One of these methods adopted for this thesis will be discussed in Chapter 5 (see section "Exchange interaction parameters").

4.3 Spin-polaron formation mechanisms; Ferron

Here we describe spin-polaron formation in the frame of the Heisenberg picture considering only the localized atomic spins in the system. We introduce an one-dimensional lattice where intersite exchange interaction J refers to the magnetic interaction between two neighbouring spins of the lattice, and J_0 is an on-site interaction which describes the on-site magnetic interaction of the spins of itinerant electrons with the localised spins of the lattice (see Fig. 4.1).

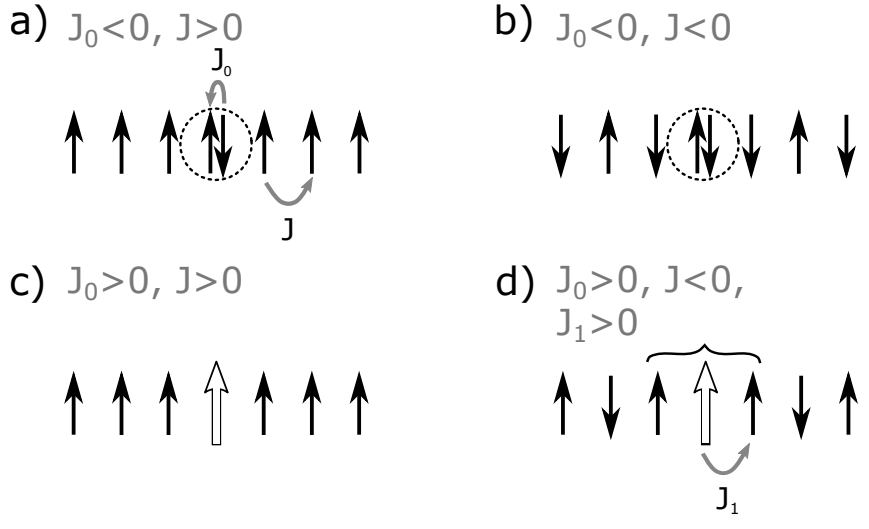

Figure 4.1. Illustration for the different type of magnetic structures stabilised due to an excess spin local magnetic interaction with the magnetic media (following named as onsite interaction). a) Exchange interaction in host is FM; the onsite interaction is AFM. b) Both exchange interaction in the host and the onsite interaction are AFM. c) Exchange interaction in the host is FM and the onsite interaction is also FM. d) Exchange interaction in the host is antiferromagnetic, however, the onsite interaction is FM. In this case a ferron-like spin-polaron forms.

A spin-polaron can occur in a variety of magnetic phases. A charge carrier strongly interacting with the magnetic subsystem affects the initial magnetic structure. Apparently, an impurity spin localised on an atomic site changes the total spin of the magnetic ion. The antiferromagnetic on-site exchange integral $J_0 < 0$, between the extra spin and spin S of the atomic shell, will lead to the diminished S-1/2 total spin. On the other hand, the ferromagnetic on-site exchange interaction $J_0 > 0$ will lead to the enhanced spin with a value of S+1/2. Therefore, in the half-filled spin chain, the AFM onsite exchange interaction between the excess spin and the host spin leads to tightly bound singlet state formation which forms a spin-hole in the spin-1/2 Heisenberg chain (Fig. 4.1 a)b)). If the onsite interaction has ferromagnetic character, a spin-polaron may form (Fig. 4.1 c)d)). In the ferromagnetic chain, spin-polaron formation does not affect the magnetic structure of the lattice. However it can be seen that in the case of an AFM lattice a spin-polaron stabilizes due to a local breaking of the magnetic order via rotation of the host spin by 180° (a spin-flip event). Ferromagnetic sign of the exchange interaction J_1 with the nearest-neighbour sites is also required. For details see (Fig. 4.1 d)). This type of the spin localisation aligns several surrounding spins in a ferromagnetic manner and in general, can result in spin-polarons with a variety of size and structure [86] (see also Paper IV of this thesis). Nagaev at first has discussed in detail this type of quasiparticle. He has introduced the corresponding term - "ferron" [68]. In materials, the ferron-like type of quasiparticle was tought to be formed by the localization of a conduction band electron (a donor-type of dopant) or a hole (an acceptor-type of dopant) in the valence band and therefore has -e or + e charge, respectively. Ferron-like spin-polaron propagates in the material as a joint entity, and above the Neel temperature, T_N collapses. Although, if the depth of the potential well created by a spin-polaron is large enough, the quasiparticle survives in the paramagnetic region as well.

Spin-polaron stability increases due to the lattice polarisation which accompanies the ferromagnetic cloud formation. In the magnetic semiconductors, strong electron interaction with optical phonons leads to co-operative spin-polaron and polarisation-polaron formation. In this case, a charge carrier trapped in the ferromagnetic region significantly polarises the surrounding lattice. The contribution of the lattice polarisation can be roughly estimated as $\frac{e^2}{\varepsilon^* R_{FM}}$, where R_{FM} is the radius of the ferromagnetic region. For certain magnetic semiconductors, the electron-lattice interaction is so significant that the contribution of the lattice polarisation energy into spin-polaron formation energy is comparable to the magnetic interaction contribution [87]. Therefore, an entangled spin-polaron and lattice polaron state forms.

4.4 Spin-polaron at finite temperature

Foremostly, a spin-polaron formation can be realized in the collective and fluctuation regimes [88]. In the collective regime, often realised at low temperatures ($T << T_N$), the maximal total spin of the spin-polaron is proportional to N, the number of the ferromagnetically coupled spins. The number of the magnetic spins, in its turn, varies depending on the parameters of the system.

In the fluctuation regime, the collective effects described above are interrupted by temperature fluctuations. In this case, a carrier adjusts its spin along the magnetic moment of the fluctuation created by the magnetic moments inside a localisation area. This adjustment is energetically favourable and has a certain lifetime. The average total spin of the spin-polaron is proportional to $\sqrt{N'}$, where N' is the number of the localised magnetic moments interacting with the carrier. It is easy to see that the relaxation of the excess spin, in this case, is much faster than the relaxation of the surrounding spins in the ferromagnetic area. Namely, in the fluctuation regime, the spin orientations are not affected by the presence of the carrier. This scenario is possible when thermal energy $k_B T$ exceeds the exchange field in the carrier localisation volume.

4.5 Langevin dynamics

An attempt to account for temperature effects in the magnetic lattice adopted in this thesis we performed using Langevin dynamics. The extended Heisenberg Hamiltonian we considered for a spin-polaron in the AFM background looks as follows:

$$\mathcal{H} = \sum_{i \neq j} |J_{ij}^{(pp)}| \mathbf{s}_i \cdot \mathbf{s}_j - \sum_{i \neq j} |J_{ij}^{(pb)}| \mathbf{s}_i \cdot \mathbf{s}_j - \sum_{i \neq j} |J_{ij}^{(bb)}| \mathbf{s}_i \cdot \mathbf{s}_j - K_{\text{ani}} \sum_i (\mathbf{s}_i \cdot \mathbf{e}_{\text{K}})^2 , \tag{4.3}$$

where $\mathbf{s}_i$ denotes the classical atomic magnetic moment on site i of the magnetic lattice. J_{ij} denote nearest-neighbour exchange parameters. Superscripts denote exchange interaction parameter between two spin-polaron sites ($J_{ij}^{(pp)}$), site of the media and spin-polaron ($J_{ij}^{(pb)}$) and two sites of the media ($J_{ij}^{(bb)}$), respectively. The direction of the anisotropy axis $\mathbf{e}_{\text{K}}$ and K_{ani} represents the parameter characterising the magnetocrystalline anisotropy. A negative value of K_{ani} corresponds to easy axis anisotropy, a positive value to easy-plane anisotropy.

The dynamics of the magnetic moments $\mathbf{s}_i$ in the magnetic system is evaluated by solving the stochastic Landau-Lifshitz-Gilbert [89, 90]

equation as:

$$\frac{\partial \mathbf{s}_i}{\partial t} = -\frac{\gamma}{1+\alpha^2}\mathbf{s}_i \times \mathbf{B}_i^{eff} - \frac{\gamma}{1+\alpha^2}\frac{\alpha}{s_i}\left[\mathbf{s}_i \times \left[\mathbf{s}_i \times \mathbf{B}_i^{eff}\right]\right], \tag{4.4}$$

where dimensionless parameter α denotes Gilbert damping and γ is the electron gyromagnetic ratio. Each atomic moment is considered to be a three dimensional vector with constant magnitude. B_i^{eff} in this equation is the local magnetic field at site i which finds as:

$$\mathbf{B}_i^{eff} = -\frac{\partial \mathcal{H}}{\partial \mathbf{s}_i} + \mathbf{b}_i(T), \tag{4.5}$$

where the first term is a partial derivative of the Eq. (4.3) with respect to moment, and therefore depends on the current magnetic configuration of the magnetic system. The second term $\mathbf{b}_i(T)$ is the stochastic field, depending on temperature and modelled as a Gaussian white noise, to account for all possible excitations. The term must fulfil the following criteria:

$$\langle b_i(t)\rangle = 0, \qquad \langle b_i(t) b_j(t')\rangle = 2D\delta_{ij}\delta(t-t'), \tag{4.6}$$

where the brackets denote averaging in time. The first criterion indicates that the time average of the stochastic field is zero. According to the second criterion, the field correlated in time $\delta(t-t')$ and in between different directions is neglected. Finally, the temperature dependent strength of this field, D can be found from the Fokker-Planck equations [91, 92] as:

$$D = \frac{\alpha}{(1+\alpha^2)}\frac{Tk_B}{s\mu_B}. \tag{4.7}$$

4.6 Spin polaron motion

As we already mentioned above, a spin-polaron is a composite object with a complex internal structure. Therefore, a realistic description of the quasiparticle and its motion has to account for perturbations in the magnetic subsystem, optical phonon excitations as well as for the magnetic and polarisation fluctuations and temperature effects. Up to now, several theoretical mechanisms have been suggested for spin-polaron motion in a magnetic lattice.

In a simplified picture, if only the spin degrees of freedom are considered in the system, a new type of magnetic polaron state named quasi-oscillatory can form [93]. A qualitative picture of the quasi-oscillatory state in an antiferromagnet is described as follows: in the case of $J_0 < 0$, onsite exchange interaction, an electron spin and spin of the atom are

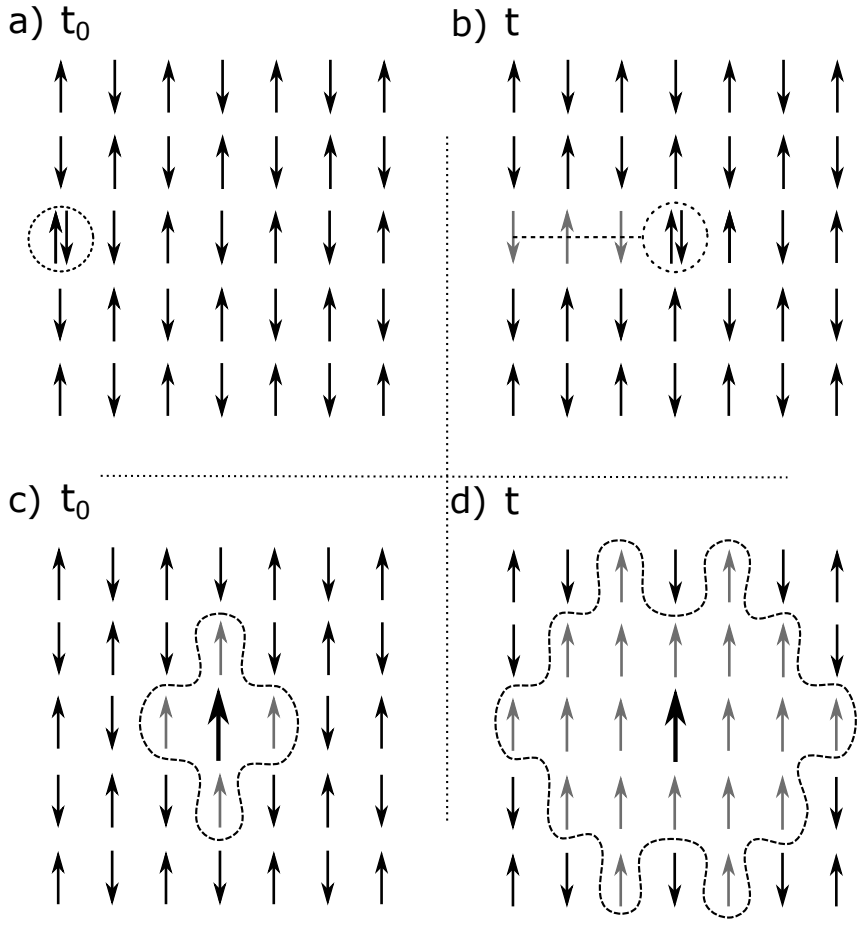

Figure 4.2. Illustration of two different mechanisms of spin-polaron propagation described in the text. a) At the initial moment, t_0 in the antiferromagnetic background a spin-hole forms. b) At the moment t spin-hole propagation leads to the formation of a string of the spin-flip states. c) Ferron-like quasiparticle formation at the initial moment t_0. d) The random walk leads to a spin-polaron with a larger radius.

antiparallel. The impurity electron localized on the initial site in this situation will create an exchange-interaction hole in the antiferromagnetic order of the host (the dashed circle in Fig. 4.2 a),b)). The electron transition from the initial site to the nearest-neighbour site will be accompanied with the spin-flip by 180°. Due to the conservation of the system total spin, the transition of the impurity electron will form a string of the spin-flip states (Fig. 4.2 b)). Each spin-flip event increases the energy of the system by $|J_1|S$, where J_1 is the lattice exchange integral and S is the total spin of the atom. Consequently, the number of spin-flip events increases as soon as the electron propagates through the lattice. Therefore the magnetic energy of the system will also increase. The reversed motion of the electron to the initial position will vanish changes incorporated by its propagation, and the system will retain the initial total energy. Therefore, the electron propagation mimics existence of a quasi-elastic force, which tends to return the electron to the initial position. The particle will perform oscillations around the initial site, and the deformation of the periodic structure will oscillate all together with the oscillating electron near its equilibrium position.

The energy of the quasi-oscillatory state can be estimated as follows:

$$U_{min} = \frac{|J_1|SR}{a}, \tag{4.8}$$

where $|J_1|S$ is the exchange energy per one spin-flip event, a is the period of the lattice, and R/a is the number of jumps that an electron performs, propagating to distance R from the initial position. Moreover, according to the uncertainty principle, the real trajectory of the electron propagation is much more complicated than we have assumed here. The simplified picture reflects the fact that the electron propagation in a limited region increases the system energy and triggers the emergence of a restoring force.

Another scenario of the electron propagation is the random walk model (electron diffusion in the lattice) [94]. According to the model, an electron performs in average $(\frac{R_{mp}}{a})^2$ jumps that increases the energy of the system by about:

$$U_{max} = |J_1|S\left(\frac{R_{mp}}{a}\right)^2. \tag{4.9}$$

Radius R_{mp}, in this case, can be referred as the radius of the magnetic polaron (Fig. 4.2 c)d)). If R_{mp} is larger than the lattice constant, the description can be continued in the frame of effective-mass approximation. A rough estimate of the spin-polaron effective mass can be obtained from the equation given by Mott and Davis [95], $m^*_{mp} = m^*_b e^{\gamma R_{mp}}$ where the numerical coefficient $\gamma \cong 1$ and m^*_b is a polaron band effective mass. Thus,

taking into account both quasi-oscillatory and diffusion mechanisms of the spin-polaron propagation the average energy due to an electron propagation $\bar{U}$ lies in the range of $U_{min} < \bar{U} < U_{max}$.

5. Polaron in the frame of Density Functional Theory

The central statement of the Density Functional Theory (DFT) is that the ground state and other properties of an electronic system can be determined from knowledge of the electron density distribution only. Seminal works applied to atoms (Tomas-Fermi model) [96, 97, 98] revealed a fundamental importance of electron density. Later Dirac [99] formulated hypothesis according to which the density function may describe atomic states within the Hartree-Fock model instead of specifying individual three-dimensional wave functions. Further, the idea developed to the theory, nowadays, mainly presented in Hohenberg-Kohn-Sham [100, 101] formulation which we consider in this chapter.

DFT applied to the correlated many-body system has driven the computational condensed matter physics and physical-chemistry to a principally new, groundbreaking level. The theory makes it possible to overcome the *exponential wall* and to calculate properties of the large, many-particle systems from the first principles. This advantages provided within the DFT formalism have a significant impact on building a microscopic theory of the polarons in solids. The theory describes polarons with high accuracy, which is remarkable given that they are quasiparticles spread in the media far beyond the characteristic lattice distance

Below we describe basic concept and models of DFT which lead out our studies of the lattice polarons presented in the next chapter.

5.1 Hohenberg - Kohn formalism

According to the Born-Oppenheimer [102] approximation, electronic and ionic degrees can be separated, in the way that the light electronic subsystem evolves in the external potential of the almost stationary, heavy nuclei. Then, the Hamiltonian describing electronic subsystem can be written as:

$$\hat{H} = \hat{T} + \hat{V}_{ext} + \hat{V}_{ee} = -\frac{\hbar^2}{2m}\sum_i \nabla_i^2 + \sum_i v(\boldsymbol{r}_i) + \frac{1}{2}\sum_{i\neq j}\frac{e^2}{|\boldsymbol{r}_i - \boldsymbol{r}_j|}, \qquad (5.1)$$

where the first term is the kinetic energy of the electrons, the second term is the external potential, and the last term corresponds to the electron-electron interaction. From the form of the Hamiltonian follows that the systems with the same number of particles N will differ from each other only by the potential interaction term. Therefore, all physical properties can be regarded as functionals of a particular, external potential. In this case the wave function can be called v-representative. Therefore, it corresponds to following Shrödinger equation:

$$(\hat{T} + \hat{V}_{ext} + \hat{V}_{ee})|\Psi[v]\rangle = E[v]|\Psi[v]\rangle, \tag{5.2}$$

where $\Psi[v]$ is the v-representative wave function of the electronic system and the total energy $E[v]$ is the expectation value of the Hamiltonian $\hat{H}$:

$$E[v] = \langle\Psi[v]|\hat{T} + \hat{V}_{ee}|\Psi[v]\rangle + \langle\Psi[v]|\hat{V}_{ext}|\Psi[v]\rangle = F[v] + \langle\Psi[v]|\hat{V}_{ext}|\Psi[v]\rangle. \tag{5.3}$$

To further evaluate the problem lets focus on the last term in Eq. (5.3). The operator $\hat{V}_{ext}$ can be defined through the external potential as:

$$\hat{V}_{ext} = \int d\tau v(\boldsymbol{r})\hat{\rho}(\boldsymbol{r}), \tag{5.4}$$

where the particle density operator is simply:

$$\hat{\rho} = \sum_{n=1}^{N} \delta(\boldsymbol{r} - \boldsymbol{r_i}). \tag{5.5}$$

Then, the expectation value of $\hat{V}_{ext}$, in general, will be defined as:

$$\langle\Psi|\hat{V}_{ext}|\Psi\rangle = \int d\tau v(\boldsymbol{r})\rho(\boldsymbol{r}), \tag{5.6}$$

where the electron density is obtained from the many-body wavefunction which in our case is the ground state function of the main Hamiltonian described in Eq. (5.1):

$$\rho(\boldsymbol{r}_1) = \langle\Psi|\hat{\rho}(\boldsymbol{r}_1)|\Psi\rangle = N \int d\tau_2 d\tau_3 \ldots d\tau_N \sum_{\sigma_1 \ldots \sigma_N} |\Psi(\boldsymbol{r}_1\sigma_1, \boldsymbol{r}_2\sigma_2 \ldots \boldsymbol{r}_N\sigma_N)|^2, \tag{5.7}$$

(the summation over the spin coordinates σ_i is performed without distinguishing spin-up and spin-down states).

Substituing Eq. (5.6) to Eq. (5.3) we obtain:

$$E[v] = F[v] + \int d\tau v(\boldsymbol{r})\rho(\boldsymbol{r}), \tag{5.8}$$

it can be seen that both the external potential and the electron density are two conjugated variables that equally contribute through the external potential to the total energy. The key idea of the Hohenberg-Kohn theory is that there is one to one correspondence between the electron density and the external potential and from the v-representative functional we can go to the ρ-representative functional. The main reason to perform this transition, as we will see further, is a possibility to describe the system using a set of one-particle equations, known as Kohn-Sham equations (see next section).

Based on the Hohenberg and Kohn [100] idea and assuming that $E[v]$ is known the Legendre transform for fixed $\rho[\boldsymbol{r}]$ will take the form:

$$F[\rho] = \inf_{v \in L^{3/2}+L^{\infty}} \left\{ E[v] - \int d\tau \rho(\boldsymbol{r}) v(\boldsymbol{r}) \right\}, \tag{5.9}$$

where, infimum is taken over the domain of v which according to Leib must belong to Banach space $L^{3/2} + L^{\infty}$ that admits decomposition of the potential into the short and long range parts. From the first-order perturbation theory follows that $\frac{\delta E}{\delta v(\boldsymbol{r})} = \rho(\boldsymbol{r})$. This automatically leads to a conjugated relation:

$$\frac{\delta F}{\delta \rho(\boldsymbol{r})} = -v(\boldsymbol{r}). \tag{5.10}$$

Now, let us consider a set of non-degenerated densities $\mathcal{M}$. According to the Hohenberg and Kohn theorem $\exists \rho \in \mathcal{M}$ that specifies a unique external potential v (to within a constant) corresponding to a unique ground state wavefunction $\Psi_0[\rho]$ (to within a phase factor). The density that minimizes the total energy while keeping external potential $v[\boldsymbol{r}]$ constant will be an exact ground state density. The general variational principle for the total energy will be obtained through the second order Legendre transform:

$$E[v] = \inf_{\rho \in \mathcal{M}} \left\{ \int d\tau \rho(\boldsymbol{r}) v(\boldsymbol{r}) + F_{HK}[\rho] \right\}, \tag{5.11}$$

where F_{HK} is a convex function and can be found as:

$$F_{HK}[\rho] = \langle \Psi[\rho] | \hat{T} + \hat{V}_{ee} | \Psi[\rho] \rangle, \tag{5.12}$$

Moreover, the ground state expectation value of an observable, $\hat{O}$, is regarded as a functional of the density:

$$O[\rho] = \langle \Psi[\rho] | \hat{O} | \Psi[\rho] \rangle. \tag{5.13}$$

For the degenerated ground state the external potential generates a linearly independent set of different ground states $\mathcal{M}'$. The expectation

value of an observable in this case, excepting the ground state total energy, will depend on a choice of the wave function and therefore the electron density from manifold $\mathcal{M}'$. This means that the ground state density, $\rho(\boldsymbol{r})$, is no longer an unique functional of the external potential $v(\boldsymbol{r})$. However, it can be proved, that the inverse mapping occur and the ground state density determines a unique external potential that has generated it. Then, the ground state energy can be found taking infimum over $\mathcal{M}'$ manifold:

$$E[v] = \inf_{n \in \mathcal{M}'} \left\{ \int d\tau \rho(\boldsymbol{r}) v(\boldsymbol{r}) + \operatorname{Tr} \hat{D}[\rho](\hat{T} + \hat{V}_{ee}) \right\}, \tag{5.14}$$

where $\hat{D}[\rho]$ is ground state density matrix with $\operatorname{Tr} \hat{D}[\rho]\hat{\rho}(\boldsymbol{r}) = \rho(\boldsymbol{r})$. The theory requires $\operatorname{Tr} \hat{D}[\rho](\hat{T} + \hat{V}_{ee})$ to be a convex function on the whole of its domain of definition.

5.2 Kohn - Sham equations

The Hohenberg-Kohn theory states that the ground state of the system is uniquely determined by the electronic density. Unfortunately, despite its conceptual beauty, the theory does not lead much ahead in solving the many-body problem since the exact form of the functional is unknown. The decisive step towards the success of the theory was achieved after Kohn and Sham [101] suggested a procedure which allows reformulating Hohenberg-Kohn theory in terms of the explicit functional of non-interacting particles.

Let us assume a system of noninteracting particles with external effective potential v_s and therefore new ground state wave function $\Phi[v_s]$. The ground state energy of the system is:

$$E_s[v_s] = \langle \Phi[v_s] | \hat{T} + \hat{V}_s | \Phi[v_s] \rangle, \tag{5.15}$$

where V_s is the potential energy functional for the system of non-interacting electrons. From this relation straightforwardly follows:

$$T_s[\rho] = \langle \Phi[v_s] | \hat{T} | \Phi[v_s] \rangle = E_s[v_s] - \int d\tau \rho(\boldsymbol{r}) v_s(\boldsymbol{r}). \tag{5.16}$$

The relation is the new Legendre transform with two following conjugated derivatives:

$$\begin{aligned} \frac{\partial E_s}{\partial v_s(\boldsymbol{r})} &= \rho(\boldsymbol{r}), \\ \frac{\partial T_s}{\partial \rho(\boldsymbol{r})} &= -v_s(\boldsymbol{r}). \end{aligned} \tag{5.17}$$

Finally assuming that $F[\rho]$ and $T_s[\rho]$ are defined on the same domain of densities, we map the system of interacting electrons to the non-interacting picture and arrive at Kohn-Sham decomposition of the initial functional in Eq. (5.12):

$$F[\rho] = T_s[\rho] + E_H[\rho] + E_{xc}[\rho], \tag{5.18}$$

where $E_H[\rho]$ term has a meaning of the Hartree energy and can be written as:

$$E_H[\rho] = \frac{1}{2}\int d\tau d\tau' \frac{\rho(\boldsymbol{r})\rho(\boldsymbol{r'})}{|\boldsymbol{r}-\boldsymbol{r'}|}. \tag{5.19}$$

$T_s[\rho]$ in Eq. (5.18) is nothing but the kinetic energy of non-interacting particles and finally $E_{xc}[\rho]$ is a new term named exchange-correlation energy. The physical meaning of this term we will discuss later. Thus, we introduced a mapping procedure of the system of interacting particles to the corresponding system of non-interacting particles which now describe a given ground state. Taking into account Eq. (5.8) and introducing all known terms in their explicit form, we obtain:

$$\begin{aligned} E[v] = -\frac{1}{2}\sum_{i=1}^{N}\int d\tau \phi_i^*(\boldsymbol{r})\nabla^2\phi_i(\boldsymbol{r}) + \int d\tau \rho(\boldsymbol{r})v(\boldsymbol{r}) + \\ \frac{e^2}{2}\int d\tau d\tau' \frac{\rho(\boldsymbol{r})\rho(\boldsymbol{r'})}{|\boldsymbol{r}-\boldsymbol{r'}|} + E_{xc}[\rho]. \end{aligned} \tag{5.20}$$

Now, if we differentiate Eq. (5.18) with respect to the density ρ we obtain following relation for the effective potential:

$$v_s(\boldsymbol{r}) = v(\boldsymbol{r}) + e^2\int d\tau' \frac{\rho(\boldsymbol{r'})}{|\boldsymbol{r}-\boldsymbol{r'}|} + v_{xc}(\boldsymbol{r}), \tag{5.21}$$

with the exchange-correlation potential:

$$v_{xc} = \frac{\delta E_{xc}}{\delta\rho(\boldsymbol{r})}. \tag{5.22}$$

The effective potential and non-interacting particle kinetic term form a set of one-particle Kohn-Sham equations. The particles described by the equation are non-interacting fermions. The Kohn-Sham wavefunction which solves eigenvalue problem is a single Slater determinant constructed from a set of orbitals that are the lowest energy solutions to:

$$(-\frac{1}{2}\nabla^2 + v(\boldsymbol{r}) + \int d\tau' \frac{\rho(\boldsymbol{r'})}{|\boldsymbol{r}-\boldsymbol{r'}|} + v_{xc})\phi_i(\boldsymbol{r}) = \epsilon_i\phi_i(\boldsymbol{r}). \tag{5.23}$$

Here, ϵ_i is the orbital energy of the corresponding Kohn-Sham orbital, ϕ_i. The density for an N-particle system, therefore, finds as:

$$\rho(\boldsymbol{r}) = \sum_{i=1}^{N} |\phi_i(\boldsymbol{r})|^2. \tag{5.24}$$

On the other hand, the exchange-correlation functional can be recast in the following form:

$$E_{xc} = \min_{\Psi \to \rho} \langle \Psi | T[\rho] + V_{ee}[\rho] | \Psi \rangle - T_s[\rho] - E_H[\rho]. \tag{5.25}$$

The exchange-correlation functional is often split into two terms as follows:

$$E_{xc} = E_x + E_c, \tag{5.26}$$

where first and second term correspond to exchange functional and a correlation functional, respectively.

5.3 Exchange correlation functionals

As we already stated, the Kohn-Sham theory highly facilitates calculations and demonstrates large perspectives for multi-atomic systems. According to the theory 3 N-degree of freedom description within the total wave function becomes reduced to a significantly more feasible problem which deals with the electron density and therefore three degrees of freedom. The theory is formally exact since it yields the exact ground state density of the real system. However, the form of the exchange-correlation functional is the most debatable subject of the theory. It carries all unknown information about the system and must be approached according to the hypothetical assumptions. Nowadays, there are plenty of different approaches for the exchange-correlation functional. A few, the most significant of them, will be discussed below.

In the simplest Local Density Approximation (LDA) [101], originally introduced by Kohn and Sham, the density is being treated locally as an uniform electron gas and therefore, the exchange-correlation energy within each volume is assumed to be:

$$E_{xc}^{LDA}[\rho] = \int d\tau \rho(\boldsymbol{r}) \epsilon_{xc}^{unif}[\rho(\boldsymbol{r})], \tag{5.27}$$

where ϵ_{xc}^{unif} is the exchange-correlation energy per particle of an uniform electron gas of density $\rho(\boldsymbol{r})$. The exchange part of the functional can be approximately determined by the Dirac functional as:

$$E_x^{LDA}[\rho] = -\frac{3}{4}(\frac{3}{\pi})^{\frac{1}{3}} \int \rho(\boldsymbol{r})^{\frac{4}{3}} dr, \tag{5.28}$$

while correlation functional $E_c^{LDA}[\rho]$ is accurately calculated using Quantum Monte Carlo method.

For the spin-polarized case, the approach is extended to the Local Spin Density Approximation (LSDA) and the functional gets the following form:

$$E_{xc}^{LSDA}[\rho_\uparrow, \rho_\downarrow] = \int d\tau \rho(\boldsymbol{r}) \epsilon_{xc}^{unif}[\rho_\uparrow(\boldsymbol{r}), \rho_\downarrow(\boldsymbol{r})]. \tag{5.29}$$

where, $\rho(\boldsymbol{r}) = \rho_\uparrow(\boldsymbol{r}) + \rho_\downarrow(\boldsymbol{r})$.

As the LDA assumes the homogeneous density everywhere in the system, it fails in situations where the density undergoes rapid changes. As a result the approach usually under-estimates the exchange energy and over-estimate the correlation energy. An improvement in this situation has been achieved by Generalized Gradient Approximation (GGA) [103, 104, 105] which considers the gradient of the electron density $\nabla\rho(\boldsymbol{r})$ within the exchange-correlation functional:

$$E_{xc}^{GGA} = \int d\tau f^{GGA}[\rho_\uparrow(\boldsymbol{r}), \rho_\downarrow(\boldsymbol{r}), |\nabla\rho_\uparrow(\boldsymbol{r})|, |\nabla\rho_\downarrow(\boldsymbol{r})|]. \tag{5.30}$$

Within the GGA, a more accurate description of the molecule geometries and lattice parameters of compounds has been achieved. It reduced the bond dissociation energy error and improved transition-state barriers. But, unlike LDA, there is no single universal form of the functional. Particularly, in our calculation, we have adopted the extremely successful parameterization for GGA functional suggested by Berdew, Burke and Ernzerhof [106].

The PBE functional incorporates the exchange and the correlation functionals:

$$E_{xc}^{PBE} = E_x^{PBE} + E_c^{PBE}. \tag{5.31}$$

The exchange functional in the PBE takes the following form:

$$E_x^{PBE}[\rho] = \int d\tau \rho(\boldsymbol{r}) \epsilon_x^{unif}(\rho) F_x^{PBE}(s) d\boldsymbol{r}, \tag{5.32}$$

with the exchange enhancement factor:

$$F_x^{PBE}(s) = 1 + \kappa - \frac{\kappa}{1 + \mu s^2/\kappa}. \tag{5.33}$$

The parameter tells how much exchange energy is enhanced over its LDA value. Here s is the dimensionless density gradient which finds as:

$$s = \frac{|\nabla\rho(\boldsymbol{r})|}{2(3\pi^2)^{\frac{1}{3}} \rho(\boldsymbol{r})^{\frac{4}{3}}}, \tag{5.34}$$

and κ and μ are numerical parameters which vary for different versions of the functional.

As for correlation functional, the PBE approach has adopted the following form:

$$E_c^{GGA}[\rho_\uparrow, \rho_\downarrow] = \int d\tau \rho[\epsilon_c^{unif}(r_s, \zeta)] + H(r_s, \zeta, t)], \tag{5.35}$$

where r_s is the local Seitz radius, $\zeta = \frac{\zeta_\uparrow - \zeta_\downarrow}{\zeta_\uparrow + \zeta_\downarrow}$ is the relative spin polarization. The following ansatz is adopted for $H(r_s, \zeta, t)$:

$$H = \frac{e^2}{a_0}\gamma\phi^3 \ln\left\{1 + \frac{\beta}{\gamma}t^2\left[\frac{1 + At^2}{1 + At^2 + A^2t^4}\right]\right\}, \tag{5.36}$$

where

$$A = \frac{\beta}{\gamma}\left[\exp\left\{-\frac{\epsilon_c^{unif} a_0}{\gamma\phi^3 e^2}\right\} - 1\right]^{-1}. \tag{5.37}$$

Here $a_0 = \frac{\hbar^2}{me^2}$ and

$$t = \frac{|\nabla\rho|}{2\phi k_s \rho}, \tag{5.38}$$

is another dimensionless gradient which is expressed through k_s, the Tomas-Fermi screening wave factor and $\phi(\zeta)$. The spin-scaling factor is written as:

$$\phi(\zeta) = \frac{(1+\zeta)^{\frac{2}{3}} + (1-\zeta)^{\frac{2}{3}}}{2}. \tag{5.39}$$

Finally, β and γ are also numerical parameters which vary their values depending on the functional version.

5.4 Projected Augmented Wave (PAW) formalism

All the electronic states are non-zero close to the nuclei, and therefore Kohn-Sham wavefunctions exhibit very sharp, oscillatory behaviour in this region. However, further out in the interstitial region where only the valence states exist, the wave functions are much smoother. Due to the features in the core region, the wave function requires a very fine grid. One way of solving this problem is the use of much smoother, effective potential (pseudopotential) which mimics existence of the collective system of nuclei and core electrons [107]. This method reduces the number of wave functions to be calculated since the KS equations are then solved

for the valence electrons only. Nowadays the idea about pseudopotentials forms the basis of a variety of effective methods employed to solve the Kohn-Sham problem.

The PAW formalism, initially proposed and implemented by Blöchl [108], advances the idea of pseudopotential allowing to calculated a smooth pseudofunction instead of the real valence wavefunction. The method can be considered as a generalization of Vanderbilt-type ultrasoft pseudopotentials [109] and the linearized augmented-plane-wave [110] method.

In the PAW method, the one electron wavefunctions $\psi_{k\nu}$ (orbitals), where $k\nu$ are k-point and band indexes, respectively, are constructed from the pseudo-orbitals $\tilde{\psi}_{k\nu}$ using the following linear transformation:

$$|\psi_{k\nu}\rangle = \left|\tilde{\psi}_{k\nu}\right\rangle + \sum_i (|\phi_i\rangle - \left|\tilde{\phi}_i\right\rangle) \left\langle \tilde{p}_i | \tilde{\psi}_{k\nu} \right\rangle, \tag{5.40}$$

where ϕ_i form partial wave basis in each PAW sphere, built upon solving the Shrödinger equation for the isolated atom. For each partial wave, the auxiliary partial wave $\tilde{\phi}_i$ is chosen. Moreover, so-called projectors $\tilde{p}_i$ are defined as dual function by using the following relation: $\left\langle \tilde{p}_i | \tilde{\phi}_i \right\rangle = \delta_{i,j}$. In interstitial region between the PAW spheres, the orbitals are constructed such way that they are identical to the exact orbitals. However, inside the spheres, the pseudo orbitals are an inaccurate approximation to the true orbitals, even not reproducing the norm of the all-electron wave function.

5.5 Hubbard-U correction

The Hubbard model is an elegant way to properly describe a large class of materials with properties that are determined by strong electronic correlations, particularly characteristic for transition elements. The transition elements which occupy three rows of the Periodic Table, extending from the alkali earth metals (Ca, Sr, Ba) with the empty d-shells to the noble metals (Cu, Ag, Au) with the fully occupied d-shells. Despite its simplicity, Hubbard model, which also accounts for on-site Coulomb interaction is a powerful tool for reproducing the main features of d-electrons which exhibit intermediate behaviour between strongly localised core electrons and free electrons in alkali metals.

Formally, the correlation energy, E_c, can be defined as the difference between the energy obtained from the Hartree-Fock approximation and the exact energy of the system, $E_c = E_{exact} - E_{HF}$. In the Hartree-Fock (HF) [111, 112] picture the electronic ground state is defined via variationally optimised single particle determinant. However, a precise description of the system with strong electronic correlations requires accounting for the full N-electron wave function together with the many-body terms of

the electronic interactions, constructed as a linear combination of multiple Slater determinants [113].

The conventional DFT also fails to describe strongly correlated electronic systems. One of the most known examples is the Mott insulators [114]. DFT predicts conducting properties for these materials what is in strict contradiction with the experimental observations. The insulating properties stem from the strong Coulomb repulsion between d-electrons. The repulsion of the electrons prevails over their kinetic energy and forces the electrons to be localised on the atomic-like orbitals. Moreover both LDA and GGA, which tend to overestimate electron delocalisation, incorrectly reproduce other physical properties of the Mott insulators, including their equilibrium crystal structure, magnetic moments, vibrational spectrum, etc. The Hubbard model naturally incorporates terms describing the electron localisation on atomic orbitals and gives better description of the material properties compare to HF approximation and conventional DFT functionals.

In the second-quantization, one-band formulation of the Hubbard Hamiltonian [115] reads as follows:

$$\hat{H} = -j \sum_{<l,m>,\sigma} (\hat{c}^{\dagger}_{l\sigma}\hat{c}_{m\sigma} + H.c.) + U \sum_{l} \hat{n}_{l\uparrow}\hat{n}_{l\downarrow}, \tag{5.41}$$

where parameter j represents the kinetic energy of the fermion hopping between nearest-neighbor sites. $\langle l,m\rangle$ denotes summation over nearest-neighbor lattice sites. The fermion with spin σ on l-th (m-th) lattice site is specified by the creation (annihilation) operator $\hat{c}^{\dagger}_{l\sigma}$ ($\hat{c}_{m\sigma}$). Parameter U denotes the potential energy arising from the on-site Coulomb repulsion and the density operator is given as $\hat{n} = \hat{c}^{\dagger}_{l\sigma}\hat{c}_{l\sigma}$.

The general expression for the total energy within LDA+U approach (the following formalism applies to other generic DFT functionals too) reads as follows [116]:

$$E^{LDA+U}[\rho^{\sigma}, \{n^{\sigma}\}] = E^{LSDA}[\rho^{\sigma}] + E^{U}[\{n^{\sigma}_{mm'}\}], \tag{5.42}$$

where ρ^{σ}, is the electronic density with spin σ (hereafter we drop dependence on spatial coordinate, so that $\rho^{\sigma} = \rho^{\sigma}(\boldsymbol{r})$) and $n^{\sigma}_{mm'}$ are the on-site atomic-orbital occupations. The Hubbard-U functional $E^{U}[\{n^{\sigma}_{mm'}\}]$ in Eq. (5.42) consists of Hubbard and so-called double counting terms which we discuss further:

$$E^{U}[\{n^{\sigma}_{mm'}\}] = E^{Hub}[\{n^{\sigma}_{mm'}\}] - E^{dc}[\{n^{\sigma}\}]. \tag{5.43}$$

The formalism is adapted in a such way that the strongly correlated electrons, usually populated on d or f orbitals, are considered in the frame of the Hubbard correction while the remaining electrons are treated within the conventional functional.

The occupation numbers are obtained by projecting the Kohn-Sham orbitals $\{\psi^\sigma\}$ onto the localised basis set of the atomic states $\{\phi\}$ as:

$$n^\sigma_{mm'} = \sum_{<k,\nu>} f_{k\nu} \langle \psi^\sigma_{k\nu} | \phi_{m'} \rangle \langle \phi_m | \psi^\sigma_{k\nu} \rangle, \tag{5.44}$$

where $f_{k\nu}$ is the occupation of the KS states with the corresponding k-points, ν-band numbers and σ spin indexes, respectively.

The screened electron-electron Coloumb interaction V_{ee} among localized atomic basis is given by the following integrals:

$$\begin{aligned} v_{ee}^{mm'',m'm'''} = \langle \phi_m, \phi_{m''} | V_{ee} | \phi_{m'}, \phi_{m'''} \rangle = \\ \int\int d\boldsymbol{r} d\boldsymbol{r'} \phi^*_m \phi_{m'} \frac{e^2}{|\boldsymbol{r} - \boldsymbol{r'}|} \phi^*_{m''} \phi_{m'''}. \end{aligned} \tag{5.45}$$

Using the notation introduced above, the Hubbard term in Eq. (5.43) in rotationally invariant formulation may be expressed as:

$$\begin{aligned} E^{Hub}[\{n^\sigma_{mm'}\}] = \frac{1}{2} \sum_{\{m\},\sigma} \{ v_{ee}^{mm'',m'm'''} n^\sigma_{mm'} n^{-\sigma}_{m''m'''} + \\ (v_{ee}^{mm'',m'm'''} - v_{ee}^{mm'',m'''m'}) n^\sigma_{mm'} n^\sigma_{m''m'''} \}. \end{aligned} \tag{5.46}$$

The double-counting term $E^{dc}[\{n^\sigma\}]$ in Eq. (5.43) is introduced in order to remove electron-electron interaction already incorporated in the $E^{LSDA}[\rho^\sigma]$ of Eq. (5.42):

$$E^{dc}[\{n^\sigma\}] = \frac{U}{2} n(n-1) - \frac{J}{2} \sum_\sigma n^\sigma (n^\sigma - 1), \tag{5.47}$$

where $n^\sigma = \sum_m n^\sigma_{mm}$ stands for the trace of occupation matrix for the localized states with spin σ and $n = \sum_\sigma n^\sigma$ represents the summation of the trace of both spins. The Eq. (5.47) contains parameter U which has the meaning of the screened Coulomb interaction:

$$U = \frac{1}{(2l+1)^2} \sum_{m,m'} v_{ee}^{mm',mm'} = F^0, \tag{5.48}$$

and the Hund exchange parameter J:

$$J = \frac{1}{2l(2l+1)} \sum_{m \neq m',m'} v_{ee}^{mm',m'm} = \frac{F^2 + F^4}{14}. \tag{5.49}$$

Basically, the simplified form of the functional, Eq. (5.42), is obtained retaining only lowest order Slater integrals F^0, at the same time neglecting higher orders, F^2, F^4 and etc. Neglecting the non-sphericity of the

electronic interactions and the differences among the couplings between parallel and anti-parallel spin electrons we arrive at the Hubbard+U approach in its simpler formulation [117]:

$$H^{Hub}[\{n^{\sigma}_{mm'}\}] = \frac{U_{eff}}{2} \sum_{\sigma} \mathrm{Tr}[\boldsymbol{n}^{\sigma}(1-\boldsymbol{n}^{\sigma})], \tag{5.50}$$

where U_{eff} is an effective value that incorporates the Coulomb interaction U and the exchange correction J as $U_{eff} = U - J$.

5.6 Self-consistent determination of Hubbard-U parameter

The appropriate Hubbard U parametrisation can be optimised on the basis of a variety of different physical properties. For example, these are ground state crystal structure [118], elastic constants [119], band-gap energy [120], valence charge distribution [121], etc.

Following, we describe one of the ways to estimate system-specified U parameter theoretically [122, 123]. This formalism stems from the idea of computing U parameter utilising constrained-density-functional calculation. In the suggested approach, a self-consistent and effective Hubbard U, is considered to be a correction of the total energy curvature with respect to the occupation of the Hubbard manifold. According to this approach, the effective Hubbard U is given by the following expression:

$$U_{eff} = \frac{d^2E[\{n\}]}{dn^2} - \frac{d^2E^{KS}[\{n\}]}{dn^2}. \tag{5.51}$$

The first term represents the total energy curvature with respect to constrained site occupation in the case of the interacting system. The curvature contains the energy cost of an electron localisation on the chosen site including all screening effects from the crystal environment. The second derivative represents the total energy curvature obtained for the non-interacting Kohn-Sham problem associated with the same system.

As it has been shown in Refs. [122, 123], the actual optimisation of the U parameter is easier to pass using a Legendre transform. After solving the Kohn-Sham equations self-consistently, we get an occupation-dependent energies:

$$\begin{aligned} E[\{\alpha_I\}] &= \min_n \left\{ E[\{n\}] + \sum_I \alpha n_I \right\}, \\ E[\{\alpha^{KS}_I\}] &= \min_n \left\{ E^{KS}[\{n\}] + \sum_I \alpha^{KS}_I n_I \right\}. \end{aligned} \tag{5.52}$$

Variation of these functionals with respect to wavefunctions show that α parameters, play role of additional potentials to the single particle term:

$$V_{tot}|\psi_{kv}^{\sigma}\rangle = V_{KS}|\psi_{kv}^{\sigma}\rangle + \alpha^{I}\sum_{m}|\phi_{m}^{I}\rangle\langle\phi_{m}^{I}|\psi_{kv}^{\sigma}\rangle \tag{5.53}$$

where localized potential shifts of strength are applied to the localized levels of associated site I. It is useful to introduce the interacting and noninteracting density response functions of the system with respect to these localized perturbations:

$$\begin{aligned} \chi_{IJ} &= \frac{\partial^2 E}{\partial\alpha_I\partial\alpha_J} = \frac{\partial n_I}{\partial\alpha_J}, \\ \chi_{IJ}^{0} &= \frac{\partial^2 E^{KS}}{\partial\alpha_I^{KS}\partial\alpha_J^{KS}} = \frac{\partial n_I}{\partial\alpha_J^{KS}}. \end{aligned} \tag{5.54}$$

The effective interaction parameter U^I associated to site I can be constructed as follows:

$$U^{I} = (\chi_{0}^{-1} - \chi^{-1})_{II}, \tag{5.55}$$

where χ^{-1} and χ_0^{-1} are inverse of the response matrixes given in Eq. (5.54). χ measures response of the system at self-consistency and χ_0 measures response accounting for the rehybridization of the electronic states upon perturbation, respectively.

5.7 Hybrid functional and Screened Coulomb potential

In the PBE functional, the many-electron exchange energy is specified by the local electron density and its derivatives. At the same time, the Hartree-Fock theory provides an exact form of the many-electron exchange energy. The accuracy of the semilocal PBE functional substantial increases by using the hybrid functional which mix the PBE exchange energy with a fraction of the nonlocal Fock exchange:

$$E_x = -\frac{e^2}{2}\sum_{\langle k,\nu\rangle\langle q,\eta\rangle} f_{k\nu}f_{q\eta}\int\int d\boldsymbol{\tau}d\boldsymbol{\tau'}\frac{\psi_{k\nu}^{*}(\boldsymbol{r})\psi_{q\eta}^{*}(\boldsymbol{r'})\psi_{k\nu}(\boldsymbol{r'})\psi_{q\eta}(\boldsymbol{r})}{|\boldsymbol{r}-\boldsymbol{r'}|}. \tag{5.56}$$

where $f_{k\nu}$ and $f_{q\eta}$ are occupational numbers corresponding to a set of one-electron Bloch states of the system $\{\psi_{k\nu}\}$.

Earlier versions of the hybrid functional [124, 125] have successfully been applied to medium sized molecules and some insulating solids with

excellent results. However, for periodic systems, which are of the main interests in solid states, the long-range nature of the Fock exchange interaction and consequently the costly computational requirements present a major difficulty for practical application. This is especially true for metallic and semiconductor systems, which often demand also a dense sampling within the Brillouin zone. Development of the hybrid functionals based on a screened Coulomb potential extended the applicability of the method to large molecules and solids.

The screened Coulomb hybrid density functional proposed by Heyd, Scuseria and Ernzerhof (HSE) [126] has been designed to produce exchange energies comparable to traditional hybrids while admixing the Fock's exchange only in the short range part. The exchange-correlation HSE functional has the following general form:

$$E_{xc}^{HSE} = aE_x^{HF,SR}(\omega) + (1-a)E_x^{PBE,SR}(\omega) + E_x^{PBE,LR}(\omega) + E_c^{PBE}. \tag{5.57}$$

The expression consists of two parameters which characterize the functional profile ω and a. The mixing coefficient a determines the magnitude of the exact exchange fraction in the short-range exchange energy, therein the screening parameter ω is employed to accomplish splitting of the full Coulomb potential $1/r$ into the short and long-range parts by means of the error function:

$$\frac{1}{r} = \frac{\mathrm{erfc}(\omega r)}{r} + \frac{\mathrm{erf}(\omega r)}{r}. \tag{5.58}$$

where $r = |\boldsymbol{r} - \boldsymbol{r'}|$. Therefore, using the decomposed Coulomb kernel the non-local Fock exchange energy in Eq. (5.57) takes the following form:

$$E_x^{SR} = -\frac{e^2}{2} \sum_{\langle k,\nu\rangle\langle q,\eta\rangle} f_{k\nu} f_{q\eta} \int\int d\boldsymbol{\tau} d\boldsymbol{\tau'} \frac{\mathrm{erfc}(\omega r)}{|\boldsymbol{r} - \boldsymbol{r'}|} \psi_{k\nu}^*(\boldsymbol{r}) \psi_{q\eta}^*(\boldsymbol{r'}) \psi_{k\nu}(\boldsymbol{r'}) \psi_{q\eta}(\boldsymbol{r}). \tag{5.59}$$

The family of HSE hybrid functionals have two remarkable limits. When $\omega = 0$ the functional is equivalent to PBE0 [127] functional and otherwise for $\omega \to \infty$ the hybrid functional asymptotically converges to standard PBE. Empirically, it has been found that the satisfactory description of bulk systems can be achieved for $\omega = 0.1 - 0.25$ [128]. Although, for the best of our knowledge a variation of ω and a parameters can be employed in order to validate the model for a certain material since the space of parameter values, for different materials, has been explored only sparsely. For the validation procedure, a variety of experimental parameters can be used such as lattice parameter, vacancy formation energies, as well as the band gap.

5.8 Exchange interaction parameters

Nowadays, there are several methods to estimate exchange interaction parameters within the quantum mechanical description of the solids. In this thesis, the material dependent exchange interaction parameters are extracted with employment of DFT+DMFT theory [129, 130].

First, to define the local set of electronic orbitals $|i,\xi,\sigma\rangle$, the electronic structure problem is solved. Here i refers to the number of the atomic site in the crystal and indicates the lattice vector R_i that uniquely points to a given ion. Moreover, ξ denotes the orbital degree and σ is the spin index with obtained $\{\uparrow\downarrow\}$ values, respectively. A generalised expression for the intersite exchange is formulated as follows:

$$J_{ij} = \frac{T}{4}\sum_{n}\left[\hat{\Delta}_i(i\omega_n)\hat{G}^{\uparrow}_{ij}(i\omega_n)\hat{\Delta}_j(i\omega_n)\hat{G}^{\downarrow}_{ji}(i\omega_n)\right], \tag{5.60}$$

where i and j are atomic sites of the interacting particles, T is the temperature, $\omega_n = 2\pi T(n+1)$ refers to n-th fermionic Matsubara frequency. Trace in the expression (5.60) is intended over the orbital degrees. $\hat{G}^{\sigma}_{ij}$ refers the intersite Green's function projected over spin σ. Finally, the term $\hat{\Delta}_i$ can be expressed as:

$$\hat{\Delta}_i(i\omega_n) = \hat{H}^{i\uparrow}_{KS} + \hat{\Sigma}^{\uparrow}_i(i\omega_n) - \hat{H}^{i\downarrow}_{KS} - \hat{\Sigma}^{\downarrow}_i(i\omega_n). \tag{5.61}$$

It has a meaning of the exchange splitting at the i-th site, estimated as a difference between the spin- and site-projected Kohn-Sham Hamiltonian $\hat{H}_{KS}$ and local self-energy $\hat{\Sigma}_i$ for spin-up and spin-down cases, respectively.

6. Results of numerical polaron modeling

During the last decade, a significant number of studies were published reporting the first principle calculations of polarons in different materials. For instance, both electron and hole polarons have been described in pure and doped compounds such as cerium dioxide [131, 132], rutile [11, 133], perovskites [121], hematite [134], hafnium dioxide [135, 136], lithium iron phosphate [137], cuprate superconductors [138], lithium peroxide, lithium carbonate [139, 140] and many more. The common conclusion of all these studies is that in order to correctly reproduce the charge localization associated with polaron formation one needs to use methods going beyond the standard density functional theory (DFT), such as DFT+U [11, 133, 137, 141], SIC [141], hybrid functionals [140, 141] or dynamic mean field theory (DMFT) [142]. Below, we present the results for a different type of polarons obtained using DFT+U and Hybrid functional methods.

6.1 Standard procedure of the polaron state localization in DFT

An extra electron (hole) in the ionic crystal or a polar semiconductor may induce a polaron formation. Usually, en extra charge can be incorporated via a defect, doping or creation of a vacancy. This process can be illustrated by considering a bivalent metal oxide MeO in the frame of the ionic bonding model. In the ideal MeO lattice, a metallic ion is in Me^{+2} ionic state. An oxygen vacancy in the compound will create two unpaired electrons adjacent to two Me atoms surrounding the vacancy so that each of the two Me atoms accompanying the defect will obtain one unbounded extra charges and become Me^{+1}. A similar situation applies to Me vacancy formation which will result with two O^{-1} oxidation states. The extra electrons on metallic sites interacting with the lattice form a bound lattice polaron (localised solution). The insufficiency of the charge on oxygen ions will lead to a hole polaron formation.

It is rarely possible to reproduce localised solutions within standard DFT theory. For this type of density configuration, both the LDA and GGA fail due to the self-interaction errors inherent in typical exchange-correlation functionals. For the case of a metal vacancy in a MeO oxide, the functional will lead to two unpaired electrons being spread across

several sites (delocalized solution). Interestingly, Hartree-Fock (HF) theory oppositely overestimates polaronic hole localisation. Therefore, both LDA/GGA and HF cannot be considered as theories adequately describing polaron states in solids.

Much success towards solving this problem has been obtained applying theoretical methods beyond DFT. Lany and Zunger [143] have well illustrated the opposite biases, which standard LDA functional and HF theory exhibit, by analysing curvatures of the total energy E as a function of the fractional occupation number n. They found that for HF theory $d^2E/dn^2 < 0$ and for LDA functional, due to residual self-interaction, $d^2E/dn^2 > 0$. In the ideal, unbiased case the energy has to be a linear function of occupation number and therefore $d^2E/dn^2 = 0$. Moreover, authors have formulated the condition to be fulfilled as:

$$\begin{aligned} E(N+1) - E(N) &= e_i(N); \\ \Pi_i + \Sigma_i &= 0. \end{aligned} \tag{6.1}$$

where $e_i(N)$ is the energy before electron addition to the system, Π_i indicates the self-interaction energy after electron addition to the orbital i, Σ_i is the energy contribution arising due to wave-function relaxation, respectively. In order to satisfy this relation, they have introduced a potential operator that acts on empty hole states but vanishes for the normally occupied states. Within DFT+U approach, similarly to the method proposed by Lany and Zunger, the self-interaction error is also being corrected. Hybrid functionals improve the description of the wavefunction as well, combining nonlocal Fock exchange term with conventional DFT functional. Thus, disadvantages provided within LDA/GGA and HF for polaronic calculations can be neglected using the proper choice of U parameter and ω-a parametrisation.

Beyond DFT approaches provided for the electron density calculation do not always guarantee localizations at specific sites. To the best of our knowledge, the correct initial geometry is another crucial factor which controls electron localization or delocalization. Electron and hole polarons in semiconductors tend to affect the bond lengths near the polaronic site. Therefore, a correct initial geometry with justified bond lengths may help to localize the charge. On the other hand, an artificial wavefunction with an excess electron or hole at specific sites may also be helpful at the beginning of the modelling.

To obtain the results presented in this thesis, we have used a variety of the methods in order to localize electrons at specific sites. We have noticed that the procedures described above may not always give the localized solutions that are expected. In some cases, to achieve a satisfactory result, it is worthy to try different technics (varying U and (ω, a) values, stretched bond lengths around polaronic sites, justified initial geometry, applying U-ramping method [144], etc.).

6.2 Hole bipolarons in MgO

In alkaline earth oxides, hole polarons can form when cation vacancies, also called V-centres, or aliovalent impurities are present [145]. According to both experiment [146, 147, 148, 149] and theory [150, 151], formation of a cation vacancy in these oxides is accompanied by hole localization in an $O^1 - O^1$ bipolaronic configuration, namely at two oxygen atoms on opposite sides of the cation vacancy, as illustrated in Fig. 6.1 a).

The localised holes possess local magnetic moments, which could be either parallel (triplet state) or antiparallel (singlet state) to each other. Some experiments showed the triplet (S=1) to be the ground state for MgO [148, 152] whereas others did not confirm it [146]. These investigations showed that neutral vacancies (V^0) were not primarily stable in bulk oxides. These defects easily trap electrons from surrounding media and collapse into more stable V^- or V^{2-} configurations. Using photoluminescence and positron annihilation spectroscopy, the concentration of Mg vacancies was found to decrease with increasing particle size accompanied by a decrease in the saturation magnetisation of the samples, with defects mostly found at the surface of the nanocrystalline [152]. The existence of a local magnetic moment in these structures allowed one to consider MgO as a strong candidate for the so-called d^0 magnets [153], a fascinating class of magnetic materials containing no d- or f-shell atoms.

As mentioned above, in order to reproduce the hole configuration one needs to use methods going beyond conventional local and semi-local approximations of DFT [141]. Moreover, the key factor leading to the formation of a localized state is the local lattice distortion around the atoms where holes localize [141], thus demonstrating the paramount importance of charge-lattice interaction for the polaron formation. This distortion is reproduced neither by LDA nor GGA; both functionals result in the metallic state for MgO [141, 154, 155].

In the following, we describe electronic structure calculation for the two-centre $O^1 - O^1$ hole-bipolaron bound to a cation vacancy in MgO calculated using a hybrid functional (HSE06, a = 0.25 and $\omega = 0.2$) employing the projector augmented wave method [108] and the PBE parametrization [106] of the exchange-correlation interaction. Calculated DOS curves show that the bipolaronic character of hole localization, associated with a cation vacancy. The hole states are 0.42 eV above the top of the valence band (see Fig 6.1 a)) and the obtained equilibrium magnetic configuration is the triplet, which is 11 meV lower in energy than the singlet state. We noticed that the magnetic moments obtained in the HSE06 calculations with a=0.25 are smaller than those from the DFT+U calculations for U_{eff}=10 eV. We find that they are directly affected by the value of the HF admixing parameter a. The calculations show that the on-site magnetic moment steadily increases with increasing HF con-

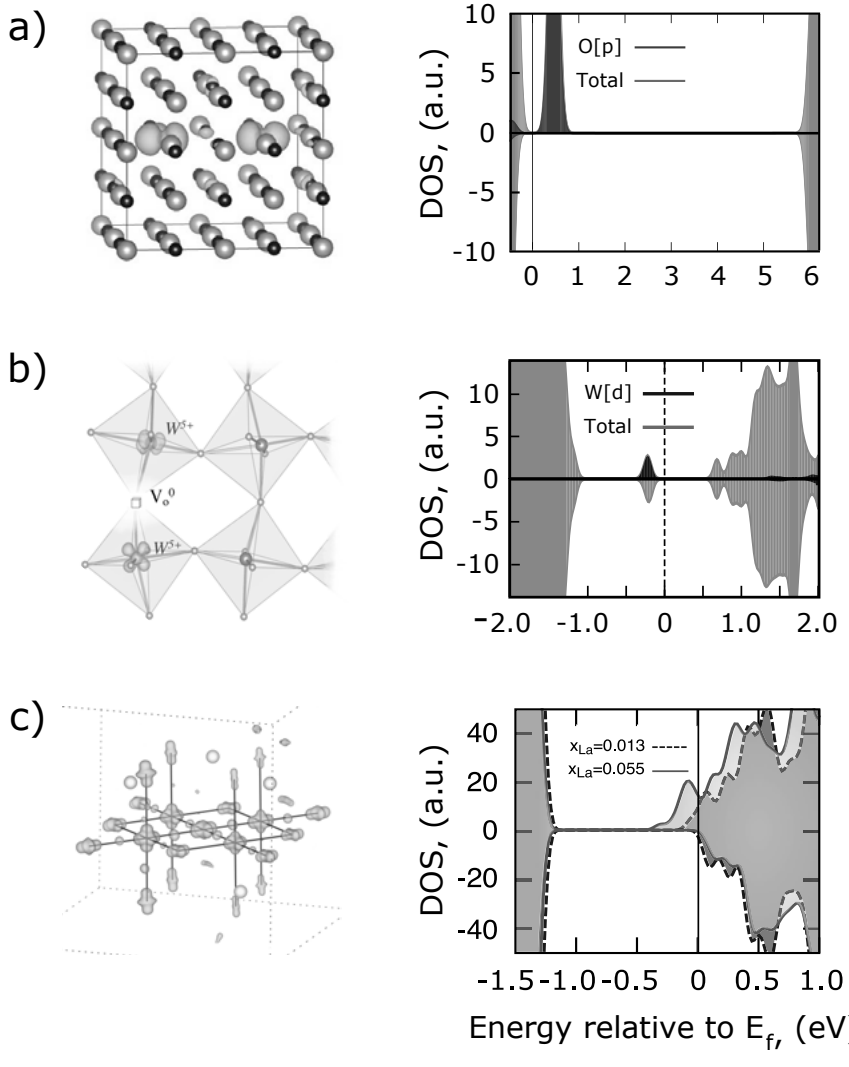

Figure 6.1. Different type of polaron states calculated in the framework of DFT+U and HSE approximations. The left panel shows localised partial charge densities of the polaron mid-gap state in a) and b) and in the vicinity of the Fermi level c). The right panel presents the corresponding density of states. a) Hole-bipolaron bound to a cation vacancy in MgO obtained via HSE06 functional. Each polaron corresponding to bipolaron is situated on the oxygen atoms surrounding the vacancy. b) Electron bipolaron along the [100] direction in $\gamma - WO_3$. Polarons are localised on tungsten d states. c) 21-site spin-polaron in La-doped $CaMnO_3$. Polaron density is spread over 21 Mn sites. b) and c) calculations are done using by DFT+U with U parameterisation optimised in the frame of linear response theory.

tribution reaching 0.77 μ_B. The increase of the a parameter shifts empty hole p-states up in the band gap, which, in turn, increases the width. For example, the values for the band gap obtained in these calculations with a=0.25 change from 5.82 eV to 7.52 eV for a = 0.5.

A comparison with calculations using DFT+U approximation shows that the band gap for MgO obtained with U_{eff}=10 eV is 4.8 eV (data not shown here) as compared to the experimental value of 7.672 eV [156], showing the typical underestimation of the band-gap of DFT based calculations. The separation between the unoccupied hole states and the top of the valence band is 1.7 eV. Hence it seems that both DFT+U and HSE methods produce localized hole solutions with a similar degree of localization in agreement with previous results [141].

We also find that holes prefer to localise in $O^1 - O^1$ bipolaron configurations. Although, one-centre $O^2 - O^0$ bipolaron (further called monopolaron), where two holes localise at the p-orbitals of the same oxygen atom are found to be metastable. The monopolaron is not the ground state and could have a rather high energy. In order to stabilise it, we take advantage of the fact that the deformation pattern around the localised charge is of paramount importance for the polaron stabilisation. To prepare the initial guess for the local atomic configuration around the monopolaron, we introduced a lattice distortion into the unit cell around one of the oxygens neighbouring the cation vacancy, and we obtained a metastable local energy minimum. The unit cell was then fully relaxed. After the relaxation, we obtained a metastable $O^2 - O^0$ polaronic configuration. The two-centre solution $O^1 - O^1$ compared to $O^2 - O^0$ bipolaron configuration is favourable by about 2 eV. Therefore, we found that the existence of both polaronic configurations in MgO could be possible.

The results of Sections 6.1 and 6.2 form the basis for the results of Paper II.

6.3 Electron polarons in oxygen-deficient $\gamma - WO_3$

Tungsten trioxide is a wide band-gap semiconductor (2.6-3.0 eV [157, 158, 159]) with perovskite-like structure. The oxide shows rich structural polymorphism [160, 161, 162], whereby oxygen octahedrons surrounding tungsten atoms vary their orientations and shape depending both on temperature and pressure. Usually, at room temperature both δ-WO_3 (triclinic $P1$ 233-290 K) and γ-WO_3 (monoclinic $P2_1/n$ 290-350 K) phases coexist [163]. Depending on the method of preparation, the samples can be characterized by various γ/δ ratios, micro-structure and defectiveness. Under certain conditions, a more exotic hexagonal h-WO_3 phase [164, 165] or amorphous a-WO_3 [166] phase can form. The structural

variety of WO_3 offers a range of optical characteristics that is important for applications relying on light absorption [167, 168, 169].

The presence of different localised charge states in WO_3 has been confirmed by numerous experiments [170, 171, 172]. The formation of polarons in this oxide has also been studied theoretically by semi-empirical models [133, 173] and more recently by ab-initio methods employing hybrid functionals [154]. More studies of the electronic and structural properties of perfect and defective WO_3 can be found in Refs. [174, 175, 176].

In the following, we present calculated bipolaron state in defective γ-WO_3 phase. In the defective oxide (with one oxygen vacancy), a bipolaron can form at the d-states of each of the two tungsten W^{5+} atoms surrounding an oxygen vacancy in the same manner as it is described for hole-polarons in MgO above.

For the calculations reported below, we have employed DFT+U functional. Moreover, to properly model small polarons in the compound, we have modelled the lattice distortions around the polaronic sites naturally supporting polaron localization [137, 141, 177, 178]. We considered an oxygen vacancy with two unpaired electrons localized on both sides of the vacancy in the $W^{5+} - W^{5+}$ configuration. Within the DFT+U_W approach, we varied U_W applied to tungsten d-states from 2 to 12 eV. We analysed the localisation patterns for different values and found that for U_{eff} = 8 eV and higher values almost precisely one electron was localised at the d-orbitals of each of the two W^{5+} tungsten atoms. The local magnetic moment for each W in this case was 0.96 μ_B. Next, we performed calculations using DFT+ U_W, U_O. The U values (U_{Op} = 9 eV and U_{Wd} = 6 eV) were determined using the linear response procedure described in Section 5.6. In this case, the local magnetic moment due to the electron localisation at the W_d-states were 0.86 μ_B.

The density of states (DOSs) obtained in the DFT+U_W, DFT+U_W,U_O show the following. The band gaps are expectedly underestimated by both versions of the DFT+U calculations: E_g (DFT+U_W) = 1.43 eV (data is not shown), E_g (DFT+U_W, U_O) = 1.64 eV (Fig 6.1 b)) that should be compared to the experimental value of 2.8 eV [179].

In the case of DFT+U_W, the localized polaronic d-states are situated at the upper edge of the valence band (data is not shown) whereas, for DFT+U_W, U_O the states situated 0.8 eV above the top of the valence band (Fig 6.1 b)). We notice that the position of the polaronic peak in the gap obtained by DFT+U_W, U_O is in good agreement with HSE06 and previously reported B3LYP results [180]. We found that in the case of DFT+U_W ,U_O the antiferromagnetic coupling of local spins is favoured over the ferromagnetic one by about 20 meV. Using DFT+U_W, U_O we also examined $DOSs$ calculated for Li-WO_3 and found them to be very similar to those calculated for the vacancy case. The only noticeable dif-

ference was a 40 meV shift of the polaronic peak down in energy. Further results of this study are also reported in Paper III of this thesis.

6.4 Spin-polarons in La-doped $CaMnO_3$

Perovskite $CaMnO_3$-$LaMnO_3$ (CMO-LMO) system exhibits an outstandingly rich magnetic and structural polymorphism [181]. $CaMnO_3$ (CMO) is an orthorhombic (Pnma) semiconductor with the band gap of 3.07 eV [182]. Its magnetic ground state is the G-type antiferromagnetic (G-AFM) structure, where each spin-up (down) atom is surrounded by 6 spin-down (up) atoms. Such a magnetic ordering is thought to be governed by the super-exchange interaction along the $Mn^{4+}(t_{2g}^3)\uparrow - O(p) - Mn^{4+}(t_{2g}^3)\downarrow$ bond chains [71]. When trivalent La^{3+} substitute atoms in the Ca^{2+} sublattice, extra valence electrons are added to the system. This extra charge can be redistributed among a large number of atoms or fully (partially) localized at the d-orbitals of particular Mn atoms driving the double-exchange interaction in the mixed-valence $Mn^{3+}(e_g^1)\uparrow - O(p) - Mn^{4+}(t_{2g}^3)\uparrow$ bond alignment [61]. The Hund coupling may then assist the spin flip at the central site of the magnetic octahedron [183], thus forming a ferromagnetic (FM) 7-site droplet or the so-called 7-site spin-polaron (SP). Such 7-site SPs can be joined together in different configurations forming larger FM droplets, for example, involving 12-, 17- or 21-sites [86]. Unlike lattice polarons, where an electron is trapped due to a strong electron-lattice interaction, spin polarons are thought to form largely due to magnetic interaction [26, 88]. However, cooperative spin-charge-lattice effects are also important for SPs as the formation of the $Mn^{3+}(e_g^1)$ state leads to the symmetry breaking by Jahn-Teller distortions becoming more pronounced as the number of Mn^{3+} ions increase. At a critical concentration, the accumulated lattice deformation energy drives the magnetic transition to the C-type antiferromagnetic (C-AFM) state, which in *La*-doped $CaMnO_3$ is accompanied by the structural transition from Pnma orthorhombic to the P_1/m monoclinic structure [86, 181, 184].

In our study, we used the DFT+U approach, employing the PAW method [108] and the PBE parametrization [106] of the exchange-correlation interaction. The choice of the Hubbard U parameter is always an important issue in the calculations of complex oxides. Here we estimated the effective U parameter (U_{eff}=U-J [117]) using the linear response method developed by Cococcioni [122], which depending on the choice of the basis set, resulted in U_{eff} (Mn_{3d}) in the range of 3.45-4.23 eV. For our calculations, however, we utilized the rotationally invariant approach [116]. This approach was shown to be more appropriate for the descrip-

tion of complex magnetic structures [123]. We used J = 0.9 eV, which is the most common value applied for this class of compounds [185].

In Fig 6.1 c), we show the density of states (DOS) we obtained for the 21-sites SPs formed in G-AFM matrix for two La concentrations. The excess electrons, donated by La, occupy the states in the shoulder near the Fermi level, which is hardly visible for x_{La}=0.013 but becomes more evident as the La concentration increases as shown in Fig 6.1 c). This shoulder consists of the e_g-states and the partial charge distribution shows that these e_g states are mostly localized at the SP sites and have $3z^2 - r^2, x^2 - y^2$ character. We also found that somewhat larger degree of the $Mn(e_g^1) - O(p)$ hybridization is observed in the double-exchange active (101) plane as compared to the others. We have also performed hybrid functional calculations (HSE06) [126, 186] of the 7-site SP configuration and obtained the very similar character of DOSs to the ones shown in Fig 6.1 c). Moreover, we have checked the significance of the spin-orbit coupling for the description of the magnetic structures in $La_xCa_{1-x}MnO_3$. We found that it has only a minor influence lowering the total energies of the considered SPs by about $10-15\%$. More results of this study can be found in Paper IV of this thesis.

7. On polaron mobility

Usually, the rate equation for polaron hopping both in the adiabatic and non-adiabatic regimes manifests an exponential type of temperature-dependence. When the probabilities to occupy the initial and the final states are equal each other, the site-to-site hopping can be described by the Arrhenius type of equation. It means that the atomic displacements that affect the electronic configurations along the transition path are in coincidence at the moment of a career jump. In the adiabatic case, the carrier moves rapidly enough to adapt to the relevant atomic motions. However, in the non-adiabatic regime, the carrier is unable to follow such atomic motion. Nonetheless, the hoping process in the non-adiabatic regime which is mainly controlled by the electron tunnelling processes, shifts to the adiabatic regime as soon as the temperature of the system increases. Thus, both the lattice configuration and electron-lattice cooperative effects manifest their key role in polaron transport properties.

Below we discuss different theoretical models of the propagating polaron and describe our modelling of polaron motion in a crystal. The results are obtained including methods presented in Chapter 4 and Chapter 5 of this thesis.

7.1 Adiabatic rate transition for the phonon assisted hopping

The hoping process of electrons can be illustrated by a family of trajectories curved on the potential energy profile plotted as a function of relative atomic displacements, (see Fig 7.1). It can be seen that there are two potential wells which correspond to the initial $-n$ and the final n sites, respectively. The lower and upper adiabatic potentials describe trajectories which the carrier follows moving from one well to the other well. There are a few possibilities for the carrier to move [187, 188]. In the non-adiabatic regime, the carrier performs a transition from the lowest to the upper adiabatic potential along the path shown by the dashed line in Fig. 7.1. A carrier makes there finite number of oscillations and then moves down to the next potential well. Therefore, even if the non-adiabatic jump is predominant, a hoping process includes some adiabatic passages. Another possibility for a career is to jump immediately to the upper adiabatic potential absorbing a photon with energy $\hbar\omega \geq E_b$, where

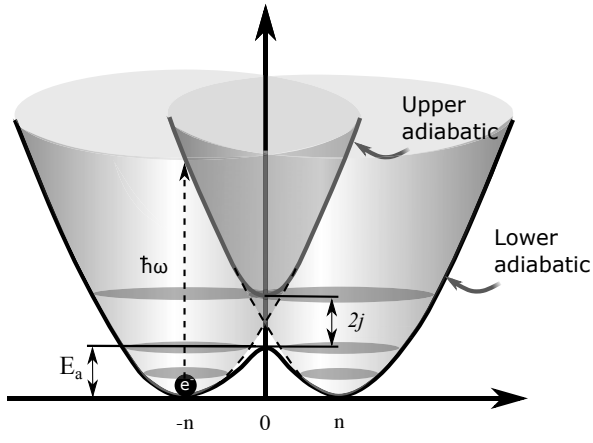

Figure 7.1. Schematic explanation of a small polaron propagation from "-n" to "n" position in the anharmonic potential within the adiabatic and non-adiabatic limit. The lower adiabatic and upper adiabatic potentials are shown by solid curves versus relative atomic displacements. E_a is the activation energy at the coincidence point ("0" coordinate) for the adiabatic hopping along the low adiabatic trajectory. With dashed lines, we show polaron trajectory in the non-adiabatic regime (see also text).

E_b is the energy of electron binding to the potential well in the lattice (discussed previously in Section 2.1). In the case when the hopping is activated by the interaction with a phonon the carrier is following the lowest adiabatic potential which is strongly anharmonic in the vicinity of its maximum. In Fig. 7.1, E_a represents the transition activation energy and can be expressed as: $E_a = \frac{1}{2}E_b - j$ [187, 188], where j possess the value equal to a half of the splitting between the two adiabatic potentials at the coincidence point (denoted by "0" in Fig 7.1).

The small polaron jump rate in the adiabatic regime refers to the Arrhenius type of equation given in the following form:

$$R_{ad} = \nu e^{\frac{-E_a}{k_B T}}, \tag{7.1}$$

where ν is a representative atomic vibration frequency. Usually, Eq. (7.1) satisfactorily describes high temperature ($T > \frac{\theta_D}{2}$) regime of a small polaron hopping in solid. However, in certain cases, adiabatic polaron hopping can manifest more complex behaviour. For example, a shift of the stiffness of the atomic vibrations accompanying polaron hopping brings an important contribution which has to be accounted for. The effects can be described using Emin-Holstein dimensional theory [189, 190, 191] developed for a polaron moving in the adiabatic regime as we show below.

The free energy associated with a carrier which occupies an initial position at "-n" is denoted as F_{-n} and express by the following polynomials:

$$F_{-n} = (\frac{T_e}{R_{-n}^2} - \frac{V_s}{R_{-n}^3} - \frac{V_l}{R_{-n}}) + f_{-n}, \tag{7.2}$$

where T_e is the coefficient characterising the carrier's kinetic energy contribution, V_l is a parameter describing the long-range electron-phonon interaction and V_s the short-range electron-phonon interaction, respectively. R_{-n} is the characteristic dimensionless radius of a polaron at the ground state. The last term in this expression, f_{-n}, denotes contribution of the atomic harmonic vibrations associated with the polaron formation.

At the coincidence point, a relation for the free energy in the case of a three-dimensional media can be written as [191, 192]:

$$F_0 = \frac{T_e}{R_0^2} - \frac{V_s}{2R_0^3} - \frac{V_l}{2}(\frac{1}{R_0} + \frac{1}{\sqrt{R_0^2 + d^2}}) + f_0, \tag{7.3}$$

where R_0 is a dimensionless characteristic radius of a polaron at the coincidence moment, $d = 2n$ is a dimensionless separation between the two centroids associated to the initial and final sites. f_0 denotes the vibrational free energy of atoms with configuration at the coincidence point.

Under the assumption that $R_{-n} = R_0$ and introducing the following relation:

$$E_a = \frac{V_s}{2R_0^3} + \frac{V_l}{2}\left(\frac{1}{R_0} - \frac{1}{\sqrt{R_0^2 + d^2}}\right), \tag{7.4}$$

the difference of the free energies for the initial configuration and at the coincidence point, reads as: $F_{-n} - F_0 = -E_a + (f_{-n} - f_0)$. Then, an expression for the polaron hopping rate can be rewritten in the following form:

$$R_{ad} = \nu \exp\left(\frac{f_{-n} - f_0}{k_B T}\right) \exp\left(\frac{-E_a}{k_B T}\right). \tag{7.5}$$

In Ref. [191] Emin has shown that the exponential pre-factor in Eq. (7.5) can be expressed as:

$$\frac{f_{-n} - f_0}{k_B T} = \frac{E_a}{\Delta_0}, \tag{7.6}$$

where Δ_0 is the electronic intersite transfer energy at the coincidence point. The physical meaning of Eq. (7.6) refers to the carrier motion induced softening processes. The effects arise due to the intersite motion

of a charge carrier which reduces the stiffness of the associated atomic vibrations. Substituting Eq. (7.6) into Eq. (7.5) yields the adiabatic jump rate in the so-called weak dispersion model:

$$R_{ad}^{w} = \nu exp\left(\frac{E_a}{\Delta_0}\right) exp\left(\frac{-E_a}{k_B T}\right), \tag{7.7}$$

which in the limit of $\Delta_0 \to \infty$ yields the adiabatic regime given by Eq. (7.1).

As for the spin-polaron hopping processes its hopping rate is usually estimated under the assumption that both lattice and magnetic degrees of freedom are contributing independently to the probability of the hopping event. Thus, the spin-lattice coupling effects are assumed to be neglectable, and the spin and lattice degree are factorised according to the following expression:

$$R = f_{mag} f_{lat} e^{-E_a/k_B T}, \tag{7.8}$$

where E_a is accounting for both contributions from the spin and the lattice perturbation, so that $E_a = E_{lat} + E_{mag}$. Moreover, f_{mag} and f_{lat} denote the magnetic and lattice pre-factors, respectively. The one-electron tight-binding approach leads to the following magnetic prefactor [193, 194]:

$$f_{mag} = 0.25\,\mathrm{sech}\left(\frac{T_N}{T}\right) e^{-\frac{k_B T_N^2}{4E_a T}}. \tag{7.9}$$

for the small polaron in the case of an AFM lattice. In Eq. (7.9) T_N is the Neel temperature [80].

7.2 Lattice-polaron hopping barriers in the frame of DFT

The following procedure can represent the polaron transfer process calculated within the ab-initio formalism. Obviously, at the very beginning, one needs to reproduce polaronic states localized in the compound. Particularly, as we have shown in Fig. 6.1, the polaron state appears localised in reciprocal space as a mid-gap state in the density of states. At the same time, the polaron localisation can be indicated in a real space. For example, the corresponding partial charge density of the mid-gap state appears as the onsite localised orbital. The first step in the polaron transition modelling is reproducing charge localisation at the initial and final sites of the polaron transition path. This can be achieved using methodologies described in Chapter 6.

Usually, the transition barriers grow as the length of the transition path increases. In order to estimate the transition state between the initial and final states, we assume that a polaron behaves according to the rules formulated for the small adiabatic polaron transfer. Indeed, according to this model, a polaron has to overcome a certain energy barrier corresponding to the coincidence point between the initial and final potential wells on the potential surface.

Further, we present the calculated energies for the hole bipolaron-to-monopolaron transition in MgO (see Fig. 7.2). The bipolaron and monopolaron states, considered here are equivalent to two-center and one-center bipolarons. The transition we modelled in the linear approximation, which roughly estimates the energy barriers for hole migration using the set of cell configurations obtained with the linear interpolation procedure [11, 139].

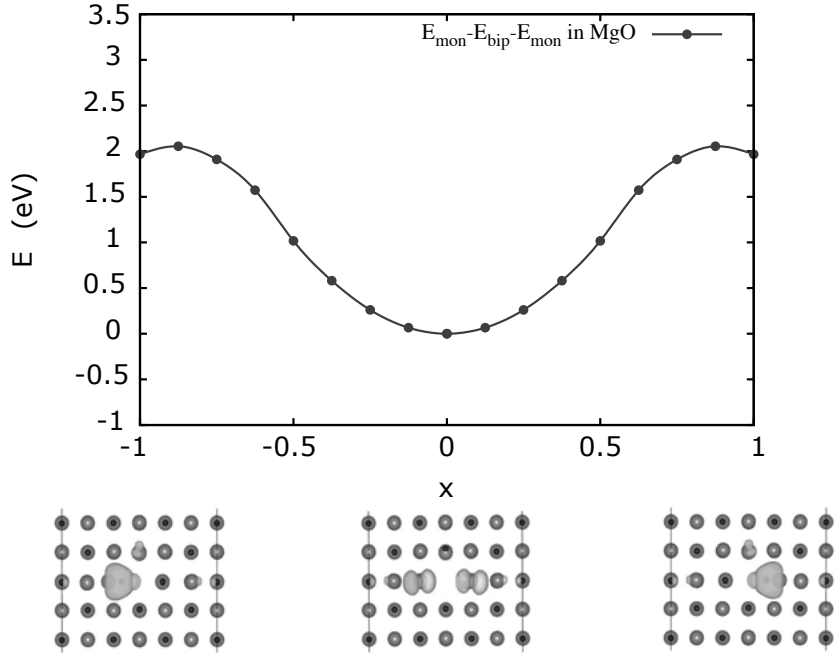

Figure 7.2. a) Monopolaron-Bipolaron-Monopolaron transition estimated in the linear approximation (see Eq. (7.10)) in pure oxides. Initial and final configurations are equivalent due to symmetry (x = -1 and x=1). We choose to shift all energies in such a way that $E_{bip}^{MgO} = 0$.

Each atomic coordinate is specified with a parameter q, and a given set of atomic coordinates is then specified by $\sum q^p$. The linear interpolation scheme along the transition path between different polaronic configura-

tions can then be written as follows:

$$\begin{aligned} \sum q^p &= -x\sum q^{m1} + (1+x)\sum q^b, \quad -1 < x < 0; \\ \sum q^p &= (1-x)\sum q^b + x\sum q^{m2}, \quad 0 < x < 1. \end{aligned} \tag{7.10}$$

The initial configuration of the transition expressed in Eq. (7.10) is the monopolaron configuration $O^2 - O^0$, where two holes are located on the first oxygen atom, which corresponds to the bipolaronic ligand accompanying the vacancy (denoted as m1 configuration, see also picture underlying Fig. 7.2). The configuration $O^1 - O^1$ is denoted as b and, finally, monopolaron configuration $O^0 - O^2$, where the both holes are localized on the second oxygen atom is denoted as m2. The resulting energies

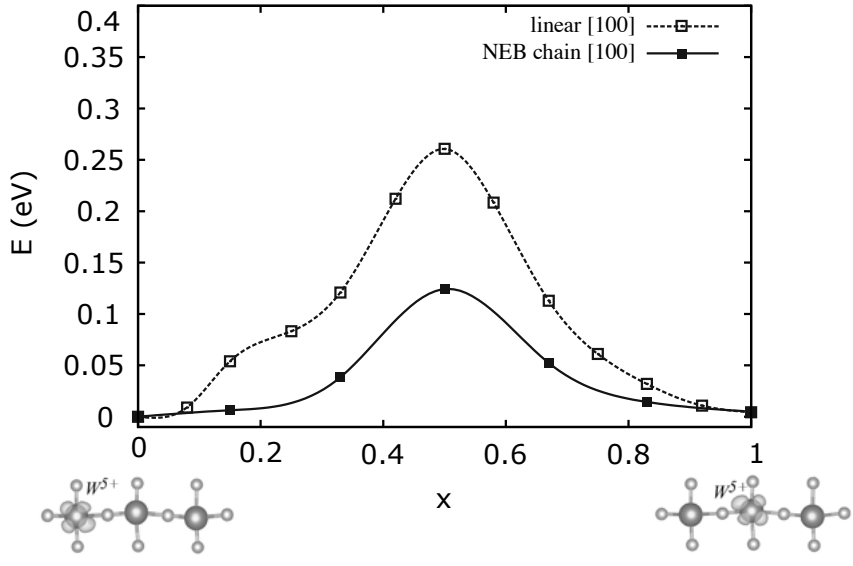

Figure 7.3. b) Energies along the transition paths of W^{5+} from one tungsten site to the other in the case of Li doped γ phase. The energies are given with respect to the energy of W^{5+}. The solid lines show the energies obtained using nudged elastic band for all the [100] crystallographic directions. For comparison, we also show the energies obtained using linear interpolation scheme calculations (dashed line). Charge distributions for W^{5+} at the initial $x = 0$ and final $x = 1$ transition points are shown for illustration at the bottom of the plot. We choose all energies such a way that the energy of the initial polaronic configuration equals zero.

for bulk MgO are shown in Fig. 7.2. The bipolaron configuration is at (0) and monopolarons at (-1) and (1) according to the notation chosen here. The curves are symmetric as in bulk MgO $O^2 - O^0$ and $O^0 - O^2$ configurations are equivalent. It can be seen that both holes perform a

transition from p-orbitals from the initial to the final sites passing bipolaron configuration where each hole is situated on the opposite oxygen atoms. Calculated energy barrier is about 2 eV. More information regarding polaron dynamics in MgO, CaO and MgO/CaO heterostructures can be found in Paper II.

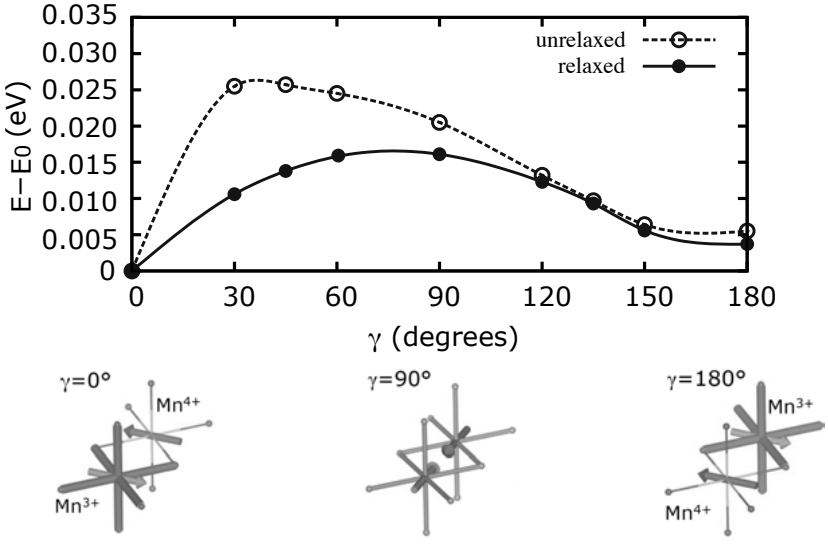

Figure 7.4. Calculated transition barriers for spin-polarons in La doped $CaMnO_3$ with restricted (dashed line) and allowed (solid line) lattice relaxation. Energies of initial and final spin-polaron configuration differ due to the different distance between the spin-polarons and the La impurity. All energies along the transition path are given with respect to the ground-state configuration (see also text). Spin rotation angle of the initial Mn^{3+} and final Mn^{4+} sites along the transition path varies in the range of $\gamma = 0° - 180°$ and measures in clock-wise (anti-clock wise) direction for initial (final) sites.

Next, we report our results of the polaron mobility in *Li* doped monoclinic WO_3. First, we consider one lithium atom situated in an octapore in the supercell of 256 atoms, i.e. $WO_3Li_{0.016}$. This is a realistic concentration often studied in experiment [195]. To study polaron mobility we used tungsten sites away from *Li* ($\sim$ 6-8 Å) simulating a free polaron propagation in the WO_3 matrix. Figure 7.3 shows the energy barriers for polaron jumping between two neighbouring W^{5+} sites in the [100] crystallographic directions. The barriers are calculated using two following methods: the linear interpolation procedure described above and nudged elastic band (NEB) method. The NEB [196, 197] is a method developed in order to find saddle points and minimum energy paths between known reactants and products. The method is based on optimization of a number of intermediate images along the reaction path. Each image

finds the lowest possible energy at the same time the equal spacing to neighbouring images is being preserved. This constrained optimization is done by adding so-called spring forces along the band between images and projecting out the force components to the potential perpendicular to the band.

As expected, the barriers obtained using linear interpolation scheme (260 meV) described above are higher than those obtained using NEB method (125 meV). These values are in surprisingly close agreement with the activation energy for polaron hopping estimated from basic models using experimental information, 180 meV [195]. Further details of our study of the polaron mobility in monoclinic WO_3 can be found in Paper III.

7.3 Spin-polaron hopping barriers from first principles

The spin-polaron is a region of ferromagnetic coupling in an AFM matrix, which is connected to the excess of electrons in this region. To study the dynamics of such polarons we adopt a concept similar to one we have introduced for lattice polarons where the spin-polaron can jump between two sites by overcoming a certain energy barrier, E_a.

Our recent studies of the static properties of spin polarons in La doped $Ca_{1-x}MnO_3$ have provided a theoretical description of the magnetic phase diagram in the La range of $0 < x < 0.10$, in good agreement with experimental data (see Paper IV). These studies have shown that spin-polarons are stabilised mostly due to the magnetic interaction at lower La concentrations and due to the lattice contribution at larger concentrations. To reduce the influence of the spin-lattice correlations, we chose to calculate barriers for polaron hopping in the low La concentration limit, namely, for $x_{La} = 0.013$. The barriers were estimated for hopping from the initial site to nearest-neighbour.

We calculated the energy barriers for polaron hopping for a seven site spin-polaron in bulk. We notice that the seven site polaron was formed in the antiferromagnetic matrix by flipping spin at one Mn site and then allowing the lattice to fully relax. We denote this magnetic and lattice configuration as the initial configuration. Spin-polaron hopping from the initial configuration to the final configuration (in Fig. 7.4 the relevant atomic sites are shown schematically and labelled as Mn^{3+} and Mn^{4+}, respectively) was controlled by changing the spin configuration. Namely, spins at the initial and final sites were simultaneously rotated by angle γ in a clockwise and anti-clockwise directions, respectively (for illustration see Fig. 7.4). The excess charge associated with the polaron could, in this way, be moved from the initial to the final configuration. The energy barrier of the polaron hopping we determined by the maximum of the

Table 7.1. *Obtained parameters over various model fitting to the calculated time periods between hopping events.*

Model	Parameters
Adiabatic	E_a = 10 meV
Weak dispersion adiabatic	E_a = 15 meV; Δ_0=12 meV
Non-adiabatic	E_a=20 meV; j = 10 meV
Magnetic polaron	E_a = 18 meV at T_N = 125 K

total energy curve along the transition path (see Fig. 7.4). It varies in the range of 14-18 meV depending on the La atom position with respect to the polaron. Our results show that in each point of the transition path lattice relaxation lowers the energy with a non-negligible value as compared to the energy of the unrelaxed lattice ($E_a \simeq$ 24-27 meV).

We also found that it was energetically favourable for the spin-polaron to move in the double-exchange active (101) plane. The barriers also varied about 1.5 meV depending on the choice of the spin rotational plane along the transition path in the non-relaxed case. However, the difference was neglected in calculations with employment of the lattice relaxation.

Moving further, as we continue discussing the spin-polaron mobility introducing the temperature effects when the polaronic centre can move through the sample. We assumed that the carrier motion of the magnetic polaron can be modelled using an Arrhenius-type process using a real-time method such as Kinetic Monte Carlo (KMC) [198]. To obtain reasonable statistics, the simulations for each temperature were performed for 100 different times with different seeds for the random number generator to obtain unbiased results. To study the dynamics of the spin-polaron system, we choose an anisotropic, 2D landscape since the spin-polaron is very likely to move in the double-exchange active (101) plane. The energy barrier was set to be E_a = 15 meV as they were obtained via our calculations described above. The attempt frequency, ν, was assumed to be $\nu = 1 \times 10^{12}$ Hz, such value is expected if the motion of the polaron as a compound object is driven by magnonic and phononic processes.

We found that the obtained average time periods between hopping events, i.e. jumps of the polaron between sites, follow an exponential behaviour as a function of temperature (Fig. 7.5). We also performed a numerical fitting of the obtained results to the rate transition within adiabatic (Eq. (7.1)), adiabatic with weak dispersion (Eq. (7.7)), non-adiabatic (Appendix 11.1, Eq. (11.35)) and non-adiabatic magnetic polaron (Eq. (7.9)) models (results are presented in Table 7.1).

As an attempt to take into account the stochastic behaviour of the system, we introduced the stochastically driven motion process. We calculated the time that it takes for the polaron to jump whenever two nearest-neighbour spins are aligned strictly antiparallel in the motion

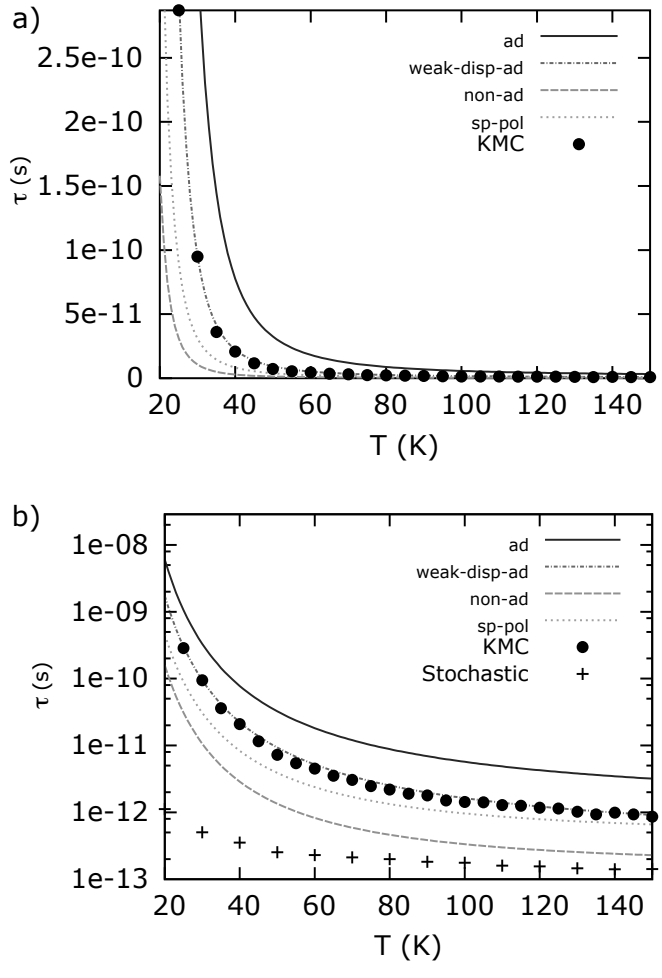

Figure 7.5. Average times between spin-polaron jumps obtained using KMC method (filled circles). The result is compared with different models: adiabatic, adiabatic with weak dispersion, non-adiabatic and non-adiabatic in case of the spin-polaron in the AFM lattice. On the bottom panel, the data is given using a logarithmic scale and also contains results for the stochastically driven motion.

plane. In Fig. 7.5 b) it can be seen that this approach also predicts an exponential-like behaviour likewise our calculations and models listed in Table 7.1. However, jumping times obtained via stochastically driven motion method differ by almost two orders of magnitude. The reasons behind such behaviour could be many, in particular, there is no influence of the lattice in the anti-parallel approach, a factor which is relevant for the energy barrier obtained from first principle calculations. The only term in this case which describes the intrinsic viscosity of the spin system is the Gilbert damping α, used for the Atomistic Spin Dynamics [199] simulations based on Langevin dynamics (discussed in Section 4.5). This parameter was set up to $\alpha = 0.5$. A full account of the results of spin-polaron mobility and the potential to use these objects in nano-technology is discussed in full detail in Paper V.

8. Conclusions and outlook

> They tried to bury us. They
> didn't know we were seeds.
>
> *Dinos Christianopoulos*

In this chapter, we summarise the results emphasised in the thesis and provide a brief outlook of the directions where some of our findings can have further development and applications.

- We have studied multi-polaron solutions in the framework of the 1D Holstein model in Paper I. We found that the periodic solutions can stabilize in a certain range of the parameters. By using the approaches previously introduced in plasma physics, we show that the periodic solutions may stabilize with respect to a periodic perturbation in a certain range of the parameters. We emphasize the importance of the universal, dnoidal solution, which previously has not been discussed in the context of the Holstein model. Thus, along with the robust stable solitonic solutions, we enlarge the set of stable solutions to be considered, to the periodic functions, which may describe the multi-polaron case. Moreover, the model was extended and studied under the influence of non-local effects that has never been done before. We show that, by increasing the complexity of the problem, the NLSE lose its complete integrability. We show that the non-local nonlinear effects produce important effects in the dynamics of solitons and polarons and ignoring these effects can become crucial for an adequate description. Particularly, we have observed that nonlocal effects influence polaron-polaron collisions by inducing an inelastic scattering via the excitation of internal modes. We show that nonlocality forces the bipolaron dynamics to develop spatial asymmetry and delocalizes bound polaronic states earlier in time than the standard solution. This result should also be considered in theories dealing with bipolaronic superconductivity.
- In Paper II, we have modelled different hole bipolaronic configurations adjacent to a cation vacancy at the (100) MgO/CaO interface. We found that the vacancy formation is substantially facilitated by the presence of the interface between the two oxides. We applied two theoretical methods, DFT+U and HSE hybrid functional, and this allowed us to obtain a correct local lattice distortion around the

defect which leads to hole localisation pattern in agreement with experimental data. The $O^1 - O^1$ bipolaronic configuration is found to be the ground state in all the studied cases. We show that at the interface, the *cis* configurations are always preferred, and the triplet and singlet magnetic configurations are degenerate within the accuracy of 1-2 meV. We found that the $O^2 - O^0$ bipolaronic solution is metastable exhibiting deeper local minima at the interface compared to those in bulk oxides. This result indicates that different bipolaronic configurations could coexist at the MgO/CaO interfaces. The study shows the possibility to control bipolaron configuration introducing an interface between two oxides. The applied methodology can be extended in order to theoretically predict V-center topology formed on interfaces between a wide range of ionic oxides.

- In Paper III, we study the applicability of $HSE06$ and two $DFT+U$ approaches to model polarons in WO_3. We have shown that the $DFT+U$ approach with two $Hubbard-U$ parameters determined and applied simultaneously to the 5d states of W (U_W=6 eV) and 2p states of O (U_O=9 eV) provides a proper description of polaron formation and transitions in WO_3. At the same time, this method allows us to calculate large cells necessary to properly model polarons and bipolarons in the crystal. Using this approach we have studied the vacancy energetics for the six non-equivalent oxygen positions and two electronic configurations: $W^{5+} - W^{5+}$ and $W^{6+} - W^{4+}$. We show that the $W^{5+} - W^{5+}$ bipolarons situated along [001] are the most favourable electronic configurations around vacancies. We have also studied polaron and bipolaron formation and energetics for Li-doped WO_3. In this case, the $W^{5+} - W^{5+}$ bipolaronic configuration aligned with [001] has again the lowest energy but winning only 8 meV over two separated W^{5+}. Our results suggest that polarons formed due to oxygen vacancies are immobile, at the same time, the W^{4+} state is metastable and the transition from $W^{5+} - W^{5+}$ to $W^{6+} - W^{4+}$ state is possible with a barrier of 150 meV. On the contrary, polarons formed in Li doped tungsten oxide are mobile with the minimum activation energy (98 meV) along the [001] direction. The W^{4+} state is 300 meV higher in energy than any studied W^{5+} configuration and, therefore, W^{4+} is unlikely to form in perfect $Li - WO_3$ without vacancies or similar structural defects.
- Further, in Paper IV, we propose an optimised approach, based on DFT+U, which allowed us to describe charge localisation and magnetic polymorphism of doped $CaMnO_3$ and Mn-oxides, in general. Moreover, it allows us to describe the La-concentration dependence of the magnetic state of La-doped $CaMnO_3$ fully from first principles. We report the optimised geometries of SPs as a function of La concentration and provide a microscopic understanding of the rela-

tive importance of exchange and lattice effects for the formation of the spin-polarons in La-doped $CaMnO_3$. In this paper, we propose an optimised methodology enabling one to describe charge localisation and magnetic polymorphism of doped $CaMnO_3$ and Mn-oxides, in general. The methodology proposed in this paper also allows us to stabilise the spin-polarons of different sizes and configurations, calculate their energies, study the degree of charge localisation and its coupling to the local distortions and, finally, describe the mechanism of their stabilisation. We perform this analysis for a wide range of La concentrations and show how stabilisation mechanism changes with concentration.

- In Paper V, we have investigated theoretically the static and dynamic properties of spin-polarons in La-doped $CaMnO_3$. In order to do this, we constructed an effective low energy Hamiltonian, in which all parameters were calculated from first principles theory. This low energy Hamiltonian is used to investigate the temperature stability of the spin-polaron, as well as the response to an external applied electric field. Technically, this involves ab-initio electronic structure theory and atomistic spin-dynamics simulations in combination with kinetic Monte Carlo simulations. In our study, we compared results from different geometries, like spin-polarons in bulk, surface or single two-dimensional layers, and significant differences were observed. Where a comparison can be made, primarily for bulk geometries, the results presented here compare well with experimental data, and previous theoretical predictions.

  We demonstrated a remarkable control of the mobility of spin-polarons in this material, and that the critical parameters deciding this, is the temperature and the strength of the applied electrical field. This opens up for technology using spin-polarons, and our simulations demonstrate that storing and erasing information magnetically, by introduction and control of electrical charge, is possible, even for rather low strength of the external electric field.

Concluding the present thesis, I would like to say that the main context of this work can be viewed as new, theoretical results in polaron physics. The results improve our understanding of several current problems in the field as well as open new possibilities for further studies both from theoretical and experimental perspectives.

Analytical studies of polarons took place since the 50's of the previous century. Currently, many aspects of a single polaron description are understood very well. However, there are still plenty of interesting questions waiting further investigations. In this context, multipolaron systems have gained particular attention in the last two decades. In this work, we attempted to extend Molecular Crystal Model in 1D, including nonlocality effects. More complex view on multipolaron systems accounting for

anisotropy, nonlocality and studies performed for 2D and 3D dimensional systems, undoubtedly will lead to new, unknown physical effects. It is especially important to continue this theoretical research in collaboration with further experimental studies.

Also, we would like to emphasize some methodological priorities laid out for further studies. Mapping to the models previously studied in the context of other physical problems makes possible to adopt new methods, from other fields of physics and mathematics. For example, in Paper I and Chapter 3 we have discussed a methodology, previously developed in plasma physics, in order to examine solution stability. Particularly, in case of NLSE, for further research it might be useful to involve methods of optic and plasma physics, as well as to adopt field theoretical methods. In general, attention must be paid to studies of quantum interacting particle systems. It is remarkable, that the opposite methodological trend also takes place. For example, as already mentioned in the Introduction, Feynman's path integral method.

Undoubtedly, analytical models might lead to limited, sometimes incorrect description of polarons in real systems. Studies with employment of first principle methods give a better description of lattice polarons, their inner structures, mobility, etc. Moreover, due to the complexity of the systems carrying polarons, experimental measurements quite often face great difficulties. In this case, a consistent theoretical description using analytical and computational methods brings important knowledge about mechanisms underlying the polaron behaviour. The theoretical and computational methods we propose in the thesis, open possibility to compare experimental data with theoretical model. For example, we show that the theoretical description admits a variety of different polaronic configurations in a crystal, which differ in charge and orbital occupation, however, some of them are metastable and will have a rather short mean lifetime. Moreover, polarons may develop certain topologies in highly anisotropic systems such as heterostructures and exhibit different transport properties depending on the way they have originated, either intercalation of defects or electron injection.

Successful studies of the lattice polarons using ab-initio implementation of the Hubbard-U approach show that further achievements can be obtained by including Holstein-like electron-phonon interactions. Another possibility is further studies of polarons in f-electron systems with employment of full-potential approaches and Dynamical mean-field theory (DMFT). Optical and spectral properties of polaronic systems can be studied using quantum many-body methods in the presence of time-dependent potentials such as Time-dependent density functional theory (TD-DFT). Valuable information can be achieved using phonon spectra calculations in order to analyze renormalization of phonon branches due to the localized state formation. Moreover, the first principle methods

we propose in order to study polarons in solids can be extended to other quasiparticles such as excitons, plasmon states, etc. In this spirit, studies of spin-polarons is a promising direction for further studies. Research on spin-polaron properties in perovskites with half-field and highly occupied e_g orbitals would be especially interesting. In such compounds, we expect a strong influence of the spin-orbit coupling, electronic correlations as well as the cooperative spin-lattice effects.

9. Svensk sammanfattning

En polaron kan enkelt beskrivas som en lokal störning av en inre struktur, som skapas av rörliga elektroner, och där den lokala störningen skapar en attraktiv potential som fångar in och lokalriserar den rörliga elektronen. Det polaroniska tillståndet utvecklas på ett självkonsistent sätt: ett lokaliserat laddningstillstånd inducerar gitterpolarisation som i sin tur fångaar in den lokalt polariserade laddningsbäraren. Polaronen har egna egenskaper som speglar dess inre struktur: radie, formationsenergi, laddning, magnetisk moment och andra kvanttal. Polaronkonceptet medger en beskrivning inom ramen för den effektiva massapproximationen, och eftersom den är en s.k. klädd kvasipartikel är den polaroniska effektmassan vanligtvis större än den effektiva massan av en vanlig elektron somrör sig fritt i ett material.

L.D. Landau introducerade ursprungligen polaron-konceptet men det var S.I. Pekar som föreslog namnet "polaron". Han studerade polaronens självenergi och effektiva massa i polära kontinuum medier. Fröhlichs modell i kontinuum gränsfallet (d v s för stora polaroner) visade sig vara ekvivalent med Pekars metod i den så kallade stark-kopplande regimen. Senare utvecklade R. Feynman en linje-integral-metod för att särskilt studera polaronproblemet. Metoden har blivit till en av dem mest använda inom statistisk mekanik och kvantfältteori. Ett annat försök för att beskriva polaroner baseras på mikroskopiska modeller som tar hänsyn till mediets interna struktur. I de modellerna beskrivs polaroner med en atomär bild (tillämpbar för mindre polaroner), vilket är ett annat tillgångssätt som skiljer sig från Fröhlichs beskrivning. Betydelsefulla publikationer inom polaronen-vetenskap gjordes på 50-talet av föra århundradet. I dagslägget är polaronstudier med det diskreta tillgångssä ett brett forskningsfält. Här bör man nämna några avancerade beräkningsbaserade och teoretiska metoder, som till exempel diagrammatisk Monte Carlo, eller exakta diagonaliserings metoden. Det har nyligen vistats att en ordentlig teoretisk analys av gitterpolaroner i en mikroskopisk beskrivning kräver att ab-initio-beräkningstekniker används. De sistnämnda kan noggrannt svara för materialens elektronvågfunktion och inkluderar rörelse av varje enskild atom i området där gitterdeformation kring lokaliserade elektronen uppstår.

Experimentella studier av polaroner är också ett intensivt forskningsfält. Dessa experiment spelar stor roll för förståelsen av en mängd olika fenomen såsom laddningstransport och optiska egenskaper hos halvledare,

högtemperatur-supraledning, och gigantisk magnetoresistans. Olika experimentella tekniker fokuserar på olika aspekter och egenskaper hos polaroner i fasta material. Till exempel optisk absorptionsspektra påvisar att ett polarontillstånd bildas, medan detaljer av det optiska absorptionspektrumet beror på storleken hos polaronerna och röntgenabsorptionsmätningar kan användas för att upptäcka när polaronband bildas. Nyligen har även mätningar med tvådimensionell elektronspektroskopi (2DES) använts för att studera koherenta vibrationer i filmer av polymerer, där man har observerat absorption av polaronpar i filmer som inte utsatts för uppvärmning. För att studera polaronkonduktivitet används mätningar av elektrisk konduktivitet och av Seebeck koefficienten. Slutligen är det också viktigt att påpeka betydelsen av experimentella studier av provens magnetiseringen eftersom dessa indikerar om spinnpolarontillstånd har bildats. Detta arbete beskriver teoretiska studier av gitter- och spinn-polaroner in flera olika system, såsom endimensionella kedjor av harmoniska oscillatorer, joniska och kovalenta oxider, samt magnetiska halvledare.

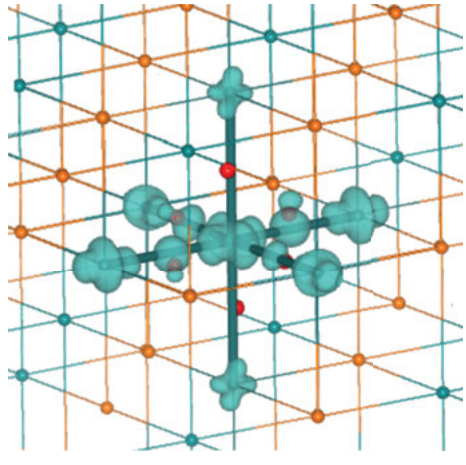

Figure 9.1. En spin-polaron i den antiferromagnetiska G-typ fasen.

I denna avhandling beskrivs teoretiska studier av gitter- och spinnpolaroner i flera system t.ex. en endimensionell kedja av harmoniska oscillatorer; joniska och kovalenta oxider; samt magnetiska halvledare. För gitterpolaroner presenterar vi först en analytisk studie där multipolaronlösningar hittades inom ramen för Holstein 1D-molekylkristallmodellen. Vi hittade en ny periodisk s.k. dnoidalösning, som tidigare inte diskuterats för multipolaronsystemet. Utöver det undersökte vi stabiliteten hos multipolaronlösningar och har visat att cnoidala och dnoidala lösningar stabiliseras i olika områden av det parametriska utrymmet. Dessutom utvidgade vi modellen med hjälp av icke-lokala effekter, vilket speglar det verkliga systemens beteende. Vi studerade också polaron-dynamik

och visade att tidsutvecklingen av det polaroniska systemet medger excitering av inre strukturer. Vi har även studerat lokalisering av hålbipolaroner, och medföljande vakansformation av en katjon i kristallstrukturerna MgO och CaO och vid gränsskiktet MgO/CaO. Ett viktigt resultat i denna studie är att grundtillståndetet är den O^1-O^1 bipolära konfigurationen, både för kristall-oxider och vid deras gränsskikt. Vi har också upptäckt att den enkel-centrerade O^2-O^0 bipolaronen är metastabil och att dess stabilitet är förstärkt vid gränsskikten jämfört med situationen inuti kristall-oxider. I denna avhandling studeras möjliga övergångar mellan några valda bipolära konfigurationer. Med samma tankesätt studerades även elektronlokalisering och polaronmobilitet i syrefattig, Li-dopad och monoklinisk tungstentrioxid. Det visar sig att små polaroner, som skapas i närvaro av syrevakanser, föredrar bipolära W^{5+}-W^{5+} konfigurationen över den metastabila W^{6+}-W^{4+} konfigurationen. Vi visar att bipolaroner är starkt bundna av syrevakanser och därmed även orörliga. Dock verkar polaroner vara rörliga om de är skapade av Li interkalation.

Avslutningsvis visar vi att spin-polaroner (SP) också kan skapas i La-dopad $CaMnO_3$, i den antiferromagnetiska G-typ fasen (se figur 9.1), men inte i den antiferromagnetiska C-typ eller A-typ fasen. I detta material är SP lösningar stabila på grund av samspelet mellan magnetiska och gitter effekter vid låga La koncentrationer och vid höga koncentrationer mestadels på grund av gittret. Det är viktigt att poängtera att det teoretiska magnetiska fasdiagrammet överensstämmer väl med tidigare rapporterade experimentella resultat. Vi har också studerat dynamiska aspekter och temperaturegenskaper för detta material och med hjälp av beräknade material-specifika utbytesparametrar har vi erhållit att 3D magnetiska polaroner i Heisenberg-gittret stabiliseras vid något högre temperatur än för 2D magnetiska polaroner. Utöver detta har vi föreslagit en metod för att beräkna övergångs barriärer för magnetiska polaroner. Resultaten i denna avhandling är sammanfattningsvist i utomordentlig överensstämmelse med tillgängliga teoretiska och experimentella resultat.

10. Acknowledgements

Foremost I would like to thank my primary supervisors Olle Eriksson and Natalia Skorodumova for inviting me to Uppsala University to complete my PhD degree. Olle, thank you for all I have learned from you about such inspiring and complex subject as magnetism. Natalia, thank you for introducing me to the fascinating world of oxides. Also, I would like to thank Manuel Pereiro which co-supervised this thesis. It was a great pleasure for me to work with you on the nonlinear polaronic systems. Dear supervisors, thanks for all your support, smart pieces of advice and patience. Here, in Uppsala, many of my dreams regarding my scientific activity, came true.

I am grateful to my coauthors Yaroslav Kvashnin, Anders Bergman and Jonathan Chico. Thank you guys for all meetings, discussions and work we have done together. I really enjoyed it and learned plenty of important stuff from you working on our common projects. Next, I would like to thank Sussane Mirbt, head of our Materialteori Division for all support and help she provides to PhD students keeping at the same time friendly and working atmosphere at our division. I am very grateful to following seniors and researchers for all interesting discussions and ideas they have shared with me during my stay in Uppsala: Börje Johansson, Jonas Fransson, Moyses Araujo, Mattias Klintenberg, Lars Nordström, Peter Oppeneer, Biplab Sanyal, Annica Black-Schaffer, Ralph Scheicher, Anton Grigoriev, Vladimir Pavlenko, Bo Thidé, Stefan Leupold, Alex Aperis, Rudra Banerjee, Igor Di Marco, Marco Berritta, Adrien Bouhon, Wei Luo, Barbara Brena, Sudip Chakraborty, Erna Delczeg, Dushko Kuzmanovski, Oscar Grånäs, Jan Rusz, Diana Iuşan, Danny Thonig, Erik Sjöqvist, Olga Vekilova, Pablo Maldonado, Attila Szilva, Johan Hellsvik and Heike Herper. Thank you, people, you are wonderful scientists and it was a great pleasure for me to work with you side by side.

I would like to thank my dear officemates: Johann Lüder, Satadeep Bhattacharjee and Patrik Thunström. Thank you for discussions and friendship. I hope that sharing with me a working space, was not too annoying and painful, since I have had very individual working hours, time to time.

I appreciate all I have done as a member of local IT support team together with Raghuveer Chimata and Soumyajyoti Haldar. It was an interesting and important experience for me to work with you. And of course I send lots of gratitudes to the head of IT group of Department

of Physics and Astronomy, Teresa Kupsc for friendful collaboration and support. The same amount of thankfulness goes to department system administrators, I enjoyed working with, Anders Sjödin and Alen Jadadic.

Further I send gratitudes for all help and patience, to our department secretary Inger Ericson. Also, I would like to mention Åsa Andersson and Marja Fahlander. Thanks for the everyday work you provide for us. It makes our activities much more easier.

Here, I would like to mention members of the student community. Dearest friends I am not afraid to seem too emotional saying that you became my newfound family. I will always remember those great times we have spent together. Thank you for everything: Anna Sinelnikova, Kristofer Björnson, Debora Rodrigues, Henning Hammar, Johan Schött, Anna and Tobias Lindström, Taizo Shibuya, Alexander Edström, Johann Schmidt, Till Brönnle, Sumanta Bhandary, Alexey Vorobyev, Francesco Cricchio, Inka Locht, Marco Battiato, Oladunjoye Awoga, Francesco Catalano, Marcio Costa, Weiwei Sun, Vancho Kocevski, Hitoshi Fujii, Lisa Unger, Beatriz Villarroel, Ramon de Almeida, Iulia Brumboiu, Robert Johansson, Samara Keshavarz, Jakob Spiegelberg, Alexander Nasedkin, Ritwik Mondal, Adam Jakobsson, Pjotr Zguns, Teeraphat Watcharatharapong, Raquel Esteban and many many others to whom I, unfortunately, forgot to mention here.

Special thanks, I send to Martin Amft for support and help he provided at the very early and most difficult times of my stay in Uppsala.

And the last but not the least, I owe to thank my family members for all love, courage and understanding they have provided during my PhD studies.

11. Appendices

11.1 On non-adiabatic transition rate

Here, we derive the semi-classical transition rate in the non-adiabatic regime guided by Holstein's paper [200]. We start from the electron-lattice harmonic Hamiltonian with augmented coupling term between the nearest-neighbour sites. Into the consideration, we take the n-th site as the initial and n+1-the site as a final site of the carrier transition in the N-site chain. In the frame of the molecular-crystal model, the corresponding Hamiltonian reads as:

$$i\hbar\frac{\partial a_n}{\partial t} = \left[\sum_m \left(-\frac{\hbar^2}{2M}\frac{\partial^2}{\partial x_m^2} + \frac{1}{2}M{\omega_0}^2{x_m}^2 + \frac{1}{2}M{\omega_1}^2 x_m x_{m+1}\right) + g x_n\right] a_n - j(a_{n+1} + a_{n-1}), \tag{11.1}$$

where a_n has a meaning of the electronic wavefunction amplitude which is a function of the "lattice-vibration" coordinates x_n and in general reads as $a_n(x_1, ...x_N)$. Similarly to the Hamiltonian introduced in Chapter 3, g in Eq. (11.1) is the electron-lattice coupling constant, and j is the nearest-neighbour overlap integral of the tight-binding electrons, respectively. ω_0 and ω_1 correspond to the individual vibration of the diatomic molecule with mass M, and the nearest-neighbour augmented vibration, respectively.

In order to simplify the initial Hamiltonian in Eq. (11.1), we transform previous equation to the normal mode coordinate representation introducing the following general relation for the vibrational degrees x_n:

$$x_n = (\frac{2}{N})^{\frac{1}{2}} \sum_k q_k \sin(kn + \frac{\pi}{4}), \tag{11.2}$$

where $k = 2\pi\kappa/N$, the integer κ lying in the range -1/2(N-1) $\leq \kappa \leq$ 1/2(N-1) and N is assumed to be an odd integer.

After inserting Eq. (11.2) in Eq. (11.1) we get:

$$\begin{aligned} i\hbar\frac{\partial a_n}{\partial t} = \sum_k [(-\frac{\hbar^2}{2M}\frac{\partial^2}{\partial q_k^2} + \frac{1}{2}M{\omega_k}^2{q_k}^2) + \\ (\frac{2}{N})^{\frac{1}{2}} g q_k \sin(kn + \frac{\pi}{4})] a_n - j(a_{n+1} + a_{n-1}). \end{aligned} \tag{11.3}$$

Next, we find it convenient to introduce a quantity $\mathscr{E}_{kn}$ as:

$$\mathscr{E}_{kn} = \sqrt{\frac{2}{N}} g \sin(kn + \frac{\pi}{4}). \tag{11.4}$$

After the transformation, the Hamiltonian described by Eq. (11.1), takes the following form:

$$i\hbar\frac{\partial a_n}{\partial t} = \sum_k \left(-\frac{\hbar^2}{2M}\frac{\partial^2}{\partial q_k^2} + \frac{1}{2}M{\omega_k}^2{q_k}^2 + \mathscr{E}_{kn}q_k \right) a_n. \tag{11.5}$$

We notice that in the stationary case, Eq. (11.5) is nothing but a Hamiltonian corresponding to a system of the N harmonic independent oscillators with the shifted equilibrium points:

$$E_n a_n = \sum_k \left(-\frac{\hbar^2}{2M}\frac{\partial^2}{\partial q_k^2} + \frac{1}{2}M{\omega_k}^2{q_k}^2 + \mathscr{E}_{kn}q_k \right) a_n. \tag{11.6}$$

Moreover, Eq. (11.6) can be rewritten in the following convenient form:

$$E_n a_n = \sum_k \left(-\frac{\hbar^2}{2M}\frac{\partial^2}{\partial q_k^2} + \frac{1}{2}M{\omega_k}^2(q_k - \frac{\mathscr{E}_{kn}}{M{\omega_k}^2})^2 - \frac{{\mathscr{E}_{kn}}^2}{2M{\omega_k}^2} \right) a_n. \tag{11.7}$$

Introducing ${q_0}' = \frac{\mathscr{E}_{kn}}{M{\omega_k}^2}$ and denoting the non shifted oscillatory eigenvalue as E', one readily obtains:

$$E_n' a_n = \sum_k [-\frac{\hbar^2}{2M}\frac{\partial^2}{\partial q_k^2} + \frac{1}{2}M{\omega_k}^2(q_k - {q_0}')^2] a_n, \tag{11.8}$$

where the eigenvalues simply find as:

$$E_n = E_n' + \sum_k \frac{{\mathscr{E}_{kn}}^2}{2M{\omega_k}^2}, \tag{11.9}$$

and the eigenfunctions are:

$$a_n = \frac{1}{\sqrt{q_0}}\phi_n^{(osc)}(\frac{q_k - q_0'}{q_0}), \tag{11.10}$$

where $q_0 = (\frac{\hbar}{M\omega_k})^{1/2}$.

In Eq. (11.10), $\phi_n^{(osc)}(\xi)$ are Chebyshev-Hermite polynomials:

$$\phi_n^{(osc)}(\xi) = \frac{1}{\sqrt{2^n n!\pi^{1/2}}} H_n(\xi) e^{-\xi^2/2}. \tag{11.11}$$

Now let us calculate the classical occurrence probability for the electron to propagate from the n-th to the n+1 site. For the calculation, we use the first order perturbation theory by omitting only lattice vibrations and

assuming that j (hopping integral) is a small parameter, perturbing the electronic amplitude a_n:

$$\begin{array}{l} i\hbar\frac{\partial a_n}{\partial t} = -gx_n(t)a_n - ja_{n+1}; \\ i\hbar\frac{\partial a_{n+1}}{\partial t} = -gx_{n+1}(t)a_{n+1} - ja_n. \end{array} \tag{11.12}$$

Taking into account that at the initial moment t_0, $a_n = 1$ and $a_{n+1} = 0$, and introducing the coincidence moment t_c at which $x_n(t_c) = x_{n+1}(t_c)$, the solution of the system given in Eq. (11.12) can be found as:

$$\begin{array}{c} a_{n+1} = -\frac{j}{i\hbar}\exp\{\frac{ig}{\hbar}\int_{t_c}^{t} x_{n+1}(t)dt\}\times \\ \int_{t_0}^{t}\exp\{\frac{ig}{\hbar}\int_{t_c}^{t}(x_n(t'') - x_{n+1}(t''))dt''\}dt', \end{array} \tag{11.13}$$

or in terms of the normal coordinates:

$$\begin{array}{c} a_{n+1} = -\frac{j}{i\hbar}\exp\{\frac{ig}{\hbar}\int_{t_c}^{t}\sum_k(\frac{2}{N})^{\frac{1}{2}}q_k(t)\sin\alpha_{kn}dt\}\times \\ \int_{t_0}^{t}\exp\{\frac{ig}{\hbar}\int_{t_c}^{t}\sum_k(\frac{2}{N})^{\frac{1}{2}}q_k(t'')\sin(\frac{k}{2})\sin(\frac{k}{2}+\alpha_{kn})dt''\}dt', \end{array} \tag{11.14}$$

where, $\alpha_{kn} = (kn + \frac{\pi}{4})$.

For further evaluation, we use a number of the following assumptions suggested in Ref. [200]. The argument of the first path integral in Eq. (11.14) is assumed to be zero as an average of all possible given classical trajectories between successive coincidence points. Also, the spacing in time between consecutive coincidence points is assumed to be large comparing with the transition time. Thus, one can replace the integration over time limits in the second path integral by integration from minus to plus infinity. The phase of the normal coordinate in the region around t_c is assumed to be stationary, so that the time variation of the q_k can be considered as a linear function near the coincidence point which allows factorisation in terms of time and velocity. Thus, we obtain:

$$a_{n+1} = -\frac{j}{i\hbar}\int_{-\infty}^{+\infty} exp\{\frac{ig}{2\hbar}(\dot{x}_n(t) - \dot{x}_{n+1}(t))(t-t_c)^2\}dt, \tag{11.15}$$

and, after integration over the time variable, we get:

$$a_{n+1} = -\frac{j}{i}e^{-\frac{i\pi}{4}}\left(\frac{2}{\hbar(\dot{x}_n(t) - \dot{x}_{n+1}(t))}\right)^{\frac{1}{2}}. \tag{11.16}$$

The transition probability of an inter-site jump, $n > n+1$, which occure in a single coincidence event is:

$$W_{(n\to n+1)} = \frac{2\pi j^2}{\hbar}\frac{1}{|\dot{x}_n - \dot{x}_{n+1}|} = \frac{\pi j^2}{\hbar}\frac{(2N)^{1/2}}{\dot{q}_k(t)\sin(\frac{k}{2})\sin(\frac{k}{2}+\alpha_{kn})}. \tag{11.17}$$

If $W_{(n\to n+1)}$ is a probability to jump per second, then the probability to jump for a coincidence event can be expressed as :

$$R_{non-ad} = P_c W_{(n\to n+1)}, \tag{11.18}$$

where P_c is probability that the coincidence will occur.

Further, P_c is calculated by using the standard description of the thermal average function:

$$P_c = \frac{F_c}{Z_c} = \frac{\int ... \int e^{\beta(H_L + g x_n)} [\delta(x_n - x_{n+1})\dot{x}_r dt][\delta(\dot{x}_n - \dot{x}_{n+1} - \dot{x}_r) dx_r] dx_1 ... dx_N d\dot{x}_1 ... d\dot{x}_N}{\int ... \int e^{\beta(H - g x_n)} dx_1 ... dx_N d\dot{x}_1 ... d\dot{x}_N}, \tag{11.19}$$

where, $\beta = \frac{1}{k_B T}$.

To evaluate Eq. (11.19), we use the standard Euler-Poisson integral [1], and we first evaluate the integration over the velocity variables of P_c:

$$F_{\dot{x}} = ... \int \int ... e^{\frac{-M\beta \dot{x}_p^2}{2}} e^{\frac{-M\beta \dot{x}_{p+1}^2}{2}} \delta(\dot{x}_p - \dot{x}_{p+1} - \dot{x}_r)\dot{x}_r dt ... d\dot{x}_p d\dot{x}_{p+1} ... \tag{11.20}$$

Here we use the delta function filter property: $\int \delta(x-y) f(x) = f(y)$ and get the following expression:

$$F_{\dot{x}} = \sqrt{\frac{\pi}{M\beta}} e^{\frac{-M\beta \dot{x}_r}{4}} \dot{x}_r dt. \tag{11.21}$$

Next, the denominator of Eq. (11.19), we find as:

$$Z_{\dot{x}} = ... \int \int ... e^{\frac{-M\beta \dot{x}_p^2}{2}} e^{\frac{-M\beta \dot{x}_{p+1}^2}{2}} ... d\dot{x}_p d\dot{x}_{p+1} ... = \frac{2\pi}{M\beta}. \tag{11.22}$$

Finally, dividing Eq. (11.21) by Eq. (11.22) we get:

$$P_{\dot{u}} = \sqrt{\frac{M\beta}{4\pi}} e^{\frac{-M\beta \dot{x}_r}{4}} \dot{x}_r dt. \tag{11.23}$$

To obtain probability per time unit one needs to divide $P_{\dot{x}}$ by dt. Then multiplying $P_{\dot{u}}$ by $W_{(n\to n+1)}$ in the limit $|\dot{x}_n - \dot{x}_{n+1}| \to |\dot{x}_r|$ and integrating over all possible values of $\dot{x}_r$ one gets:

$$P_{\dot{x}} W_{(n\to n+1)} = \int \sqrt{\frac{M\beta}{4\pi}} e^{\frac{-M\beta \dot{x}_r}{4}} \frac{2\pi j^2}{\hbar} d\dot{x}_r = \frac{2\pi j^2}{\hbar}. \tag{11.24}$$

[1] In derivations, we often use Euler-Poisson integral with real and complex coefficients: $\int e^{-(ax^2+bx+c)} dx = \sqrt{\frac{\pi}{a}} e^{\frac{b^2-4ac}{4a}}$, $\int e^{-iax^2} dx = \sqrt{\frac{\pi}{a}} e^{-\frac{\pi}{4}}$

To evaluate integration over the coordinate variables x_n it is more convenient to use normal mode representation which is already introduced above:

$$P_{q_k} = \frac{F_{q_k}}{Z_{q_k}} = \frac{\int ... \int e^{\beta\left(\sum_k \frac{1}{2} M {\omega_k}^2 {q_k}^2 + g q_k \sin\alpha_{kn}\right)} \delta\{(\frac{2}{N})^{\frac{1}{2}} (\sum_k q_k \sin\alpha_{kn} - \sum_k q_k \sin\alpha_{k(n+1)})\} dq_1 ... dq_N}{\int e^{\beta\left(\sum_k \frac{1}{2} M {\omega_k}^2 {q_k}^2 + (\frac{2}{N})^{\frac{1}{2}} g q_k \sin\alpha_{kn}\right)} dq_1 ... dq_N}. \tag{11.25}$$

Using the following property of the delta function: $\delta(x) = \frac{1}{2\pi} \int_{-\infty}^{+\infty} e^{ix\gamma} d\gamma$ we can rewrite the numerator of (11.25) in the following way:

$$\delta\left[x_n - x_{n+1}\right] = \int_{-\infty}^{+\infty} e^{i(\frac{2}{N})^{\frac{1}{2}} (\sum_k q_k \sin\alpha_{kn} - \sum_k q_k \sin\alpha_{k(n+1)})\gamma} d\gamma. \tag{11.26}$$

Evaluation of all parts readily leads to:

$$F_{q_k} = \frac{1}{2\pi} \prod_k \left(\frac{2\pi}{\beta M \omega_k^2}\right)^{\frac{1}{2}} \int_{+\infty}^{-\infty} exp\left(\sum_k \frac{((i\gamma - g\beta)\sin\alpha_{kn} - i\gamma \sin\alpha_{k(n+1)})^2}{NM\omega_k^2 \beta}\right) d\gamma; \tag{11.27}$$

$$Z_{q_k} = \prod_k \left(\frac{2\pi}{\beta M \omega_k^2}\right)^{\frac{1}{2}} \left(\sum_k \frac{(g\beta \sin\alpha_{kn})^2}{NM\omega_k^2 \beta}\right). \tag{11.28}$$

Dividing the given quantities, we obtain the following relation:

$$P_{q_k} = \frac{1}{2\pi} \int_{+\infty}^{-\infty} exp\left(\sum_k \frac{((i\gamma - g\beta)\sin\alpha_{kn} - i\gamma \sin\alpha_{k(n+1)})^2 - (g\beta \sin\alpha_{kn})^2}{NM\omega_k^2 \beta}\right) d\gamma. \tag{11.29}$$

Next, we pair terms with opposite sights of k and using trigonometric relations, simplify P_{q_k} to the following form:

$$P_{q_k} = \frac{1}{2\pi} \int_{+\infty}^{-\infty} exp\left(\sum_k \frac{-2(\gamma^2 + i\gamma\beta)(1 - \cos k)}{NM\omega_k^2 \beta}\right) d\gamma. \tag{11.30}$$

For further evaluation, we introduce the following replacement: $\epsilon = \gamma + \frac{ig}{2kT}$. Changing integration limits can be easily done by considering that the real part of the integration limit is infinity although the imaginary coefficient is a finite number. Thus, we can write: $\lim_{\gamma \to \pm\infty} = (\gamma \pm \frac{ig^2\beta^2}{2}) = \pm\infty$, and

$$P_{q_k} = \frac{1}{2\pi} \int_{+\infty}^{-\infty} exp\left(\sum_k \frac{-(4\epsilon^2 + g^2\beta^2)(1 - \cos k)}{2NM\omega_k^2 \beta}\right) d\epsilon. \tag{11.31}$$

Then, introducing the quantity E_a either for discrete number of k or in the limit when summation over k can be replaced by integration we get:

$$E_a = \frac{1}{N}\sum_k \frac{g^2(1-\cos k)}{NM\omega_k^2} = \frac{1}{N}\int \frac{g^2(1-\cos k)}{NM\omega_k^2}dk. \tag{11.32}$$

Also, one can write :

$$P_{q_k} = \frac{1}{2\pi}\int_{+\infty}^{-\infty} e^{(-\frac{4\epsilon^2}{g^2\beta}E_a - E_a\beta)}d\epsilon. \tag{11.33}$$

Finally, integration over ϵ gives:

$$P_{q_k} = \frac{g}{2\pi}(\frac{\pi\beta}{4E_a})^{\frac{1}{2}}e^{-E_a\beta}. \tag{11.34}$$

Multiplying all quantities represented by (11.24) and (11.34) one finally gets the following relation for the small polaron transition rate in the non-adiabatic regime:

$$R_{non-ad} = W_{(n\to n+1)}P_{\dot{q}_k}P_{q_k} = \frac{j^2}{\hbar}(\frac{\pi\beta}{4E_a})^{\frac{1}{2}}e^{-E_a\beta}. \tag{11.35}$$

References

[1] L. D. Landau. Electron motion in crystal lattices. *Phys. Z. Sowjetunion*, 3:664, 1933.

[2] S. I. Pekar. Local quantum states of electrons in an ideal ion crystal. *J. Phys. USSR*, 10:341, 1946.

[3] H. Fröhlich. Electrons in lattice fields. *Advances in Physics*, 3:325, 1954.

[4] R. P. Feynman and A. R. Hibbs. *Quantum Mechanics and Path Integrals*. McGraw-Hill: New York, 1965.

[5] N. N. Bogolubov. New adiabatic form of perturbation theory in the problem of interaction of a particle with quantum field. *Ukrainian Math. J.*, 11(2), 1950.

[6] N. N. Bogolubov and N. N. Bogolubov. *Some Aspects of Polaron Theory*, volume 4. World Scientific, 1988.

[7] T. Holstein. Studies of polaron motion: Part i. the molecular-crystal model. *Annals of Physics*, 8:325–342, 1959.

[8] K. Van Houcke, E. Kozik, N. Prokof'ev, and B. Svistunov. Diagrammatic monte carlo. *Physics Procedia*, 6:95–105, 2010.

[9] U. Schollwöck. The density-matrix renormalization group. *Reviews of modern physics*, 77:259, 2005.

[10] J. M. Zhang and R. X. Dong. Exact diagonalization: the bose-hubbard model as an example. *Eur. J. Phys.*, 31:591, 2010.

[11] N. Aaron Deskins and Michel Dupuis. Electron transport via polaron hopping in bulk tio$_2$: A density functional theory characterization. *Physical Review B*, 75:195212, 2007.

[12] N. F. Mott. High temperature superconductivity; the spin polaron theory. *Contemporary Physics*, 31:373–385, 1990.

[13] O. Verzelen, R. Ferreira, and G. Bastard. Excitonic polarons in semiconductor quantum dots. *Phys. Rev. Lett.*, 88:146803, 2002.

[14] M. Saitoh. Theory of strongly coupled ripplonic polarons at finite temperatures. *J. Phys. C: Solid State Phys.*, 16:6995, 1983.

[15] G. Capone, V. Cataudella, D. Ninno, and G. Iadonisi. Plasmapolaron selfenergy and effective mass in uniaxial polar crystals. *Phys. Stat. Sol. (b)*, 197:381, 1996.

[16] T. Ohsawa, T. Kabata, O. Kimura, M. Onoda, and K. Yoshino. In situ conductivity, electron spin resonance and absorption spectra measurements in polyaniline during electrochemical doping. *Japanese Journal of Applied Physics*, 28:996, 1989.

[17] D. Emin. Optical properties of large and small polarons and bipolarons. *Phys. Rev. B*, 48:13691–13702, 1993.

[18] E. Pellegrin, J. Zaanen, H.-J. Lin, G. Meigs, C. T. Chen, G. H. Ho, H. Eisaki, and S. Uchida. O 1s near-edge x-ray absorption of

$la_{2-x}sr_xnio_{4+\delta}$: Holes, polarons, and excitons. *Phys. Rev. B*, 53:10667–10679, 1996.

[19] A. De Sio, F. Troiani, Margherita Maiuri, Julien Réhault, Ephraim Sommer, James Lim, Susana F. Huelga, Martin B. Plenio, Carlo Andrea Rozzi, Giulio Cerullo, Elisa Molinari, and Christoph Lienau. Tracking the coherent generation of polaron pairs in conjugated polymers. *Nature Commun.*, 7:13742, 2016.

[20] S. R. Sehlin, H. U. Anderson, and D. M. Sparlin. Semiempirical model for the electrical properties of $la_{1-x}ca_xcoo_3$. *Phys. Rev. B*, 52:11681–11689, 1995.

[21] R. X. Smith, M. J. R. Hoch, P. L. Kuhns, W. G. Moulton, A. P. Reyes, G. S. Boebinger, J. Mitchell, and C. Leighton. Spin polarons in $la_{1-x}sr_xcoo_3$ single crystals. *Phys. Rev. B*, 78:092201, 2008.

[22] D. Emin. Transport properties of small polarons. *Journal of Solid State Chemistry*, 12:246–252, 1975.

[23] N. F. Mott. Polaron models of high-temperature superconductivity. *Physica C*, 205:191–205, 1993.

[24] Gaurab Rimal and Jinke Tang. Magnetic hard gap due to bound magnetic polarons in the localized regime. *Scientific Reports*, 7:42224, 2017.

[25] Alexandre S. Alexandrov (Ed.). *Polarons in Advanced Materials*. Springer, 1988.

[26] David Emin. *Polarons*. Cambridge University Press, 2013.

[27] N. N. Bogolubov. *Polarons:Collected Papers*, volume 2. Kiev: Naukova Dumka, 1970.

[28] J. T. Devreese (Ed.). *Polarons in Ionic Crystals and Polar Semiconductors*. Amsterdam: North-Holland, 1972.

[29] S. I. Pekar. *Investigations in Electron Theory of Crystals*. Gostekhizdat, 1951.

[30] J. T. Devreese. Fröhlich polarons from 0d to 3d: concepts and recent developments. *J. Phys.: Condens. Matter*, 19:255201, 2007.

[31] T. D. Lee, F. E. Low, and D. Pines. The motion of slow electrons in a polar crystal. *Physical Review*, 90:297–302, 1953.

[32] R. P. Feynman. Slow electrons in a polar crystal. *Physical review*, 97:660, 1955.

[33] J.T.Devreese and F.Brosens. On the validity of the feynman-jensen inequality expressed in the hamiltonian formulation for a polaron in a magnetic field. *Solid State Communications*, 7:593–596, 1993.

[34] A. S. Mishchenko, N. V. Prokof'ev, A. Sakamoto, and B. V. Svistunov. Diagrammatic quantum monte carlo study of the fröhlich polaron. *Phys. Rev. B*, 62:6317, 2000.

[35] F. Grusdt, Y. E. Shchadilova, A. N. Rubtsov, and E. Demler. Renormalization group approach to the fröhlich polaron model: application to impurity-bec problem. *Scientific Reports*, 5:12124, 2015.

[36] A. S. Alexandrov. Many-body effects in the normal-state polaron system. *Phys. Rev. B*, 46:2838, 1992.

[37] I. A. Makarov and S. G. Ovchinnikov. Cooperative effect of doping and

temperature on the polaronic band structure in strongly correlated electron systems with strong electron-phonon interaction. *arXiv:1612.02781*, [cond-mat.str-el], 2015.
[38] I. A. Makarov, E. I. Shneyder, P. A. Kozlov, and S. G. Ovchinnikov. Polaronic approach to strongly correlated electron systems with strong electron-phonon interaction. *Phys. Rev. B*, 92:155143, 2015.
[39] M. Leijnse, M. R. Wegewijs, and K. Flensberg. Nonlinear thermoelectric properties of molecular junctions with vibrational coupling. *Phys. Rev.B*, 82:045412, 2010.
[40] A. S. Alexandrov and N. F. Mott. *Polarons and bipolarons*. Singapore, River Edge, NJ : World Scientific, 1995.
[41] Chungwei Lin, Bingnan Wang, and Koon Hoo Teo. Optimal boson energy for superconductivity in the holstein model. *Phys. Rev. B*, 93:224501, 2016.
[42] V. Coropceanu, J. Cornil, D. A. da Silva Filho, Y. Olivier, R. Silbey, and J.-L. Brèdas. Charge transport in organic semiconductors. *Chem. Rev.*, 107:926–952, 2007.
[43] I. G. Lang and Y. A. Firsov. Mobility of small-radius polarons at low temperatures. *Sov. Phys. JETP*, 18:262, 1964.
[44] F. Marsiglio. Pairing in the holstein model in the dilute limit. *Physica C*, 244:21–34, 1995.
[45] A. Dobry, A. Greco, S. Koval, and J. Riera. Exact diagonalization study of the two-dimensional t-j-holstein model. *Phys. Rev. B*, 52:13722–13725, 1995.
[46] J. Bonča, S. A. Trugman, and I. Batistić. Holstein polaron. *Phys. Rev. B*, 60:1633–1642, 1999.
[47] R.H. McKenzie, C.J. Hamer, and D.W. Murray. Quantum monte carlo study of the one-dimensional holstein model of spinless fermions. *Phys. Rev. B*, 53:9676–9687, 1996.
[48] M. Capone, P. Carta, and S. Ciuchi. Dynamical mean field theory of polarons and bipolarons in the half-filled holstein model. *Phys. Rev. B*, 74:045106, 2006.
[49] Victor Lakhno. A translation invariant bipolaron in the holstein model and superconductivity. *SpringerPlus*, 5:1277, 2016.
[50] W. Casteels, J. Tempere, and J. T. Devreese. Bipolarons and multipolarons consisting of impurity atoms in a bose-einstein condensate. *Physical Review A*, 88:013613, 2013.
[51] A. J. Heeger. Charge storage in conducting polymers: Solitons, polarons, and bipolarons. *Polymer Journal*, 17:201–208, 1985.
[52] P.A. Bobbert, T.D. Nguyen, F.W. van Oost, B. Koopmans, and M. Wohlgenannt. Bipolaron mechanism for organic magnetoresistance. *Phys Rev Lett.*, 99:216801, 2007.
[53] Yan-Min Li. A possible picture for high-tc superconductivity in ba(or sr)la-cu-o compounds. *Solid State Communications*, 62:677–680, 1987.
[54] A. S. Alexandrov and G. M. Zhao. Isotope effects in high-tc cuprate superconductors as support for the bipolaron theory of superconductivity. *New Journal of Physics*, 14:013046, 2012.

[55] G. Pöschl and E. Teller. Bemerkungen zur quantenmechanik des anharmonischen oszillators. *Zeitschrift für Physik*, 83:143, 1933.
[56] L.A. Turkevich and T.D. Holstein. Small-oscillation theory of the one-dimensional large optic polaron. *Phys. Rev. B*, 35:7474, 1987.
[57] G. Kopidakis, C. M. Soukoulis, and E. N. Economou. Electron-phonon interactions and recurrence phenomena in one-dimensional systems. *Phys. Rev. B*, 49:7036–7039, 1994.
[58] M. Abramowitz and A. I. Stegun. *Handbook of mathematical functions with formulas, graphs, and mathematical tables*. Dover Publications, Inc (Reprinted by Dover Publications, Inc.), 1992.
[59] V.E. Zakharov and L.A. Ostrovsky. Modulation instability: The beginning. *Physica D*, 238:540–548, 2009.
[60] V. Pavlenko and V. Petviashvili. Stability of the nonlinear periodic waves in plasma. *Journal de Physique Colloques*, 40:621–622, 1979.
[61] C. Zener. Interaction between the d-shells in the transition metals. ii. ferromagnetic compounds of manganese with perovskite structure. *Phys. Rev.*, 82:403, 1951.
[62] P. W. Anderson and H. Hasegawa. Considerations on double exchange. *Phys. Rev.*, 100:675–681, 1955.
[63] P.-G. de Gennes. Effects of double exchange in magnetic crystals. *Phys. Rev.*, 118:141, 1960.
[64] W. P. Su. Spin polarons in the two-dimensional hubbard model: A numerical study. *Phys. Rev. B*, 37:9904–9906, 1988.
[65] Yosuke Nagaoka. Ferromagnetism in a narrow, almost half-filled s band. *Phys. Rev.*, 147:392–405, 1966.
[66] E. L. Nagaev. Spin polaron theory for magnetic semiconductors with narrow bands. *Physica Status Solidi (b)*, 65(1):11–60, 1974.
[67] A. Mauger. Magnetic polaron: Theory and experiment. *Phys. Rev. B*, 27:2308–2324, 1983.
[68] E. L. Nagaev. Localized ferrons and the mott transition via the ferromagnetic phase in doped antiferromagnetic semiconductors. *Physics of the solid state*, 43:54–60, 2001.
[69] M. A. Krivoglaz. Fluctuon states of electrons. *Sov. Phys. Usp.*, 16:856, 1974.
[70] A. Aharoni. *Introduction to the theory of ferromagnetism*. Oxford, 1996.
[71] H. A. Kramers. L'interaction entre les atomes magnétogènes dans un cristal paramagnètique. *Physica*, 1:182, 1934.
[72] P. W. Anderson. Antiferromagnetism. theory of superexchange interaction. *Phys. Rev.*, 79:350, 1950.
[73] J. B. Goodenough. Theory of the role of covalence in the perovskite-type manganites [la,m(ii)]$\mathrm{mno_3}$. *Phys. Rev.*, 100:564, 1955.
[74] J. B. Goodenough. An interpretation of the magnetic properties of the perovskite-type mixed crystals $\mathrm{la_{1-x}sr_xcoo_{3-\lambda}}$. *J. Phys. Chem.*, 6:287–297, 1958.
[75] J. Kanamori. Superexchange interaction and symmetry properties of electron orbitals. *J. Phys. Chem. Solid*, 10:87–98, 1959.
[76] M.A. Ruderman and C. Kittel. Indirect exchange coupling of nuclear

magnetic moments by conduction electrons. *Phys. Rev.*, 96:99–102, 1954.
[77] T. A. Kasuya. A theory of metallic ferro- and antiferromagnetism on zener's model. *Prog. Theory Phys.*, 16:45–57, 1956.
[78] K. Yosida. Magnetic properties of cu-mn alloys. *Phys. Rev.*, 106:893–898, 1957.
[79] P. Langevin. Magnètisme et thèorie des electrons. *Ann. Chim. Phys.*, 5:70–127, 1905.
[80] Charles Kittel. *Introduction to solid state physics (7th ed.)*. New York: Wiley, 1996.
[81] P. Weiss. L'hypothhse du champ molèculaire et la propriètè ferromagnètique. *J. Phys., vol.*, 6:661–690, 1907.
[82] W. Heisenberg. Zur theorie des ferromagnetismus. *Zeits.f.Physik*, 49:619–636, 1928.
[83] D. R. Inglis. The heisenberg theory of ferromagnetism. *Phys. Rev.*, 42:442, 1932.
[84] A. I. Liechtenstein, M. I. Katsnelson, V. P. Antropov, and V. A. Gubanov. Local spin density functional approach to the theory of exchange interactions in ferromagnetic metals and alloys. *J. Magn. Magn. Mater.*, 67:65–74, 1987.
[85] M. Pajda, J. Kudrnovský, I. Turek, V. Drchal, and P. Bruno. Ab initio calculations of exchange interactions, spin-wave stiffness constants, and curie temperatures of fe, co, and ni. *Phys. Rev. B*, 64:174402, 2001.
[86] H Meskine and S Satpathy. Self-trapped magnetic polaron in electron-doped $camno_3$. *Journal of Physics: Condensed Matter*, 17:1889, 2005.
[87] M. Umehara. Photoinduced localized magnetic polaron and luminescence in eu chalcogenides, especially in eute. *Phys. Rev. B*, 52:8140–8149, 1995.
[88] D. R. Yakovlev and W. Ossau. *In: Gaj J., Kossut J. (eds) Introduction to the Physics of Diluted Magnetic Semiconductors. Springer Series in Materials Science, vol 144.* Springer, Berlin, Heidelberg, 2010.
[89] L. D. Landau and E. M. Lifshitz. Theory of the dispersion of magnetic permeability in ferromagnetic bodies. *Phys. Z. Sowietunion*, 8:153, 1935.
[90] T. L. Gilbert. A lagrangian formulation of the gyromagnetic equation of the magnetic field. *Physical Review*, 100:1243, 1955.
[91] A. D. Fokker. Die mittlere energie rotierender elektrischer dipole im strahlungsfeld. *Ann. Phys.*, 348:810–820, 1914.
[92] M. Planck. Über einen satz der statistischen dynamik und seine erweiterung in der quantentheorie. *Sitzungsberichte der Preussischen Akademie der Wissenschaften zu Berlin*, 24:324–341, 1917.
[93] L. N. Bulaevskii, E. L. Nagaev, and D. I. Khomskii. A new type of auto-localized state of a conduction electron in an antiferromagnetic semiconductor. *Sov. Phys. JETP*, 27:836, 1968.
[94] P. Horsch and A. Ramšak. Spin-polaron wave function for a single hole in an antiferromagnet. *Journal of Low Temperature Physics*, 95:343–352, 1994.

[95] N. F. Mott and E. A. Davis. *Electronic Processes in Non-Crystalline Material*. Clarendon Press, Oxford, 1971.
[96] E. Fermi. Un metodo statistico per la determinazione di alcune prioprietà dell'atomo. *Rend. Accad. Naz. Lincei*, 6:602–607, 1927.
[97] E. Fermi. Eine statistische methode zur bestimmung einiger eigenschaften des atoms und ihre anwendung auf die theorie des periodischen systems der elemente. *Z. Phys.*, 48:73–79, 1928.
[98] L. H. Thomas. The calculation of atomic fields. *Proc. Cambridge Philosophical. Soc.*, 23:542–548, 1927.
[99] P. A. M. Dirac. Note on exchange phenomena in the thomas atom. *Math. Proc. Cambridge Philosophical. Soc.*, 26:376–385, 1930.
[100] P. Hohenberg and W. Kohn. Inhomogeneous electron gas. *Phys. Rev.*, 136:B864–B871, 1964.
[101] W. Kohn and L. J. Sham. Self-consistent equations including exchange and correlation effects. *Phys. Rev.*, 140:A1133–A1138, 1965.
[102] M. Born and R. Oppenheimer. Zur quantentheorie der molekeln. *Annalen der Physik*, 389:457–484, 1927.
[103] David C. Langreth and M. J. Mehl. Beyond the local-density approximation in calculations of ground-state electronic properties. *Phys. Rev. B*, 28:1809–1834, 1983.
[104] A. D. Becke. Density-functional exchange-energy approximation with correct asymptotic behavior. *Phys. Rev. A*, 38:3098–3100, 1988.
[105] John P. Perdew, J. A. Chevary, S. H. Vosko, Koblar A. Jackson, Mark R. Pederson, D. J. Singh, and Carlos Fiolhais. Atoms, molecules, solids, and surfaces: Applications of the generalized gradient approximation for exchange and correlation. *Phys. Rev. B*, 46:6671–6687, 1992.
[106] John P. Perdew, Kieron Burke, and Matthias Ernzerhof. Generalized gradient approximation made simple. *Phys. Rev. Lett.*, 77:3865, 1996.
[107] D. R. Hamann, M. Schlüter, and C. Chiang. Norm-conserving pseudopotentials. *Phys. Rev. Lett.*, 43:1494–1497, 1979.
[108] P. E. Blöchl. Projector augmented-wave method. *Phys. Rev. B*, 50:17953–17979, 1994.
[109] David Vanderbilt. Soft self-consistent pseudopotentials in a generalized eigenvalue formalism. *Phys. Rev. B*, 41:7892–7895, 1990.
[110] G. Kresse and J. Hafner. Norm-conserving and ultrasoft pseudopotentials for first-row and transition elements. *Journal of Physics: Condensed Matter*, 6:8245, 1994.
[111] D. R. Hartree. The wave mechanics of an atom with a non-coulomb central field. part i. theory and methods. *Proc. R. Soc. London*, 24:89–110, 1928.
[112] V. Fock. Näherungsmethode zur lösung des quantenmechanischen mehrkörperproblems. *Z. Phys.*, 61:126, 1930.
[113] J. C. Slater. A simplification of the hartree-fock method. *Phys. Rev.*, 81:385–390, 1951.
[114] N. F. Mott. The basis of the electron theory of metals, with special reference to the transition metals. *Proceedings of the Physical Society.*

Section A, 62:416, 1949.
[115] J. Hubbard. Electron correlations in narrow energy bands. *Proceedings of the Royal Society of London*, 276:238–257, 1963.
[116] A. I. Liechtenstein, V. I. Anisimov, , and J. Zaanen. Density-functional theory and strong interactions: Orbital ordering in mott-hubbard insulators. *Proceedings of the Royal Society of London*, 52:R5467, 1995.
[117] S. L. Dudarev, G. A. Botton, S. Y. Savrasov, C. J. Humphreys, and A. P. Sutton. Electron-energy-loss spectra and the structural stability of nickel oxide: An lsda+u study. *Phys. Rev. B*, 57:1505–1509, 1998.
[118] Yoyo Hinuma, Hiroyuki Hayashi, Yu Kumagai, Isao Tanaka, and Fumiyasu Oba. Comparison of approximations in density functional theory calculations: Energetics and structure of binary oxides. *Phys. Rev. B*, 96:094102, 2017.
[119] M. Sanati, R. C. Albers, T. Lookman, and A. Saxena. Elastic constants, phonon density of states, and thermal properties of uo_2. *Phys. Rev. B*, 84:014116, 2011.
[120] Roland Gillen, Stewart J. Clark, and John Robertson. Nature of the electronic band gap in lanthanide oxides. *Phys. Rev. B*, 87:125116, 2013.
[121] Paul Erhart, Andreas Klein, Daniel Åberg, and Babak Sadigh. Efficacy of the dft + u formalism for modeling hole polarons in perovskite oxides. *Phys. Rev. B*, 90:035204, 2014.
[122] Matteo Cococcioni and Stefano de Gironcoli. Linear response approach to the calculation of the effective interaction parameters in the LDA + U method. *Phys. Rev. B*, 71:035105, 2005.
[123] Burak Himmetoglu, Andrea Floris, Stefano de Gironcoli, and Matteo Cococcioni. Hubbard-corrected dft energy functionals: The lda+u description of correlated systems. *International Journal of Quantum Chemistry*, 114:14–49, 2014.
[124] K. Kim and K. D. Jordan. Comparison of density functional and mp2 calculations on the water monomer and dimer. *J. Phys. Chem.*, 98:10089–10094, 1994.
[125] P. J. Stephens, F. J. Devlin, C. F. Chabalowski, and M. J. Frisch. Ab initio calculation of vibrational absorption and circular dichroism spectra using density functional force fields. *J. Phys. Chem.*, 98:11623–11627, 1994.
[126] Jochen Heyd, Gustavo E. Scuseria, and Matthias Ernzerhof. Hybrid functionals based on a screened coulomb potential. *J. Chem. Phys.*, 118:8207, 2003.
[127] Carlo Adamo and Vincenzo Barone. Toward reliable density functional methods without adjustable parameters: The pbe0 model. *The Journal of Chemical Physics*, 110:6158–6170, 1999.
[128] Aliaksandr V. Krukau, Oleg A. Vydrov, Artur F. Izmaylov, , and Gustavo E. Scuseria. Influence of the exchange screening parameter on the performance of screened hybrid functionals. *The Journal of Chemical Physics*, 125:224106, 2006.
[129] M. I. Katsnelson and A. I. Lichtenstein. First-principles calculations of magnetic interactions in correlated systems. *Phys. Rev. B*,

61:8906–8912, 2000.
[130] Y. O. Kvashnin, O. Grånäs, I. Di Marco, M. I. Katsnelson, A. I. Lichtenstein, and O. Eriksson. Exchange parameters of strongly correlated materials: Extraction from spin-polarized density functional theory plus dynamical mean-field theory. *Phys. Rev. B*, 91:125133, 2015.
[131] N. V. Skorodumova, S. I. Simak, B. I. Lundqvist, I. A. Abrikosov, and B. Johansson. Quantum origin of the oxygen storage capability of ceria. *Phys. Rev. Lett.*, 89:166601, 2002.
[132] O. Hellman, N. V. Skorodumova, and S. I. Simak. Charge redistribution mechanisms of ceria reduction. *Phys. Rev. Lett.*, 108:135504, 2012.
[133] Y. Bravo A. Stashans. Large hole polarons in sc-doped tio_2 crystals. *Mod. Phys. Lett. B*, 27:1350113, 2013.
[134] Nicole Adelstein, Jeffrey B. Neaton, Mark Asta, and Lutgard C. De Jonghe. Density functional theory based calculation of small-polaron mobility in hematite. *Phys. Rev. B*, 89:245115, 2014.
[135] Marshall Stoneham. The strange magnetism of oxides and carbons. *Journal of Physics: Condensed Matter*, 22:074211, 2010.
[136] Keith P. McKenna, Matthew J. Wolf, Alexander L. Shluger, Stephan Lany, and Alex Zunger. Two-dimensional polaronic behavior in the binary oxides m-hfo_2 and m-zro_2. *Phys. Rev. Lett.*, 108:116403, 2012.
[137] F. Zhou T. Maxisch and G. Ceder. Ab initio study of the migration of small polarons in olivine lix $fepo_4$ and their association with lithium ions and vacancies. *Phys. Rev. B.*, 73:104301, 2006.
[138] P. E. Spencer, J. H. Samson, P. E. Kornilovitch, and A. S. Alexandrov. Effect of electron-phonon interaction range on lattice polaron dynamics: A continuous-time quantum monte carlo study. *Phys. Rev. B*, 71:184310, 2005.
[139] Shyue Ping Ong, Yifei Mo, and Gerbrand Ceder. Low hole polaron migration barrier in lithium peroxide. *Phys. Rev. B*, 85:081105, 2012.
[140] J. M. Garcia-Lastra, J. S. G. Myrdal, R. Christensen, K. S. Thygesen, and T. Vegge. Dft+ u study of polaronic conduction in li2o2 and li2co3: implications for li-air batteries. *J. Phys. Chem. C*, 117:5568–5577, 2013.
[141] A. Droghetti, C. D. Pemmaraju, and S. Sanvito. Polaronic distortion and vacancy-induced magnetism in mgo. *Phys. Rev. B.*, 81:092403, 2010.
[142] E. Cappelluti, S. Ciuchi, and S. Fratini. Polaronic signatures in the optical properties of the electron-doped cuprate superconductor $nd_{2-x}ce_xcuo_4$. *Phys. Rev. B.*, 79:012502, 2009.
[143] Stephan Lany and Alex Zunger. Polaronic hole localization and multiple hole binding of acceptors in oxide wide-gap semiconductors. *Phys. Rev. B*, 80:085202, 2009.
[144] B. Meredig, A. Thompson, H. A. Hansen, C. Wolverton, and A. van de Walle. Method for locating low-energy solutions within DFT$+u$. *Phys. Rev. B*, 82:195128, 2010.
[145] Y. Chen and M. M. Abraham. Trapped-hole centers in alkaline-earth oxides. *J. Phys. Chem. Solids*, 51:747, 1990.
[146] J. E. Wertz. Spin resonance studies of defects in magnesium oxide. *J. Phys. Chem. Solids*, 28:136, 1959.

[147] B. H. Rose and L. E. Halliburton. Esr hyperfine investigation of the v^0 centre in mgo. *J. Phys. C: Solid State phys.*, 7:3981, 1974.
[148] L. A. Kappers, F. Dravnieks, and J. E. Wertz. Electron spin resonance and optical studies of the double-hole (v^0) centers in mgo. *J. Phys. C: Solid State Phys.*, 7:1387–1399, 1974.
[149] M. M. Abraham and Y. Chem. V^- and v^0 centers in cao single crystals. *Solid state Communication*, 16:1209, 1975.
[150] A. M. Stoneham, A. P. Pathak, and R. H. Bartram. Ground-state of 2-hole centers in oxides. *Journal of Physics C: Solid State Physics*, 9:73–80, 1976.
[151] Philippe Baranek, Giordano Pinarello, Cesare Pisani, and Roberto Dovesi. Ab initio study of the cation vacancy at the surface and in bulk mgo. *Phys. Chem. Chem. Phys.*, 2:3893–3901, 2000.
[152] N. Kumar, D. Sanyal, and A. Sundaresan. Defect induced ferromagnetism in mgo nanoparticles studied by optical and positron annihilation spectroscopy. *Chem. Phys. Lett.*, 477:360, 2009.
[153] I. S. Elfimov, A. Rusydi, S. I. Csiszar, Z. Hu, H. H. Hsieh, H.-J. Lin, C. T. Chen, R. Liang, and G. A. Sawatzky. Magnetizing oxides by substituting nitrogen for oxygen. *Phys. Rev. Lett.*, 98:137202, 2007.
[154] Fenggong Wang, Zhiyong Pang, Liang Lin, Shaojie Fang, Ying Dai, and Shenghao. Magnetism in undoped mgo studied by density functional theory. *Phys. Rev. B.*, 80:144424, 2009.
[155] Feng Gao, Jifan Hua, Chuanlu Yang, Yujun Zheng, Hongwei Qin, Li Sun, Xiangwei Kong, and Minhua Jiang. First-principles study of magnetism driven by intrinsic defects in mgo. *Solid State Communications*, 149:855–858, 2009.
[156] R. C. Whited, C. J. Flaten, and W. C. Walker. Exciton thermoreflectance of mgo and cao. *Solid State Communications*, 13:1903–1905, 1973.
[157] Malin B. Johansson, Gunnar A. Niklasson, and Lars Österlundb. Structural and optical properties of visible active photocatalytic wo3 thin films prepared by reactive dc magnetron sputtering. *J. Mater. Res., Vol.*, 27:3130, 2012.
[158] C.G. Granqvist. Electrochromic tungsten oxide films: Review of progress 1993-1998. *Sol. Energy Mater. Sol. Cells*, 60:201–262, 2000.
[159] Gratian R. Bamwenda, Kazuhiro Sayama, and Hironori Arakawa. The effect of selected reaction parameters on the photoproduction of oxygen and hydrogen from a wo_3-fe^{2+}-fe^{3+} aqueous suspension. *Sol. Energy Mater. Sol. Cells*, 122:175–183, 1999.
[160] S. Tanisaki. Crystal structure of monoclinic tungsten trioxide at room temperature. *J. Phys. Soc. Jpn.*, 15:573–581, 1960.
[161] R. Diehl and G. Brandt. Crystal structure of triclinic wo3. *Acta Crystallogr.*, 34:1105, 1978.
[162] P. W. Woodward, A. W. Sleight, and T. J. Vogt. Structure refinement of triclinic tungsten trioxide. *J. Phys. Chem. Solids*, 56:1305, 1995.
[163] K.H.Cheng, A.J.Jacobson, and M.S.Whittingham. Hexagonal tungsten trioxide and its intercalation chemistry. *Solid State Ionics*, 5:355–358,

1981.

[164] B. Gerand, G. Nowogrocki, J. Guenot, and M. Figlarz. Structural study of a new hexagonal form of tungsten trioxide. *Journal of Solid State Chemistry*, 29:429–434, 1979.

[165] O. Yu. Khyzhun, Yu. M. Solonin, and V. D. Dobrovolsky. Electronic structure of hexagonal tungsten trioxide: Xps, xes, and xas studies. *Journal of Alloys and Compounds*, 320:1, 2001.

[166] J. G. Zhang, D. K. Benson, C. E. Tracy, S. K. Deb, A. W. Czandema, and C. Bechinger. *Chromic mechanism in amorphous WO_3 films.* 190th Electrochemical Society Meeting, 1996.

[167] K. Miyake, H. Kaneko, M. Sano, and N. Suedomi. Physical and electrochromic properties of the amorphous and crystalline tungsten oxide thick films prepared under reducing atmosphere. *Journal of Applied Physics*, 55:2747, 1984.

[168] A. Antonaia, M.L. Addonizio, C. Minarini, T. Polichetti, and M. Vittori-Antisari. Improvement in electrochromic response for an amorphous:crystalline wo3 double layer. *Electrochimica Acta*, 46:2221, 2001.

[169] S. S. Sun and P. H. Holloway. Modification of the electrochromic response of wo3 thin films by oxygen backfilling. *Journal of Vacuum Science and Technology*, 2:336, 1984.

[170] Lars Berggren, Andris Azens, and Gunnar A. Niklasson. Polaron absorption in amorphous tungsten oxide films. *Journal of Applied Physics*, 90:1860, 2001.

[171] M. F. Saenger, T. Höing, T. Hofmann, and M. Schubert. Polaron transitions in charge intercalated amorphous tungsten oxide thin films. *Phys. Status Solidi A*, 4:914, 2008.

[172] Esra Ozkana, Se-Hee Leea, C. Edwin Tracy, J. Roland Pittsa, and Satyen K. Deb. Comparison of electrochromic amorphous and crystalline tungsten oxide films. *Solar Energy Materials and Solar Cells*, 79:439–448, 2003.

[173] E. Iguchi and H. Miyagi. A study on the stability of polarons in monoclinic wo3. *J. Phys. Chem. Solids*, 54:403–409, 1993.

[174] G. A. de Wijs and R. A. de Groot. Structure and electronic properties of amorphous w03. *Phys. Rev. B*, 60:16463, 1999.

[175] D. B. Migas, V. L. Shaposhnikov, V. N. Rodin, and V. E. Borisenko. Tungsten oxides. i. effects of oxygen vacancies and doping on electronic and optical properties of different phases of wo3. *Phys. Rev. B*, 108:093713, 2010.

[176] N. L. Heda and B. L. Ahuja. Electronic properties and electron momentum density of monoclinic wo3. *Comp. Mat. Science.*, 72:49, 2013.

[177] D. A. Andersson, S. I. Simak, B. Johansson, I. A. Abrikosov, and N. V. Skorodumova. Modeling of Ceo_2, ce_2o_3, and Ceo_{2-x} in the LDA$+u$ formalism. *Phys. Rev. B*, 75:035109, 2007.

[178] Sergiu Arapan, Sergei I. Simak, and Natalia V. Skorodumova. Volume-dependent electron localization in ceria. *Phys. Rev. B*,

91:125108, 2015.
[179] M. M. Johansson, B. Zietz, G. A. Niklasson, and L. Österlund. Optical properties of nanocrystalline wo_3 and wo_{3-x} thin films prepared by dc magnetron sputtering. *Journal of Applied Physics*, 115:213510, 2014.
[180] Fenggong Wang, Cristiana Di Valentin, and Gianfranco Pacchioni. Semiconductor-to-metal transition in wo_{3-x}: Nature of the oxygen vacancy. *Phys. Rev. B*, 84:073103, 2011.
[181] Adriana Moreo, Seiji Yunoki, and Elbio Dagotto. Phase separation scenario for manganese oxides and related materials. *Science*, 283:2034, 1999.
[182] J. H. Jung, K. H. Kim, D. J. Eom, T. W. Noh, E. J. Choi, Yu. Jaejun, Y. S. Kwon, and Y. Chung. Phase separation scenario for manganese oxides and related materials. *Phys. Rev. B*, 55:15489, 1997.
[183] C. Herring. *Magnetism*, volume 2. Academic, New York, 1965.
[184] C. D. Ling, E. Granado, J. J. Neumeier, J. W. Lynn, and D. N. Argyriou. Inhomogeneous magnetism in la-doped $camno_3$. i. mesoscopic phase separation due to lattice-coupled ferromagnetic interactions. *Phys. Rev. B*, 68:134439, 2003.
[185] Vladimir I. Anisimov, Jan Zaanen, and Ole K. Andersen. Band theory and mott insulators: Hubbard u instead of stoner i. *Phys. Rev. B*, 44:943–954, 1991.
[186] Jochen Heyd and Gustavo E. Scuseria. Efficient hybrid density functional calculations in solids: Assessment of the heyd-scuseria-ernzerhof screened coulomb hybrid functional. *J. Chem. Phys.*, 121:1187, 2004.
[187] I. G. Austin and N. F. Mott. Polarons in crystalline and non-crystalline materials. *Advances in Physics*, 18:41–102, 1969.
[188] S. Mildner, J. Hoffmann, P. E. Blöchl, S. Techert, and C. Jooss. Temperature- and doping-dependent optical absorption in the small-polaron system $pr_{1-x}ca_xmno_3$. *Phys. rev. B*, 92:035145, 2015.
[189] D. Emin and T. Holstein. Studies of small-polaron motion iv. adiabatic theory of the hall effect. *Ann. Phys.*, 53:439, 1969.
[190] David Emin. Formation and hopping motion of molecular polarons. *Phys. Rev. B*, 61:14543–14553, 2000.
[191] David Emin. Generalized adiabatic polaron hopping: Meyer-neldel compensation and poole-frenkel behavior. *Phys. Rev. Lett.*, 100:166602, 2008.
[192] D. Emin. Formation and hopping motion of molecular polarons. *Phys. Rev. B*, 61:14543–14553, 2000.
[193] Nai Li Huang Liu and David Emin. Double exchange and small-polaron hopping in magnetic semiconductors. *Phys. Rev. Lett.*, 42:71–74, 1979.
[194] David Emin and Nai Li Huang Liu. Small-polaron hopping in magnetic semiconductors. *Phys. Rev. B*, 27:4788–4798, 1983.
[195] A. L. Larsson, B. E. Sernelius, and G. A. Niklasson. Optical absorption of li- intercalated polycrystalline tungsten oxide films: comparison to large polaron theory. *Solid State Ionics*, 165:35, 2003.
[196] G. Henkelman and H. Jónsson. A climbing image nudged elastic band

method for finding saddle points and minimum energy paths. *J. Chem. Phys.*, 113:9901–9904, 2000.

[197] G. Henkelman and H. Jónsson. Improved tangent estimate in the nudged elastic band method for finding minimum energy paths and saddle points. *J. Chem. Phys.*, 113:9978–9985, 2000.

[198] Arthur F. Voter. Chapter: Introduction to the kinetic monte carlo method. In *Radiation Effects in Solids*, pages 1–23. Springer Netherlands, 2007.

[199] B. Skubic, J. Hellsvik, L. Nordström, and O. Eriksson. A method for atomistic spin dynamics simulations: implementation and examples. *Condensed Matter*, 20:315203, 2008.

[200] T. Holstein. Studies of polaron motion. part ii. the "small" polaron. *Annals of Physics*, 8:343–389, 1959.

Acta Universitatis Upsaliensis

Digital Comprehensive Summaries of Uppsala Dissertations from the Faculty of Science and Technology 1631

Editor: The Dean of the Faculty of Science and Technology

A doctoral dissertation from the Faculty of Science and Technology, Uppsala University, is usually a summary of a number of papers. A few copies of the complete dissertation are kept at major Swedish research libraries, while the summary alone is distributed internationally through the series Digital Comprehensive Summaries of Uppsala Dissertations from the Faculty of Science and Technology. (Prior to January, 2005, the series was published under the title "Comprehensive Summaries of Uppsala Dissertations from the Faculty of Science and Technology".)

Distribution: publications.uu.se
urn:nbn:se:uu:diva-340947

ACTA
UNIVERSITATIS
UPSALIENSIS
UPPSALA
2018